University of Alberta

SPATIAL ANALYSIS OF THERMAL AGING OF OVERHEAD POWER TRANSMISSION LINES

by

Md. Mafijul Islam Bhuiyan

A thesis submitted to the Faculty of Graduate Studies and Research in partial fulfillment of the requirements for the degree of **Master of Science**.

in

Software Engineering and Intelligent Systems

Department of Electrical and Computer Engineering

Fall 2011
Edmonton, Alberta

Abstract

To meet increasing power needs of industrialized and urbanized consumers, power transmission companies are pressed to elevate the transmitted load in overhead power transmission lines. Increased loads impose thermal and mechanical stress, causing risks of transmission reliability. These risks can be mitigated by developing computational diagnostic tools for better scheduling of line inspections and maintenance.

The thesis introduces a novel methodology for spatial analysis of conductor thermal aging based on historical weather data that can be performed at three different levels: point, line, and area. By utilizing this paradigm, the thermal state of an energized transmission line can be visualized, initiating a new dimension in thermal aging research.

An advanced model for dynamic re-rating of existing transmission lines is introduced in the thesis to reduce the risk of sag. The performance of the thermal aging and re-rating models is examined using simulation data from the BC Hydro power transmission network.

Acknowledgements

This project is accomplished successfully with the help, support, and guidance of many people. First, I would like to express my heartiest gratitude to my parents for giving continuous mental support and encouragement.

Many thanks are directed to Dr. Petr Musilek for his insightful and knowledgeable guidance and supervision throughout my M.Sc. program. I would also like to express my gratefulness to Dr. Jana Heckenbergerova for many hours of discussions with her regarding different problems related to research project. I owe a very special debt of gratitude to the late Dr. Don Koval for his cordial support as an expert in power transmission systems.

Contents

List of Tables

List of Figures

Chapter 1

Introduction

1.1 Motivation

Like all things, conductors in overhead power transmission lines are subject to aging, and this process can cause critical equipment in a power transmission network to fail permanently. Therefore, the assessment of aging characteristics of power transmission lines and other equipment plays a major role in asset management systems. The term "aging" is used to represent the degradation of system components as a result of chronological age, cumulative service stress, and higher event stress [11]. The more severe causes of overhead power conductor aging include annealing due to high line temperatures, corrosion from environmental pollution, and heavy wind and ice loads.

Thermal aging due to elevated line temperatures has a significant impact on the lifetime of overhead power conductors. The recent competitive market has changed the methods of operating and planning power systems. For instance, due to an increase in demand for power, the transmission loading pattern has changed dramatically and the new loads often cause high stress on transmission lines. This problem can be minimized by building new lines, or by raising the maximum current capacity of existing lines [12]. The former approach is not supported by the public due to the visibility and environmental impact of transmission lines. Therefore, increasing

the current capacity of existing transmission lines is the only pragmatic solution. Raising the maximum permissible operating temperature of overhead transmission lines is the trend most responsible for thermal aging [13].

High power transmission line temperature causes annealing that reduces the tensile strength of aluminum strands in an Aluminum Conductor Steel Reinforced (ACSR) [14]. The strength loss accumulates over the lifetime of the conductor [15]. Although line temperatures are mainly affected by current throughput, they also depend on parameters such as material and environmental properties which cannot be regulated during system operations. As geographical and meteorological parameters are not consistent across the entire backbone power transmission system, aging is not uniformly distributed along the transmission line corridor; aging varies not only throughout the power system, but also along individual spans [16]. Hence, to compute spatially resolved thermal aging of large power transmission lines, a high resolution numerical weather prediction model has been applied to receive environmental conditions virtually at each point of the transmission system.

If a conductor's temperature exceeds its thermal limit due to high line current, it elongates because of thermal expansion; this increases its sag and decreases the clearance to objects beneath the conductor [17]. However, the increment of sag is also susceptible to mechanical loading over a long period of time, including high wind speed and heavy ice loads. The maximum load limit of a transmission line depends on the maximum allowable sag, which is set to eliminate the possibility of injury to people, flashovers, and outages of the power transmission network [15].

Present detection of sag and aging includes expensive visual air (helicopter) or ground inspections or analysis of readings obtained from tower sensors [18]. Sensors located on towers are prone to failure from exposure to severe meteorological conditions and from a scarcity of operating power supply. Since the cost of purchasing, installing, and maintaining sensors is high, they are not installed on every

tower, which results in limited coverage of the transmission network. On the other hand, computer simulation systems for sag and aging estimation can be run at low cost from a centralized location to encompass the complete power transmission network. Historical weather information along the transmission corridor can be used in this computer modeling to allow researchers to assess long term trends or forecast future events. For these reasons, computational modeling of spatial thermal aging and ground clearance of transmission networks represents significant economic advantages for the power transmission and distribution industry.

This thesis examines the aging of power transmission lines and develops a paradigm for the spatial analysis of aging that can perform at three different levels: point, line, and area - presenting a complete spatio-temporal scenario of thermal behavior of power transmission systems. This project focuses on the achievement of optimal line current without compromising ground clearance and thermal aging. Thermal aging and sag analyses allow power transmission engineers to manage power transmission assets effectively, to schedule line maintenance and inspections economically, and to design future transmission lines. A power transmission asset management system can help to identify and prevent potential power network outages by applying early intervention techniques. A model that evaluates spatial aging of different components of a large complex power system could eventually take into account other sources of aging such as natural and chemical aging.

1.2 Thesis objectives

The development of a model for spatio-temporal thermal aging analysis is the primary objective of this thesis. This paradigm consists of four components: the Weather Research and Forecasting Advanced Research Weather (WRF) numerical weather prediction model, an IEEE standard for computing line temperature and

ampacity [19], an approach to compute the percentage of loss of strength (LoS) due to annealing [3], a spatial aging model to localize critical segments and hot spots of power transmission lines. A sag analysis model is also designed considering thermal aging and mechanical (e.g., wind and ice) loads. These models contribute to the field of power transmission line asset management systems in the following ways:

- The development of a spatial aging model that incorporates all the influencing meteorological, geographical, and conductor parameters, is capable of localizing critical segments and hot spots of power transmission lines that are subject to thermal overload.

- Evaluation of seasonal influence on conductor thermal state; ampacities in hot spots and cold spots are examined. Spatial aging analysis is performed for different seasons by implementing seasonal ratings based on quantiles of calculated ampacities.

- An expert system is designed to determine the deterioration grade that represents the current condition of an energized power transmission conductor. A knowledge based fuzzy inference model is included to perform diagnosis and maintenance of an exposed ACSR conductor.

- A model for dynamic re-rating of an existing transmission line to reduce the risk of current sag, tension, and estimate available ground clearance is introduced. The model offers an efficient utilization of transmission lines without imposing risks of flashover and outage.

- A simple risk analysis technique that considers sag and LoS [%] is introduced to predict the consequences of thermal overload and contribute to decisions regarding line throughput.

1.3 Thesis organization

In chapter 2, a literature review of electrical conductors is presented regarding the following topics: the material states of a conductor, accelerated aging of electrical basbar (strip of copper and aluminum) joints, different approaches to loss of strength computations, corrosion effects due to environmental pollution, and the effects of emissivity and solar absorption coefficients. The background of the WRF modeling system is discussed and several sag calculation methods used to compute available ground clearance, are also described. Chapter 3 comprises methodologies to assess thermal aging, including the spatial analysis and seasonal distribution of thermal aging and the sensitivity analysis of spatial thermal aging. A case study of a transmission line in the province of British Columbia, Canada, is presented. A knowledge based expert system to estimate the current condition of an aluminum conductor steel reinforced (ACSR) is introduced in chapter 4. The proposed expert system is evaluated in a case study that examines large conductors. Ground clearance and sag analyses are illustrated in chapter 5 by considering metallurgical creep forced by thermal expansion, wind force, and ice mass load. Chapter 6 contains a summary of the work performed, presents the main contributions of the thesis, discusses limitations of the thesis, and proposes future work.

Chapter 2

Literature review

2.1 Conductor construction

2.1.1 Conductor materials

Three different types of materials: copper, aluminum, and steel, as well as their alloys, are generally used to manufacture bare phase and overhead conductors in power transmission lines. A few decades ago, overhead conductors were made mostly of copper due to its good electrical conductivity and tensile strength; copper wires can still be seen on older transmission lines. Due to its low cost and low weight relative to copper, and its analogous electrical properties, aluminum is mostly used as the conducting material in overhead transmission lines built recently. Though aluminum has good conductivity, it is susceptible to corrosion, thermal deterioration, and chemical aging. Moreover, the stiffness and tensile strength of aluminum is lower than that of copper [20]. Hence, design engineers are concerned with strengthening the conductors and predicting the remaining tensile strength, particularly for longer spans, of transmission lines in order to prevent or forecast any kind of outage.

Steel is usually added to aluminum to add strength to a power conductor. Steel strands added to the aluminum provide electrical conductivity and higher mechanical strength, allowing the conductor to perform efficiently under severe thermal

overloading and harsh atmospheric conditions. However, steel is also highly vulnerable to corrosion and hence is generally galvanized with zinc for protection [20]. A layer of grease is applied to protect the contact area between aluminum and steel strands and to block galvanic corrosive agents. This grease layer exists for $10-15$ years unless the line is thermally overloaded and exposed to very hot ultraviolet radiation over an extended period [21]. Therefore, the resultant conductors have both increased corrosion resistance and increased conductivity compared to galvanized steel.

2.1.2 Conductor types

The type of conductor used for a power transmission line depends on the anticipated voltage load, the geographical location, and environmental conditions. All aluminum conductors (AAC), having high corrosion protection, are usually deployed in coastal areas. They are also used where the mechanical and thermal load is not so high. Nowadays, the all aluminum alloy conductor (AAAC) is preferred because of its high ratio of strength to weight that offers lower sag on longer transmission line spans. The aluminum conductor alloy reinforced (ACAR) is also used for special applications; it consists of various proportions of aluminum, aluminum alloy, and steel wires [22].

Figure 2.1: All aluminum Conductor (AAC)[23]

Figure 2.2: Aluminum Conductor Steel Reinforced (ACSR)[23]

Figure 2.3: Alcan Cable Aluminum Conductor Alloy Reinforced (ACAR) [24]

A high-temperature conductor such as the steel supported aluminum conductor (SSAC) is normally utilized for high voltage power transmission lines where a high degree of reliability is required. This type of conductor permits elevated temperature operation with lower line sag. Its total mechanical load is borne by high strength steel strands whereas the fully annealed aluminum strands are deployed only for transmitting current and they do not take any load. More recently, aluminum zirconium alloy wires have been used in high-temperature, high-ampacity conductors as they can carry high currents. Invar alloy wires are used for the core to strengthen steel strands [22]. However, these conductors have reduced strength relative to standard ACSR and are not preferred in areas where high winds and heavy ice loads are expected. Furthermore, the expense of installing SSAC is high due to the requirement of pre-stressing prior to clipping and sagging [25].

Aluminum conductor steel reinforced (ACSR) is currently used in most overhead transmission lines. This type of conductor is capable of tolerating elevated temperatures up to 95 °C. For short times during emergencies, the maximum per-

missible temperature is 125 °C [26]. It is also preferred where heavy wind and ice loads are a regular phenomenon. Although conventional ACSR are designed with a circular cross-sectional area, the most recent compact ACSR is manufactured by the trapezoidal shaping of wires that ensures less susceptibility to loss of tensile strength for the same cross-sectional area of the conductor. Sometimes, concentric gaps inside the conductor are emplaced to achieve better aerodynamic performance and damping of wind-induced vibrations [22].

2.2 Aging of conductor joints and splices

The reliability of power transmission lines depends on the aging behavior of both splice-conductor interfaces and conductors. The interface between two conductors and electrical joints are the most significant factors to be considered in estimating a power conductors lifespan [26].

A rising demand for power and the scarcity of new power transmission infrastructure are responsible for the elevation of operating temperatures in existing transmission lines. These higher operating temperatures cause accelerated aging of splices, or electrical joints. The results are manyfold:

- Resistance in electrical joints is increased drastically, which makes the transmission of electricity less efficient,
- Thermal conductivity is reduced,
- Connector binding stress is reduced,
- The separation of the power line and failure due to the deterioration in the connector clamping strength is the most severe consequence [26].

Bergmann et al. [27] described a mathematical model that can be deployed to predict the aging behavior of electrical joints. The model is controlled by several

influencing parameters, including construction of the joint, conductor materials, loading construction, and assembly technology.

Joint resistance R_j is the most important parameter in assessing the current condition of an electrical joint or splice. Two processes that increase joint resistance are responsible for the aging of electrical joints: (i) conductor material creep reduces the contact force and can increase the joint resistance dramatically, (ii) chemical reactions on constriction areas increase joint resistance and speed up the aging of the joint. These two aging processes can occur simultaneously although their intensities are not same [27].

Chemical reactions contribute significantly to electrical joint aging. The constriction areas formed due to the uneven contact surface between two conductors are usually corroded by chemical reactions occurring between the conducting materials and the environment [28] [29]. The resulting inhomogeneous current fields produce very high electrical resistance in the joint. Hence, the contact surface of the joint becomes unable to carry current. On the other hand, the resistance between intermetallic phases (for example Al and steel, St) of a composite conductor becomes higher as atoms transfer from one metal to another through diffusion. This migration takes place in the presence of an electric field, particularly in areas of higher temperature, like constriction areas [30]. The three stages of chemical aging are [31]:

- Formation,
- Relative stability,
- Accelerated aging.

In the formation stage, spontaneous chemical reactions produce an elevated resistance in joints. The product of the chemical reactions is an oxide layer that covers

the surfaces of the constriction area. The oxide layer protects the constriction area and further chemical reactions become very slow. Since the oxide layer behaves like a depletion region for associated chemical reactions, stable constriction areas are developed during this phase. Figure 2.4 depicts the three stages of aging behavior in constriction areas.

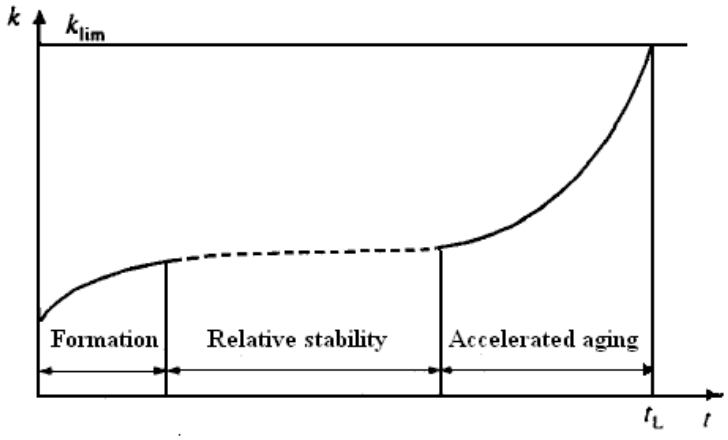

Figure 2.4: Stages of aging behavior of an electrical joint [27]

The joint resistance as well as the relative stability increases slightly in the second phase of aging, due to the presence of the protective oxide layer. However, power P_j losses are incurred and the joint temperature ϑ_j becomes high. This process can be correlated with joule heating $R_j I^2$ and is expressed as:

$$\Delta\vartheta_j \sim P_j = R_j \cdot I^2, \tag{2.1}$$

where R_j is joint resistance [ohms] and I is the current [amps], and $\Delta\vartheta_j$ is the temperature rise in joint.

In the final stage of electrical joint aging, the chemical processes are accelerated at elevated temperature and the joint resistance increases drastically. In severe cases the melting temperature of the metal is reached in the constriction areas. However, the joint resistance becomes smaller when the constriction area becomes larger due

to this melting process. The effect of this alternating resistance in a joint depends on design and loading criteria. Eventually, the joint fails when the melting is complete.

A time dependent mathematical model is essential to evaluate joint aging and predict the remaining lifespan of the joint [27]. In this model, the performance factor k is introduced to relate different types and dimensions of joints. It can be expressed as:

$$k = \frac{R_j}{R_r}, \tag{2.2}$$

where R_j is joint resistance, and R_r is reference resistance.

The formation phase of the aging process can be expressed as follows:

$$k' \sim \frac{1}{t^m}, \tag{2.3}$$

where t is the load period and m is a constant parameter. According to this equation, the thickness of the growing protective layer is proportional to the speed of contact aging, K'.

The speed of aging of a busbar joint depends on the speed of the chemical reactions in the constriction area; the higher the joint temperature T, the higher the speed of the chemical reactions. This correlation can be explained using the Arrhenius-law:

$$k' \sim d\ e^{-\left(\frac{b}{RT_a}+\frac{1}{2}\right)}, \tag{2.4}$$

where R is the gas constant, T_a is the temperature on the constriction area, and d and b are constant parameters.

Finally, the speed of contact aging can be represented by equations (2.3) to (2.4) as:

$$k' \sim (k - k_{id})\frac{d\ e^{-\left(\frac{b}{RT_a}+\frac{1}{2}\right)}}{t^m}, \tag{2.5}$$

where $(k - k_{id})$ is the proportionality constant of aging speed [27].

2.3 Thermal aging and current carrying capacity of a conductor

The maximum operating temperature of the conductor is the most significant parameter for computing the thermal aging and the current-carrying capacity of power transmission lines [15]. The temperature of a power transmission line can be determined from load current and meteorological data [32] using a procedure based on IEEE Standard 738 [19]. By applying the heat balance equation (2.6), the temperature of a conductor can be calculated [19] for a steady state power transmission system:

$$q_c + q_r = q_s + I^2 \cdot R(T_c), \tag{2.6}$$

where q_c is the heat lost due to convection and q_r is conductor radiation heat loss, q_s is the heat gained from solar radiation, and T_c represents conductor operating temperature. $I^2R(T_c)$ describes the Joule heating due to positive resistance values of the conductor where resistance is a function of conductor temperature. Other parameters that influence conductor temperature are not considered in IEEE Standard 738 as their effect is negligible under most circumstances. Equation 2.6 is solved numerically to determine T_c using an iterative procedure. Each term in equation 2.6 is described below and is explained in more detail in [19].

Solar heat flux Q_{se} depends on the projected area of the conductor A', its elevation above sea level H_c, and the azimuth of the sun and conductor Z_s and Z_c, respectively. Q_{se} gains the most heat by solar radiation. It is computed as:

$$q_s = \alpha \cdot Q_{se} \cdot \sin\left(\cos^{-1}\left(\cos(H_c) \cdot \cos(Z_s - Z_c)\right)\right) A'. \tag{2.7}$$

Convective heat loss that depends on wind speed can be calculated by:

$$q_{c,0} = 0.0205 \cdot {\rho_f}^{0.5} \cdot D^{0.75} \cdot (T_c - T_a)^{1.25}, \tag{2.8}$$

$$q_{c,1} = \left[1.01 + 0.0372 \cdot \left(\frac{D \cdot \rho_f \cdot V_w}{\mu_f}\right)^{0.52}\right] k_f \cdot K_\beta \cdot (T_c - T_a), \tag{2.9}$$

$$q_{c,2} = 0.0119 \cdot \left(\frac{D \cdot \rho_f \cdot V_w}{\mu_f}\right)^{0.6} k_f \cdot K_\beta \cdot (T_c - T_a), \tag{2.10}$$

where $q_{c,0}$ corresponds to natural convection (zero wind speed), and $q_{c,1}$ and $q_{c,2}$ represent forced convection for low and high wind speeds, respectively; T_a is ambient temperature, D is the conductor diameter, ρ_f is the density of air, V_w is the wind speed, k_f is the thermal conductivity of air at temperature $(T_a + T_c)/2$, and μ_f is the dynamic viscosity of air. K_β is a wind direction corrective parameter used for non-perpendicular wind; it is calculated by:

$$K_\beta = 1.194 - \sin(\beta) - 0.194 \cdot \cos(2\beta) + 0.368 \cdot \sin(2\beta), \tag{2.11}$$

where β is the angle between the wind direction and a perpendicular to the conductor axis.

A power transmission line may be in risk of damage when operated at elevated temperatures. As a result of line overheating, aluminum strands in an ACSR generally elongate and lose their tensile strength due to high temperature annealing [15]. High temperature annealing is the primary cause of permanent damage to aluminum strands in an ACSR. Hence high operating temperatures are primarily responsible for conductor aging.

Current carrying-capacity of an ACSR depends also on conductor ground clearance or allowable midspan sag [33]. Minimum conductor ground clearance is a crucial parameter that gives the lowest limit to prevent flashover or outage. As an overhead transmission line elongates permanently due to thermal aging, sag increases with time. Thus, the current carrying capacity of a conductor depends on

operating temperature, available ground clearance, and conductor elongation due to thermal aging [34].

2.3.1 Historical review of thermal aging models

Many research projects have been undertaken all over the world to determine the thermal aging of overhead transmission lines. Consequently, several methods have been developed to estimate the loss of conductor tensile strength. The review of thermal aging models that follows is organized chronologically to give the reader a sense of theory development.

2.3.1.1 Beers et al. (1963) [1]

Although the paper is related to transmission line ratings, the authors illuminate the annealing effects on conductors due to thermal overloading. The method described in this paper for calculating the annealing effect includes weather-data analyses that use a digital computer for extensive computations, and a graphical method for annealing calculations. The authors state that ratings of a new transmission line should be based on its loss of tensile strength, which can be influenced by parameters such as conductor characteristics, load flow, and ambient conditions (e.g., wind speed, wind direction, temperature).

The method described in the paper consists of five steps. First, data are organized in a tabular format to represent the total duration of wind and ambient temperature responsible for elevating the line temperature. The elevated temperatures are high enough to cause annealing during the expected lifespan of the conductor. Second, assumed load currents during normal or emergency conditions are assigned. Third, the maximum permissible loss of conductor strength due to annealing is ascribed. Fourth, a table of line temperatures and their frequencies is computed using transmitted current, wind velocity, and ambient temperature according to the House

and Tuttle method [34]. Fifth, the total loss of strength due to annealing is evaluated by the graphical method. In this paper, 65 °C was chosen as the minimum annealing temperature. For a case study, the authors collected five years of local weather data from the Weather Bureau of the U.S. Department of Commerce, which had been prorated to 30 years, and a correction factor was applied.

2.3.1.2 Koval et al. (1970) [2]

In this paper, the authors discussed a digital and numerical approach for calculating the permanent loss of tensile strength due to high temperature annealing. In [1], it was shown that the annealing curves can be represented by a series of second-order logarithmic polynomials. The authors used equation (2.12) to estimate the permanent loss of strength due to annealing in the aluminum strand of an ACSR.

$$S(t_1) = A0(t_1) + A1(t_1) \cdot \log[TIME(t_1)] + A2(t_1) \cdot \log[TIME(t_1)]^2, \qquad (2.12)$$

where t_1 is conductor temperature, $TIME(t_1)$ is the duration of exposure time at a given conductor temperature in hours, $S(t_1)$ is the estimated loss of strength due to annealing, and $A0$, $A1$, and $A2$ are polynomial coefficients.

The following equation can be used to compute the equivalent time loading $[TIME_{eq}(t_l)]$ at different conductor temperatures t_2,

$$TIME_{eq}(t_2) = 10^x, \qquad (2.13)$$

where

$$x = -\frac{1}{2} \cdot \frac{A1(t_2)}{A2(t_2)} \pm \sqrt{\frac{S(t_1) - A0(t_2)}{A2(t_2)} + \frac{1}{2} \cdot \left(\frac{A1(t_2)}{A2(t_2)}\right)^2}. \qquad (2.14)$$

To compute the total loss of strength due to annealing over the specified lifespan of a conductor, the frequency of all annealing temperatures must be determined. First, the loss of strength is evaluated for 65 °C. The equivalent time of 65 °C loading is then converted in terms of the 70 °C loss of strength by applying equations (2.13)

and (2.14). The frequency of temperature 70 °C is then added to this equivalent time and the loss of strength for the exposure at 65 °C and 70 °C temperatures is calculated. This process is continued until all the annealing temperatures are considered.

2.3.1.3 Harvey (1972) [3]

Harvey described a method that estimates the loss of strength of aluminum strands in different conductor types, such as AAAC, ACSR, and SAC (made from EC-H19 strands), during high temperature operation. This empirical paradigm represents a relationship between time, conductor temperature, and remaining strength. The estimated remaining tensile strength from the models and the actual remaining strength are compared in this paper. According to [3], the loss of tensile strength can be expressed as a function of conductor diameter: larger diameter conductors will deteriorate more slowly than smaller diameter ones. This diameter effect is accounted for in the developed models. Moreover, the maximum permissible line temperature without an annealing effect is chosen as 100 °C. The mathematical models for the three different conductors are:

$$\text{SAC, } RS = (-0.24 \cdot T + 134) \cdot t^{-(0.001T - 0.095)\frac{1}{d}}, \text{ if (- } 0.24 \cdot T \text{ + } 134 \text{)} > 100, \text{ use } 100; \tag{2.15}$$

$$\text{AAAC, } RS = (-0.52 \cdot T + 176) \cdot t^{-(0.001T - 0.118)\frac{1}{d}}, \text{ if (- } 0.52 \cdot T \text{ + } 176 \text{)} > 100, \text{ use } 100; \tag{2.16}$$

$$\text{ACSR, } RS = RS \text{ of } EC \cdot \left(\frac{STR_{EC}}{STR_T}\right) + 100 \cdot \left(\frac{STR_{ST}}{STR_T}\right) \cdot 1.09, \tag{2.17}$$

where RS is the remaining percentage of tensile strength, T is the line temperature [°C], t is exposed time duration [hrs], d represents strand diameter [inches], STR_{EC}, STR_{ST}, and STR_T are the initial strengths of EC strands, steel strands, and total conductor, respectively. Here, EC-H19 is one type of aluminum alloy.

2.3.1.4 Morgan (1996) [4]

By examining different published experimental data, Morgan demonstrated that the loss of strength of a conductor is related more to the percentage reduction in cross-sectional area during wire drawing, than to the diameter of the conductor, as shown earlier by Harvey [3]. The following equation was derived by Morgan for aluminum and aluminum alloy wires,

$$\ln\ln\left[\frac{1}{1-Y}\right] = A' + \frac{B'}{T}\cdot\ln t + \frac{C'}{T} + D'\cdot\ln\frac{R}{80}, \tag{2.18}$$

where R is the percentage reduction in cross-sectional area, Y is the fractional loss of strength, T is the absolute temperature, and A', B', C', and D' are constant parameters derived from various experimental data. The author also shows that the loss of strength in a 2.67 mm aluminum strand, calculated by applying the above equation, is almost analogous to the corresponding experimental data. Figure 2.5 compares strength losses computed by the three approaches described in section 2.3.1.

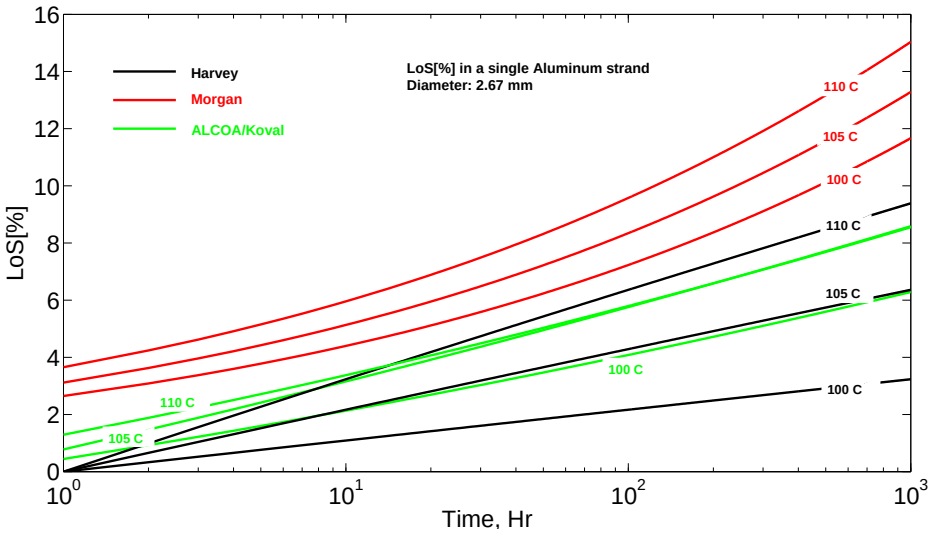

Figure 2.5: Comparisons of loss of strength calculation methods

2.3.2 Environmental pollution

2.3.2.1 Aluminum dust

The lifetime of an overhead transmission line can be shortened by the accumulation of dust or pollutant, as a layer of dust or pollutant can raise the temperature of the transmission line. Three concentric parallel layers of steel, aluminum, and accreted dust are encompassed in the dusty composite conductor depicted in Figure 2.6.

During the lifetime of a transmission line, the total emission of energy can be calculated as:

$$E = I^2 \cdot R_T \cdot T = (I_{st}^2 \cdot R_{st} + I_{al}^2 \cdot R_{al}) \cdot T, \tag{2.19}$$

where I is equivalent to line currents at two different layers: I_{st} in steel strands and I_{al} in aluminum strands; R_T is the total resistance which is equivalent to two parallel resistances, R_{st} and R_{al}.

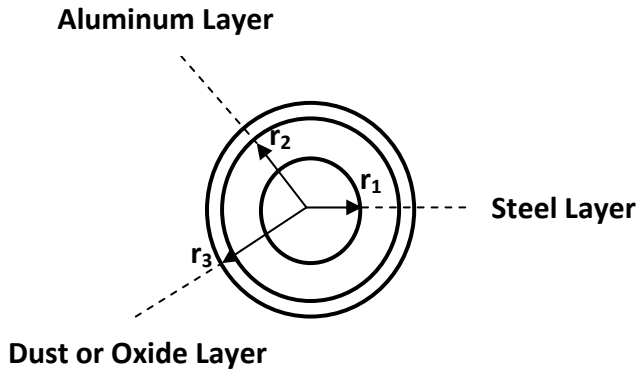

Figure 2.6: Different layers of dust covered conductor [35]

A dust layer, particularly a layer of aluminum oxide (Al_2O_3), accreted on the surface of a transmission line, resists the emission of heat through convection and radiation processes. Moreover, the resistance of the transmission line increases due to the thermal and electrical properties of the dust layer. Hence, the current-carrying capacity of the transmission line decreases. As a consequence, the frequency of exceeding the maximum permissible line temperature rises and the lifespan of the

transmission line is reduced. In the presence of the dust layer, the emission of energy (E_d), can be computed as:

$$E_d = I^2 \cdot R_{T_d} \cdot T_d = (I_{st}^2 \cdot R_{st} + I_{al}^2 \cdot R_{al} + I_d^2 \cdot R_d) \cdot T_d, \tag{2.20}$$

where I represents the equivalent line current in three current portions I_{st}, I_{al}, and I_d in the different layers, where I_d refers to current at dust layer; R_{T_d} is the total resistance equivalent to three parallel resistances R_{st}, R_{al}, and R_d in the three different layers; and resistance at each layer is directly proportional to the temperature rise of the corresponding layer; R_d and I_d represent the resistance and current of the dust layer, respectively [35].

2.3.2.2 Corrosion

An energized power transmission ACSR gradually deteriorates if exposed to atmospheric pollutants. The most severe deterioration occurs at sleeve joints, spacers, and dampers. Environmental corrosion of a conductor reduces its tensile strength depending on the impact of various types of pollutants and Al dust, as well as on the history of atmospheric pollution.

Two types of corrosion phenomena, atmospheric and galvanic, usually take place in power transmission conductors. Corrosive agents, often compounds containing sulphur, ammonium, or chlorine, are responsible for atmospheric corrosion [36]. Atmospheric corrosion often attacks the zinc coating on steel wires without decaying the aluminum strands. It usually occurs with the help of atmospheric conditions such as rain, fog, or snow. The corrosive effect is then gradually transferred to the cross sectional area of the steel strands [21]. Galvanic corrosion usually ensues in the contact area of two different metals, aluminum and steel in the case of compound conductors. If the zinc layer is corroded it creates electrolytic cells between the aluminum and zinc layers. As a result, the aluminum strands are corroded through electrolytic cells [21]. The adverse effects of these corrosive agents

affect the mechanical and electrical properties of the conductor. Transmission lines located in industrial areas are at risk of atmospheric corrosion, whereas galvanic corrosion typically occurs in coastal areas due to salt water spray [36].

2.3.3 Emissivity

The emissivity coefficient of the outer surface of a power transmission condutor is a major factor in regulating its current-carrying capacity [37]. Therefore, absorption and emission of heat by conductors mostly depend on solar absorption and emissivity coefficients, respectively. A high emissivity coefficient implies that more heat radiates from the conductor [38]. The emissivity coefficient for a new stranded aluminum conductor is approximately $0.2-0.25$ [37]. This value increases rapidly due to several factors, including years Y in service, weather conditions, and environmental pollution. A correlation between atmospheric pollutants and emissivity ε is expressed by the following empirical equation [33]:

$$\varepsilon = 0.23 + 0.7\left[\frac{Y}{1.22+Y}\right]. \tag{2.21}$$

Hence, the emissivity of a well weathered conductor can be raised to 0.85 after being energized for more than eight years.

2.3.4 Solar absorption coefficient

Solar heating can increase conductor temperature, depending on the season of the year, the time of day, geographical location, orientation of the transmission line, and the clarity of the atmosphere. The solar absorption coefficient is a conductor characteristic that represents the portion of available solar energy that can be absorbed by the conductor. The absorptivity coefficient changes gradually with the age of conductor. The value of the coefficient for a new aluminum conductor is about $0.4-0.5$, whereas it can reach 0.93 for a conductor that has operated for more than eight years [38].

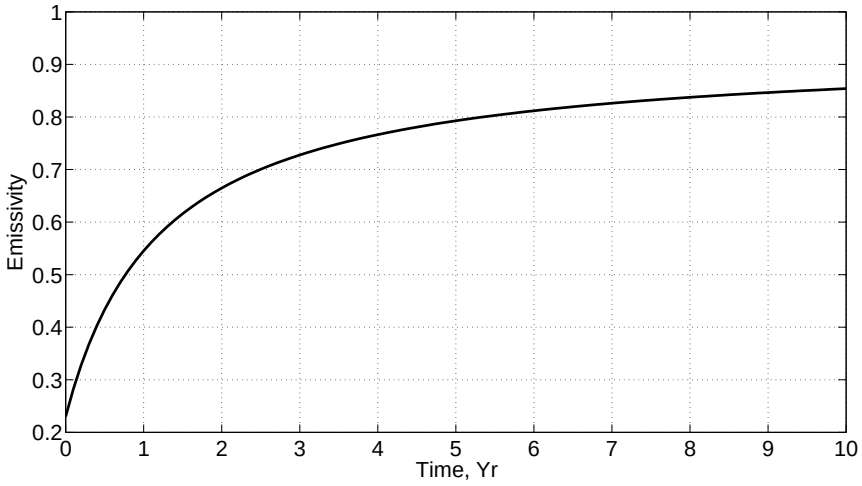

Figure 2.7: Change of emissivity coefficient over time

Both the solar absorption coefficient and emissivity of a conductor depend on years in service, location, and environmental pollution. The relationship between these two important conductor properties in a particular geographical location was depicted in Figure VIII-1 in [38]. The figure shows that emissivity is lower than solar absorptivity during entire conductor lifetime. In addition, the difference between these parameters is almost 0.2 within 15 years of service. If years of conductor service exceed 15, the difference becomes lower, leading to a steady value of 0.12.

2.4 Historical review of sag calculation

The maximum current-carrying capability of a power transmission line depends on the maximum allowable sag. Sag in excess of the maximum allowable poses risks of injury to people and damage to critical equipment in the power transmission network [15]. Subsequently, it is essential to monitor whether the conductor will not collapse under high mechanical load while not compromising the ground clearance [10]. Hence, sag computation is a very significant factor to keep the transmission line operating in an optimal way. In the power sector, many research programs

have been performed, particularly in North America and Europe, to estimate sag under different conditions using graphical and numerical approaches, among other techniques.

2.4.1 Lummis et al. (1955) [5]

In this paper, the authors discussed how to calculate the sag and tension, and described a method to compute vertical and swing clearances. They identified error parameters that are unavoidable during transmission line design, such as wind direction and speed, inelastic/plastic creep, and transfer of conductor from sheave to suspension clamp. Due to the many sources of error, they used a catenary equation for a suspended conductor. The limitations of the approximated catenary equation are manifold. However, it works satisfactorily under most ordinary conditions. Subsequently, it was shown that for an inclined tower span the actual ground clearance near the half of the higher support point will be smaller than the computed ground clearance if the maximum sag error is on the order of 30 cm.

The authors applied a different approach for computing sag at the dead end span. Dead end spans are the marginal structures of an overhead power transmission line which support the full weight of the conductor. They also use strain insulators that do not permit longitudinal and horizontal movement of transmission line [15]. Particularly, in short dead-end spans where the weight of the insulation string is very high, clearances should be kept to a minimum level. An approximate solution for computing sag for this condition takes the summation of moments of the point of support as follows,

$$S_1 = \frac{wl}{2H} \cdot (L - 2l) + \frac{Wl^2}{2H}, \tag{2.22}$$

since $H = wC$,

$$S_1 + S_2 = \frac{l}{2C} \cdot (L - 2l) + \frac{(L - 2l)^2}{8C} + \frac{Wl^2}{wC}, \tag{2.23}$$

where (S_1+S_2) is the total sag, w is the linear weight of conductor per unit length, W represents the weight of the insulator, L is the tower span, l is the total length of the conductor, C is the catenary constant, and H is the horizontal load component.

2.4.2 Seppa (1994) [6]

Seppa investigated the influence of several factors on the sag calculation of transmission line spans. He also mentioned a few parameters that are often neglected, but have substantial impact on line design.

He identified parameters that can influence the sag-tension-temperature relationship, but are ignored in the IEEE standards, such as vertical wind speed, standard deviation of wind speed and direction, and temperature distribution in the cross-sectional area of the conductor. The vertical wind speed due to turbulence has a significant cooling effect, reducing the line temperature and sag as well. "Subconductor eclipse" is another example that can change sag and tension substantially in a particular time period of a sunny day. When the shadow of one subconductor falls on another subconductor as the bundle is inclined, it can make a sag difference of up to 15 cm. In addition, the temperature difference between two subconductors can be as high as 3.5 °C. The tension or sag spike due to subconductor eclipse generally occurs at 3 p.m. to 4 p.m. according to the altitude of sun.

2.4.3 Keshavarzian et al. (2000) [7]

The authors derived a sag computation method for multispan power transmission lines where each segment has a different temperature. This method depends on the rotational stiffness of suspension insulator strings. The modified ruling span concept is also applied here by altering some fundamental assumptions. This method aims to determine the unbalanced force at each conductor support along with temperature changes, and then compute the entailed suspension clamp longitudinal

movements. Finally, conductor sags and tensions are evaluated. The method is based on an iterative procedure, so it does not require any finite element nonlinear computation. It can be represented by the equations:

$$(\delta_i - \delta_{i-1}) = 8(D^2_{R,\,t} - D^2_R) \cdot S_i \cdot \frac{\left[1 - \left(\frac{S_i}{S_R}\right)^2\right]}{3 \cdot S^2_R}, \tag{2.24}$$

$$\Delta_{i,\,t} = \frac{[(H_{i+1,\,t} - H_{i,\,t}) + K_{i,\,t} \cdot \Delta_{i-1,\,t} + K_{i+1,\,t} \cdot \Delta_{i+1,\,t}]}{K_{i,\,t} + K_{i+1,\,t} + k_i}. \tag{2.25}$$

The former equations are used to determine the longitudinal and horizontal movement of each suspension clamp that depends on the position of the suspension insulator string. D_R is the sag of the ruling span, S_i is span length, and S_R is ruling span length. The latter equation is used to evaluate actual longitudinal movements of the suspension clamps for 1 to $n-1$, Δ_1 to Δ_{n-1} supports. However, it is required to compute Δ_{i+1} and t to evaluate $\Delta_{i,t}$. Therefore, an iterative method is applied to calculate the longitudinal movements of the suspension clamps, $\Delta_{i,t}$. This iteration process is initiated by assuming $\Delta_{i,t}$ to be same as $\delta_{i,t}$. Other parameters are H_i, K_i, and k_i, representing horizontal tension, span stiffness, and suspension insulator stiffness, respectively.

2.4.4 Alawar et al. (2005) [8]

This paper presents a hybrid numerical method (HSM) to estimate the bilinear sag behavior of a bimetallic power conductor, e.g., an ACSR. The HSM is an enhanced and modified version of a numerical sag method (NSM) developed by Southwire [39]. The HSM is more accurate than the NSM, and it is as efficient as the graphical method developed by ALCOA using stress-strain curves.

Two parallel processes are deployed in the HSM to calculate the sag and tension of a bimetallic conductor, whereas in the NSM a single procedure is involved. In the HSM, one process, the evaluation of sag using the properties of the whole conductor, is analogous to the NSM. However, the other procedure in the HSM

is performed using only the core (e.g., steel) properties. The schematic diagram adopted from this method is depicted in Figure 5.5, chapter V. The authors compared the HSM with commercial sag computation software (SAG10) that produces nearly identical results.

2.4.5 Muhr et al. (2006) [9]

This paper demonstrated a sag calculation for two different overhead power transmission lines. The authors considered several influencing factors such as thermal overloading, environmental impact, aging, the deflection of tension insulators, and, most importantly, the mechanical elongation due to everyday stress. They depicted a relationship among conductor structure, load distribution, and mechanical elongation. This relationship shows that conductors with higher ratios of steel and aluminum components are less susceptible to irreversible and thermal elongation. They also proposed that the risk of flashover due to sag can be minimized by measuring the creeping, sag, and available ground clearance in certain intervals of time.

2.4.6 Massaro et al. (2008) [10]

The impact of plastic creep elongation at elevated temperature on the sags and tensions for a conventional conductor is described in this paper. Different creep estimator equations for different conductor types at different operating temperatures are also described. The following equations are adopted from [40] [41].
All Aluminum Conductor (AAC):

$$\text{Ambient Temperature: } \varepsilon_c = K \cdot \sigma^{1.3} \cdot t^{0.16}, \tag{2.26}$$

$$\text{High Temperature: } \varepsilon_c = M \cdot T^{1.4} \cdot \sigma^{1.3} \cdot t^{0.16}, \tag{2.27}$$

Steel Reinforced Conductors (ACSR):

$$\text{Ambient Temperature: } \varepsilon_c = 2.4 \cdot (\%RS)^{1.3} \cdot t^{0.16}, \tag{2.28}$$

$$\text{High Temperature: } \varepsilon_c = 0.24 \cdot (\%RS) \cdot T \cdot t^{0.16}, \tag{2.29}$$

where ε_c is the primary creep strain, σ is stress (tension/area), t is exposed time [hrs], T is conductor temperature [°C], K and M are constants, and $\%RS$ represents the tension as the percentage of rated tensile strength. The authors also provided some graphical views of the sensitivity study of sag with different operating hours at different temperatures.

2.5 Weather Research and Forecasting (WRF) model

The Weather Research and Forecasting (WRF) modeling system is a next-generation mesoscale forecast system that is capable of understanding and predicting mesoscale weather. The model is designed to work effectively in a massively parallel computing environment. The system permits two dynamical core solvers, including the nonhydrostatic mesoscale model (NMM) and the Advanced Research WRF (ARW) model. It is efficient for applications where broad spectrum data (meters to thousands of kilometers) need to be analyzed.

The WRF Software Framework (WSF) is designed to accommodate several dynamical solvers, programs for real data initialization, data assimilation systems, and standard physics interfaces that can plug physics packages into the solvers. Therefore, WRF is one of the most efficient systems in numerical weather prediction (NWP) model history [42].

NWP models usually deal with motions on a broad range of temporal and spatial scales. Therefore, full partial differential equations are solved at discrete locations using a finite difference approximate numerical approach. Parameterization is an approximation approach used in the NWP model to determine the value of

an unknown parameter from known terms. In the NWP model, parameterizations are used for physical characteristics such as radiation, boundary-layer, vegetation, and surface effects. Moreover, different numerical algorithms can be designed to approximate the solutions of partial differential equations. These are known as numerical parameterizations. The computer code involved in numerical parameterization is interpreted as a numerical model.

It is impossible, due to computational time constraints, to produce weather forecasts using NWP for every location in the atmosphere. Therefore, the model is applied in regularly spaced locations known as grid points. Each grid point contains a particular volume of air, called a grid volume. Each grid point consists of three different Cartesian directions: the values of X and Y describe surface position, whereas Z describes elevation. Each grid cell is extended with different variables, including specific humidity, potential temperature, cloudiness, liquid water content, etc. [43].

WRF, one of the most efficient NWP models, can play vital roles in the power sector. Meteorological parameters, such as wind speed and direction, ambient temperatures, precipitation rate, and solar radiation, can be obtained using the WRF model with high spatial and temporal resolution. Optimal line current in the dynamic thermal rating (DTR) system for a backbone power transmission network can be determined after analyzing these weather parameters. Other applications include an ice accretion forecasting system [44] developed using the WRF model that reduces the risk of power outage due to icing events. Forecasting of wind direction and wind speed using the WRF model for a particular geographical location can be used to predict the amount of power generation from a wind farm in different seasons.

Chapter 3

Thermal aging methodology

This chapter outlines an aging model encompassing several methodologies related to evaluation of loss of tensile strength and spatial analysis of thermal aging. Historical weather conditions along the selected transmission line were derived from historical datasets, and aging computations were made using IEEE Standard 738. A sensitivity study was performed to determine the dependency of output and input parameters of model. The confidence intervals for output parameters were identified. The results of several case studies are illustrated at the end of each section, showing the applicability of this model to the power transmission industry. Aging behavior and static thermal ratings in different seasons are analyzed in the final section of the chapter.

3.1 Evaluation of conductor loss of tensile strength[1]

Elevated operating temperatures impose significant thermal stress on, and possibly thermal damage to a conductor. Several consequences including annealing, creep, and reduction of tensile strength can occur if the overhead transmission conductor is operated beyond its maximum current-carrying capacity. These effects reduce the lifespan of the conductor. Specifically, annealing and other adverse effects prevail

[1] *A version of this section has been published. Md. M. I. Bhuiyan , P. Musilek, J. Heckenbergerova, D. Koval, 2010 Canadian Conference on Electrical and Computer Engineering, CCECE 2010, Calgary, AB, May 2-5.*

when the temperatures rises over 95 °C in aluminum based conductors [45] such as the aluminum conductor steel reinforced (ACSR), and the all aluminum conductor (AAC).

The percent loss of tensile strength of an aluminum strand, L_{Al}, can be evaluated as follows [3]:

$$L_{Al} = 100 - (-0.24T_c + 134) \cdot t^{-\frac{1.6}{0.63 \cdot d}(0.001 \cdot T_c - 0.095)}, \tag{3.1}$$

where t is the exposure time [hrs], d represents the strand diameter [mm], and T_c is conductor temperature [°C].

The loss of tensile strength for each value of discretized line temperature can be calculated using equation (3.1). The cumulative loss of strength over the simulation period can be determined by quantizing the actual conductor temperatures (above 95 °C) into ranges corresponding to the conductors temperature distributions, and by accumulating their contributions [2] to the loss of tensile strength. This computation is applicable only to the loss of strength of a single aluminum strand. The total loss of tensile strength in a compound conductor L_c can be evaluated using a method that considers its composition and material properties [46]. Particularly, this method takes into account the strand diameter r, the number of strands n, and the strand strength S of the individual components (e.g., aluminum, Al, and steel, St). The total strength of the conductor before S and after S' annealing can be calculated by applying equations (3.2) and (3.3), respectively:

$$S = \frac{\pi}{4}\left(r_{Al}^2 \cdot S_{Al} \cdot n_{Al} + r_{St}^2 \cdot S_{St} \cdot n_{St}\right), \tag{3.2}$$

$$S' = \frac{\pi}{4}\left[\left(1 - \frac{L_{Al}}{100}\right) \cdot r_{Al}^2 \cdot S_{Al} \cdot n_{Al} + r_{St}^2 \cdot S_{St} \cdot n_{St}\right]. \tag{3.3}$$

In the final step, the percent total loss of strength of the compound ACSR is determined as follows,

$$L_c = \left(\frac{S - S'}{S}\right) \cdot 100\%. \tag{3.4}$$

3.1.1 Calculation of line temperature time series

Line temperatures of a particular tower span are calculated over a specified period by implementing IEEE Standard 738-2006 [19] which takes parameters such as weather information, conductor characteristics, and geospatial data as inputs. In the next step, annealing line temperatures (above 95 °C) are filtered out from the whole line temperature distribution. Subsequently, the frequency histogram of the annealing temperature is produced to determine the ranges and occurrences of those temperatures. Finally, several annealing temperatures are quantized from the frequency histogram and the corresponding exposure durations are calculated from their frequencies according to the time resolution of weather data.

3.1.2 Proposed methodology

The proposed methodology for determining thermal aging phenomena of power transmission lines relies on the following information about the construction of lines, geographical locations, and their environment:

- physical characteristics such as type and size of the conductors;
- elevation and geospatial location;
- load data (current or historical dataset based on typical load profiles); and
- weather information that includes current and historical records of temperature, wind direction and speed, solar radiation, precipitation rate, etc.

The proposed methodology, illustrated in Figure 3.1, uses the following five steps for evaluating conductor thermal aging [47]:

I. Evaluation of a time series of conductor temperatures applying measured or assumed load current and interpolated weather information;
II. Determination of occurrence, severity, and exposure time of thermal overload

after analyzing the time series of temperatures (e.g., by constructing a frequency histogram);

III. Identification of a number of class intervals in the range of overload temperatures determined in step II, and construction of annealing curves for temperatures representing the indentified intervals;

IV. Determination of cumulative loss of tensile strength due to annealing by integrating contributions from all class intervals identified in step III, considering exposure time computed in step II;

V. Evaluation of combined loss of tensile strength considering dimension and configurations of conductor components.

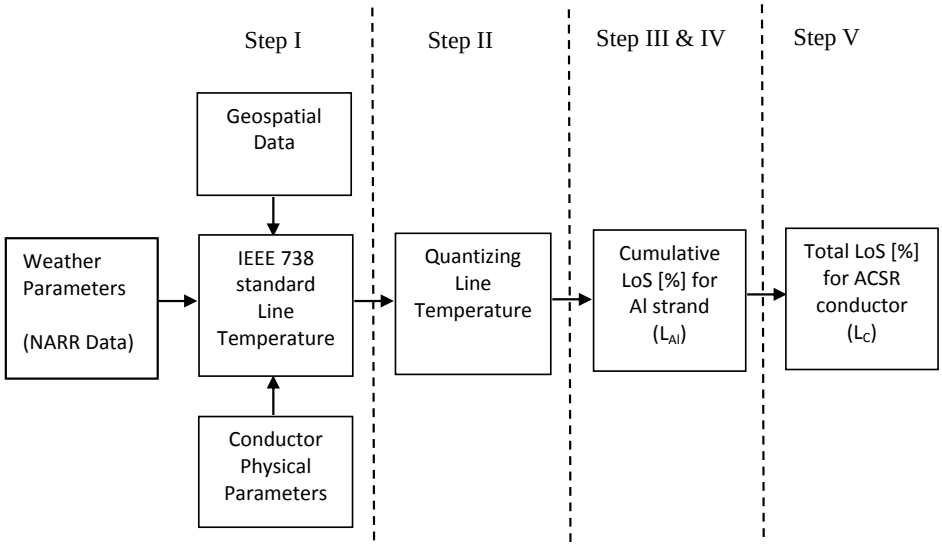

Figure 3.1: Schematic diagram of proposed methodology

3.1.3 Case study

An overhead backbone power transmission line was chosen in the Province of British Columbia, Canada, to exhibit the use of the proposed methodology. The south end of the transmission line is near Pavilion Clinton Road and it runs about 330 km north to Prince George. There are 867 transmission towers from the begin-

ning to the end of the line. A tower located at the southern part of the transmission line (latitude -121.7 °, longitude 51.0 °) was selected to illustrate this methodology. The ACSR Finch was assumed to be the conductor of the transmission line. Its aluminum strand diameter and nominal current are 3.65 mm and 1110 A, respectively [48].

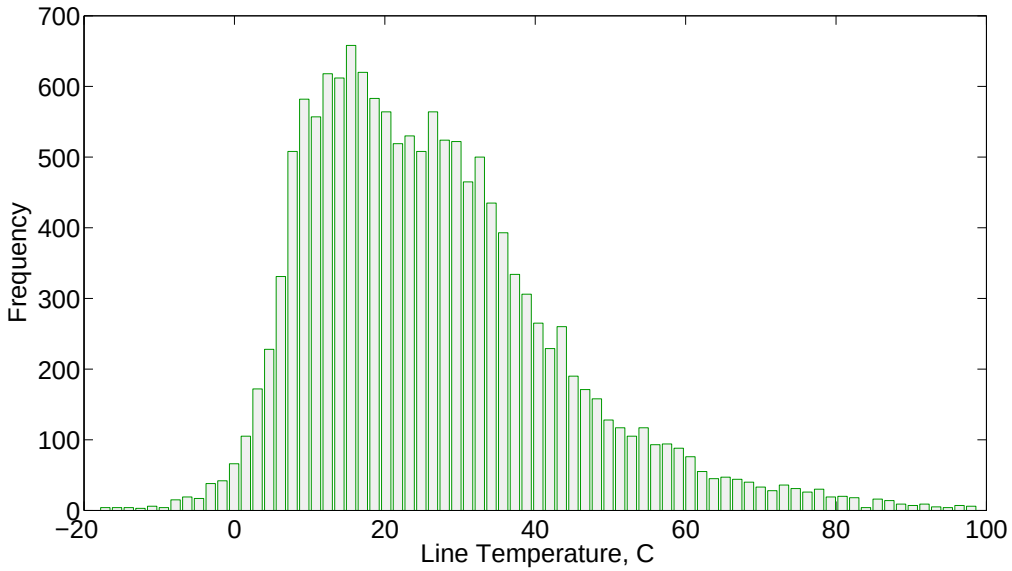

Figure 3.2: Temperature frequency histogram for nominal current over a five year period

Weather data including horizontal wind speed and direction, ambient temperature, atmospheric pressure, specific humidity, and short- and long-wave radiation, along the power transmission line has been derived from the North American Regional Reanalysis (NARR) historical dataset [49]. It spans a five year period from 01/2000 to 12/2004 with 3-hour time resolution. These meteorological variables are applied for computing the line temperature as explained in [32].

Various static load currents such as 1110 A (nominal), 1221 A (10% above nominal), 1332 A (20% above nominal), and 1443 A (30% above nominal) are considered in this case study. Though load currents are not static in a typical operating condition, the static load currents considered reflect the general aging character-

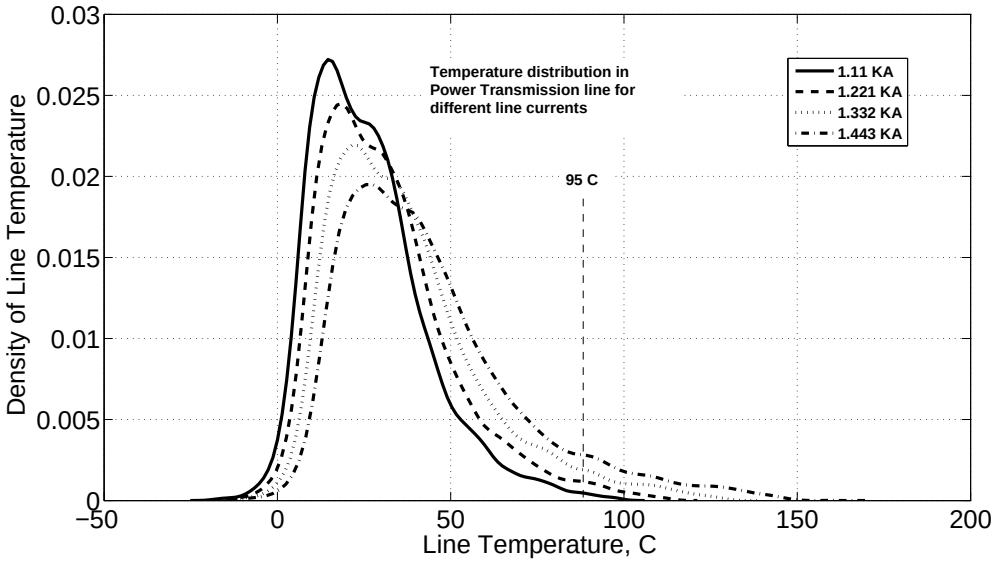

Figure 3.3: Temperature distribution of different load currents over a five year period

istics of transmission lines. Methodology described earlier was applied using the meteorological variables and the considered static load currents. A frequency histogram of conductor temperatures is depicted in Figure 3.2 for a period of five years and for the nominal current. Figure 3.3 shows the line temperatures for the nominal and higher load currents. It is observed that the temperature distribution profiles shift toward higher temperatures with increasing current. Temperature distributions in the form of frequency histograms have been used to determine the exposure duration for different annealing temperatures over five year period. Thermal overload temperatures (above 95 °C for aluminum) and their exposure times are summarized in Table 3.1, and depicted in Figures 3.4−3.7.

Table 3.1: Exposure time according to the frequency of conductor temperatures for three different currents over a five year period

1110 A		1221 A		1332 A		1443 A	
Temp [°C]	Time [hrs]	Temp [°C]	Time [hrs]	Temp [°C]	Time [hrs]	Temp [°C]	Time [hrs]
96.00	6	96	63	97	144	98	507
96.30	3	98	39	100	177	105	453
96.60	9	99	45	104	153	111	381
96.67	3	101	48	107	141	118	282
97.10	3	103	18	110	129	124	252
97.46	3	105	39	114	102	131	216
97.75	3	107	24	117	75	137	135
98.03	3	108	12	121	63	144	84
98.33	3	111	21	124	45	150	6
98.62	6	113	21	128	30	157	3

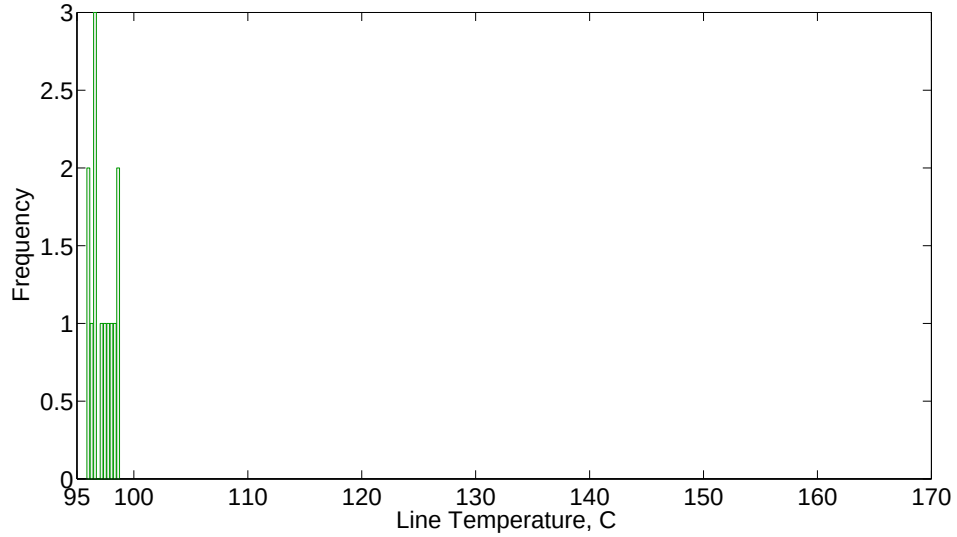

Figure 3.4: Histogram of temperatures above 95 °C for nominal current (1110 A)

The total loss of tensile strength in aluminum strands is illustrated with a graphical method [46] in Figures 3.8−3.11. The process is initiated by applying the exposure duration (6 hours) to the first annealing curve for a temperature of 96 °C (Figure 3.8). The equivalent exposure time at the following temperature (98 °C) can be determined by the horizontal projection on that annealing curve. The exposure time at 98 °C is then added to this equivalent time and the process is continued until all selected temperatures have been encountered. Finally, the percentage of total tensile

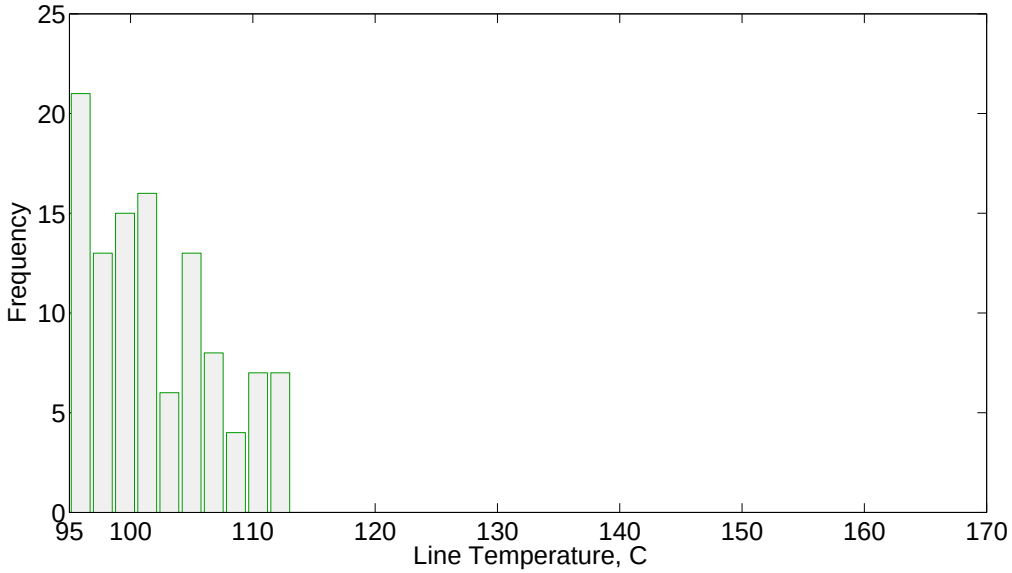

Figure 3.5: Histogram of temperatures above 95 °C for 1221 A

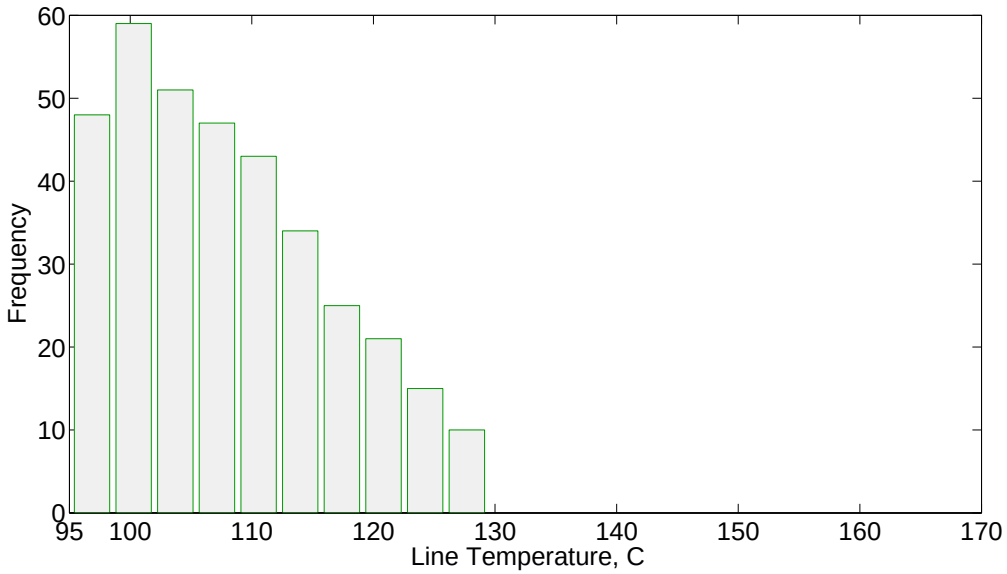

Figure 3.6: Histogram of temperatures above 95 °C for 1332 A

strength loss in the single strand corresponds to the projection of the final point on the vertical axis, equal to 0.703% for a load current of 1100 A. The same procedure is applied to the other three load currents, as depicted in Figures 3.9, 3.10, and 3.11. The overall loss of tensile strength is substantially reduced because of the steel core

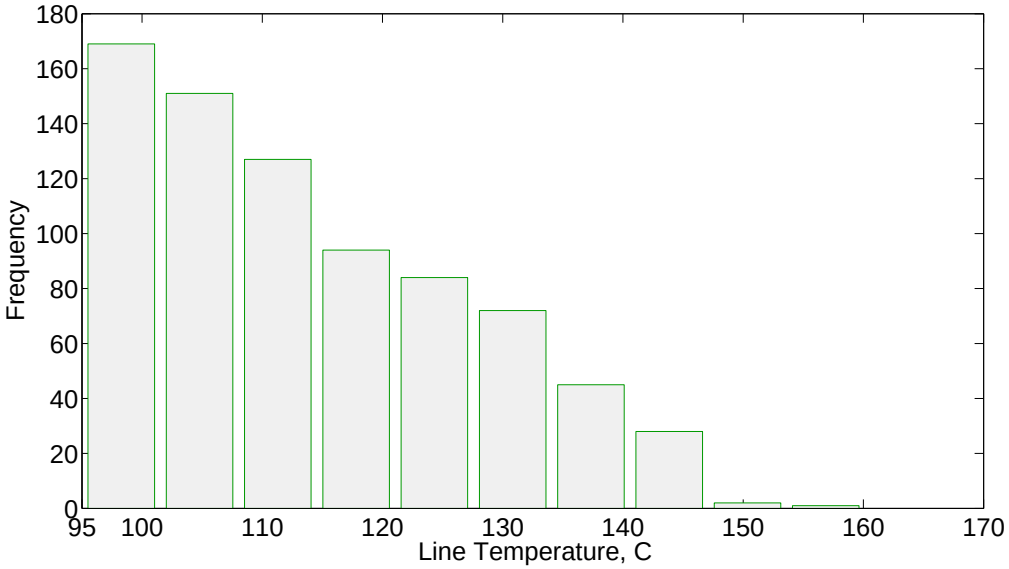

Figure 3.7: Histogram of temperatures above 95 °C for 1443 A

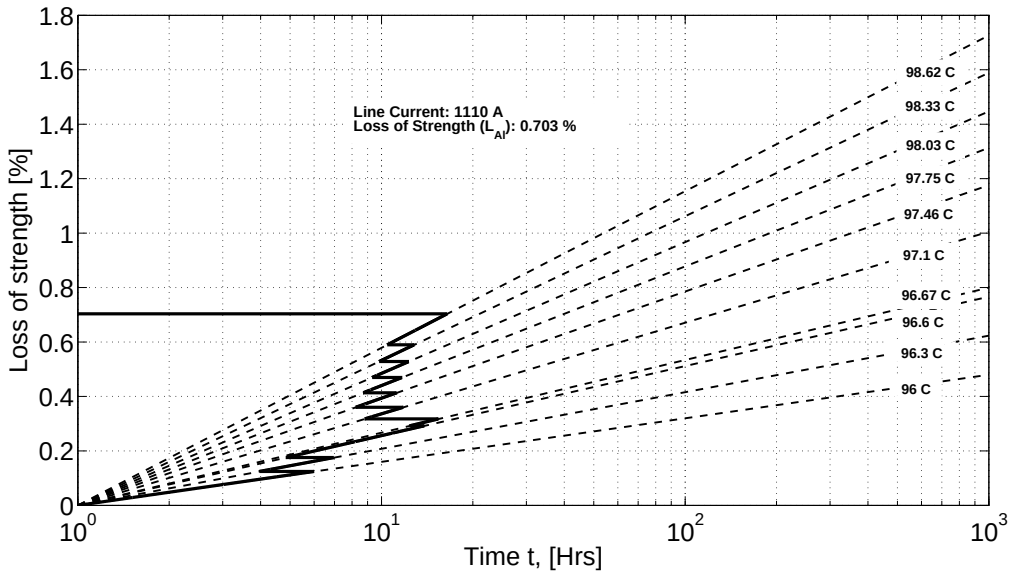

Figure 3.8: Graphical determination of loss of tensile strength for nominal current over five year period

in ACSR Finch. The loss of strength of the compound ACSR and the individual aluminum strands computed at each load current are listed in Table 3.2.

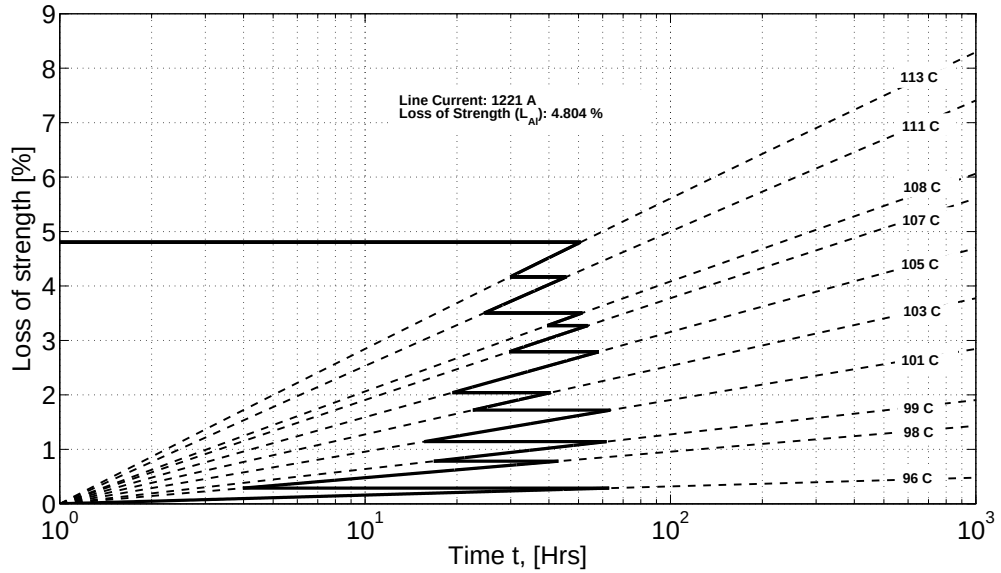

Figure 3.9: Graphical determination of loss of tensile strength for 1221 A over five year period

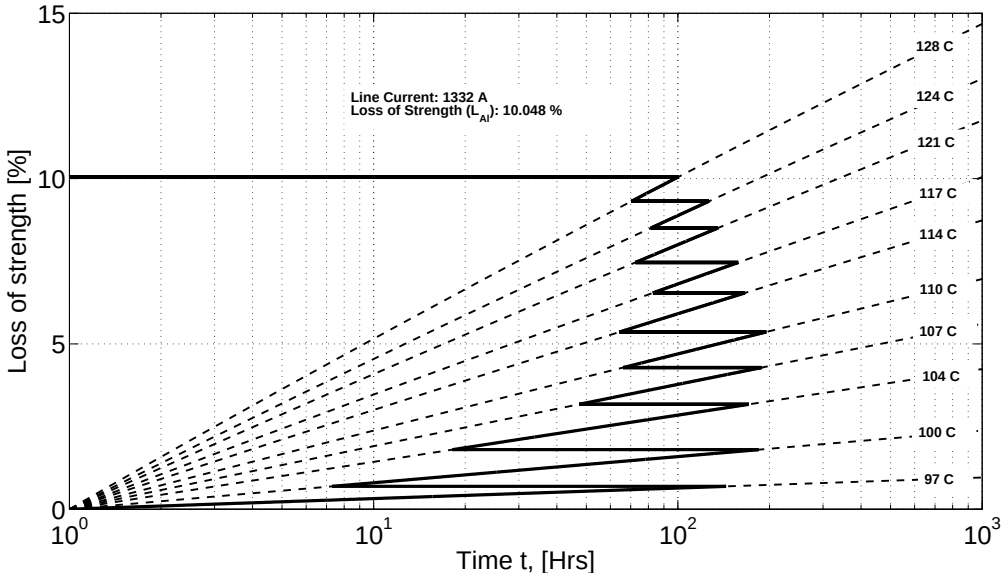

Figure 3.10: Graphical determination of loss of tensile strength for 1332 A over five year period

3.2 Spatial analysis of thermal aging[2]

This section introduces a new methodology for spatial analysis of thermal aging. It can be performed at three different levels: point, line, and area. Thermal aging

[2] *A version of this section has been submitted for publication. P. Musilek, J. Heckenbergerova, Md. M. I. Bhuiyan, IEEE Transaction Power Delivery.*

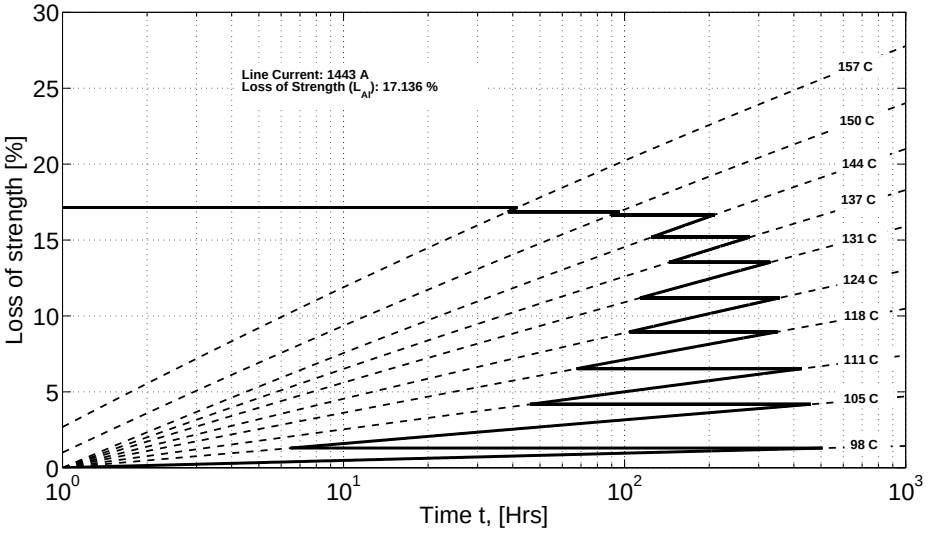

Figure 3.11: Graphical determination of loss of tensile strength for 1443 A over five year period

Table 3.2: Loss of tensile strength in aluminum strands and compound conductor (ACSR "Finch") over a five year period

Current [A]	Loss of tensile strength	
	Aluminum strand	ACSR conductor
1110	0.703 (%)	0.388 (%)
1221	4.804 (%)	2.652 (%)
1332	10.048(%)	5.546 (%)
1443	17.136(%)	9.459 (%)

at a single point (tower) on a transmission line is investigated by applying a point analysis at a known hot spot, or in an area identified as susceptible to thermal deterioration during line inspection [14]. Using a line analysis, the point analysis can be extended to every single point along a transmission corridor, or within a transmission system. Locations of the critical points can be identified either from the locations of towers supporting the conductors, or by using a regular grid. The locations also depend on the desired resolution of the analysis. Line analysis is useful in determining the spatial distribution of aging effects and for identifying critical aging segments and hot spots on a transmission line [50]. Area analysis takes into account a geographic area to evaluate the potential aging of a conductor operating

with a certain load current, assuming it is located at each point on a grid established over that area. Area analysis is particularly useful for planning new transmission corridor, to ensure the maximum lifespan of installed transmission assets in the selected route. An appropriate optimization technique needs to be implemented for planning transmission systems using this approach.

These analyses of spatial thermal aging depend on parameters related to conductor, environment, ambient weather, and load current. Conductor parameters include the conductor type and construction, the absorptivity and emissivity of its surface, and its temperature-resistance coefficient. Environment parameters take into account the route of the transmission line in terms of latitude and longitude, elevation above the sea level, and its height above the ground. Weather parameters are ambient temperature, wind velocity, and incoming and reflected solar radiation. This information can be obtained using a suitable NWP model, or by applying bilinear or bicubic interpolation [51] of the historical reanalysis data to the point(s) of interest. Load current parameters are usually chosen from the historical records of transmitted load current over the period of interest. However, a known mean load and assumed (weekly) load profiles can be used in the absence of historical records.

3.2.1 Implementation of proposed methodologies

Proposed methodologies using probabilistic and statistical approaches are demonstrated in this section. They are applied to the line temperature data over a specified period. Statistical analyses, which include average and sample standard deviation or variance, and standardization, are implemented in the line analysis method using spatial aging series. The standard deviation and standardization of a sample dataset can be computed using equations (3.5) and (3.6). The standard deviation shows how the data are dispersed from the average value, while the normalization or standardization interprets the number of standard deviations an observation is above or

below the average; both are dimensionless quantities. Standardization provides an unbiased data series where the average is zero and the variance equals unity.

Standard deviation:

$$\sigma = \sqrt{\frac{1}{N}\sum_{i=1}^{N}(x_i - \mu)^2}, \tag{3.5}$$

Standardization:

$$L_c^{std} = \frac{L_c - \mu}{\sigma}. \tag{3.6}$$

3.2.1.1 Point analysis

The process of computing the loss of strength in a single transmission tower, described in section 3.1.2, is known as the point analysis method. It involves the following five steps:

I. Determination of the time series of line temperatures using measured or assumed load data and weather data hindcast using a NWP model, or interpolated from gridded historical weather datasets;

II. Analysis of the time series to calculate the frequency and exposure time of thermal overload; threshold values of line temperatures must be determined for the thermal overload conditions, depending on the type and material of the conductor;

III. Selection of a number of class intervals above the threshold temperature found in step II, and determination of annealing magnitudes for temperatures $T_c$representing the selected intervals;

IV. Determination of the cumulative loss of tensile strength due to annealing by combining the contributions from all class intervals computed in step III, taking into account exposure times from step II;

V. Determination of the total loss of tensile strength L_c for a compound conductor, considering the dimensions and configuration of its components.

3.2.1.2 Line analysis

The line analysis methodology for conductor aging consists of the following five steps and operates based on data collected from the point analysis method:

I. Determination of the spatial series $\{L_c\}$ of conductor aging along the transmission line corridor or network of interest;

II. Calculation of sample statistics such as mean μ and standard deviation σ of the aging series $\{L_c\}$;

III. Determination of standardized aging series $\{L_c^{std}\}$, where mean $\mu(L_c^{std}) = 0$, and its variance is equal to unity, $\mathrm{Var}(L_c^{std}) = 1$;

IV. Determination of critical segments along the transmission line whose standardized loss of strength is greater than or equal to the standard deviation $\{L_c^{std}\}$ i.e.,

$$L_c^{std} \geq 1. \tag{3.7}$$

V. Identification of a hot spot for each critical aging segment by applying the global maxima approach.

3.2.1.3 Area analysis

Area analysis is essentially considered for the planning of a new power transmission line. It takes into account a geographic location to evaluate potential aging of a particular conductor operating at a certain load, as though it were located at each point on the area of interest. The following steps, adopted from [52], are essential to determine the optimal routing of the transmission line:

I. In accordance with the previous aging analyses, historical weather information that covers the entire area of interest is extracted. After processing the weather data, the required meteorological parameters necessary to solve the heat balance equation are determined.

II. Four possible line segment orientations to neighboring nodes are determined to reduce the computational complexity.

III. Thermal aging is computed for each segment of transmission line in the area of interest assuming a particular ACSR. In order to compute the thermal aging of each line segment, the line temperatures and their corresponding frequencies are computed using the point analysis method to evaluate thermal aging. These aging values represent the weight of each segment into a graph structure where all the possible directed paths are considered as line routes.

IV. Eventually, to distinguish the best possible line route from the weighted graph, a shortest path graph search algorithm (e.g., Floyd-Warshall) [53] is used. The chosen line route should have the lowest thermal aging, maximizing the lifespan of the transmission assets.

3.2.2 Identification of critical aging segments and hot spots

Critical aging segments and hot spots can be identified by implementing the line analysis method described in the introduction to section 3.2. However, an additional constraint was imposed to avoid a high frequency of short critical segments; that is, the minimal distance between two segments is 5 towers. The first step of line analysis is to determine thermal aging at each point using point analysis method. Let us consider, for example, the following spatial series consists of 10 values of the total loss of tensile strength at contiguous points along a transmission line:

$$L_c = \{\ 0.8,\ 1.2,\ 1.6,\ 1.4,\ 0.5,\ 0.5,\ 0.7,\ 0.8,\ 1.7,\ 1.6\ \}.$$

In the next step, the sample mean, μ= 1.08, and standard deviation, σ = 0.4732, of this series are computed. The standardized spatial series is calculated in step III as:

$$L_c^{std} = \{\ -0.59,\ 0.253,\ 1.09,\ 0.67,\ -1.22,\ -1.22,\ -0.803,\ -0.59,\ 1.31,\ 1.098\ \},$$

using equation (3.6). The critical aging segments are identified as the sets of contiguous tower locations with standardized aging greater than or equal to the standard deviation of $\{L_c^{std}\}$. In this example, there are two critical segments corresponding to 3rd and $9-10$th tower locations with total aging $\{1.09\}$ and $\{1.31,\ 1.098\}$, respectively. The hot spots are identified using the local maxima of each segment as mentioned in step V. Therefore, the hot spots are located at the 3rd and 9th positions and the corresponding aging values are 1.6 and 1.7, respectively.

The critical aging segments and hot spots determined by applying this methodology identify the tower locations along the transmission corridor as having elevated aging. However, to investigate whether the conductor at these locations exceeds the level of aging that imposes a reliability risk, the absolute values of aging have to be compared with the permissible maximum aging.

3.2.3 Sensitivity study of spatial aging with variable loads[3]

Sensitivity analysis investigates how the output from a model deviates when the input parameters of the model are varied, and thus it examines the consistency and robustness of the model [54]. Sensitivity analysis aims to determine the confidence intervals for model outputs. In this sensitivity study of the aging model, the effects of different current loads were examined in the sample transmission line. Specifically, the identified critical aging segments (CAS) and hotspots of the transmission line were meticulously analyzed. The results of the sensitivity study are described in the last part of the case study section.

[3] *A version of this section with case study has been published. Jana Heckenbergerova, Md. Mafijul Islam Bhuiyan and Petr Musilek, 12th International Scientific Conference on Electrical Power Engineering (EPE), 2011.*

3.2.4 Case study

To illustrate the different spatial analyses described earlier on a real power transmission system, a sample transmission line 5L011 was selected. The southern part of the test line starts near Kelly Lake, and continues 330 km north to Williston near Prince George. The compound ACSR Finch (outside diameter of 32.84 mm, and nominal current of 1100 A [48]) test line is supported by more than 865 transmission towers. The towers are numbered sequentially starting with 1 from the southern end of the transmission line for the convenience of the study. The nonuniformity of the orography and landscape of the studied area is depicted in the elevation profile of the transmission corridor in Figure 3.12.

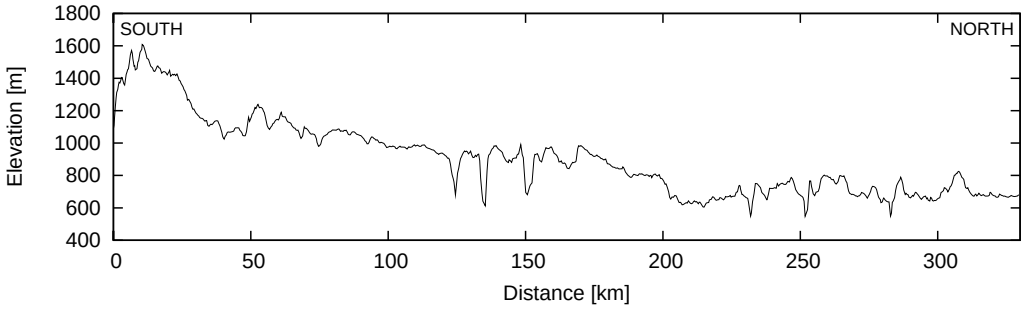

Figure 3.12: Elevation profile of line 5L011

Weather data along the power transmission line was extracted from the North American Regional Reanalysis (NARR) historical dataset [49]. NARR datasets have a 3-hour time resolution on a regular horizontal grid of 32 $\times$ 32 km and 45 vertical levels. A bilinear interpolation method was applied to attain 1-hour time resolution data from the time period of 01/2005 to 12/2009. Meteorological variables derived from the data were used to calculate the conductor temperature. They include horizontal wind speed and direction, temperature, atmospheric pressure, specific humidity, and short and long-wave radiation [19]. Ambient temperature and wind speed and direction had the most significant impact on line temperature.

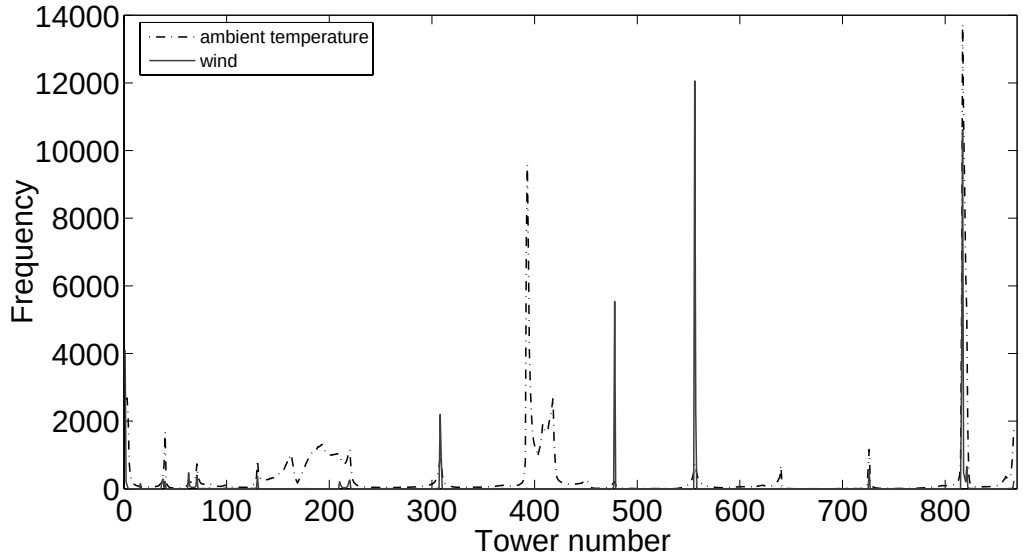

Figure 3.13: Frequency histogram of the location of maximum wind speed and ambient temperature [2005-2009]

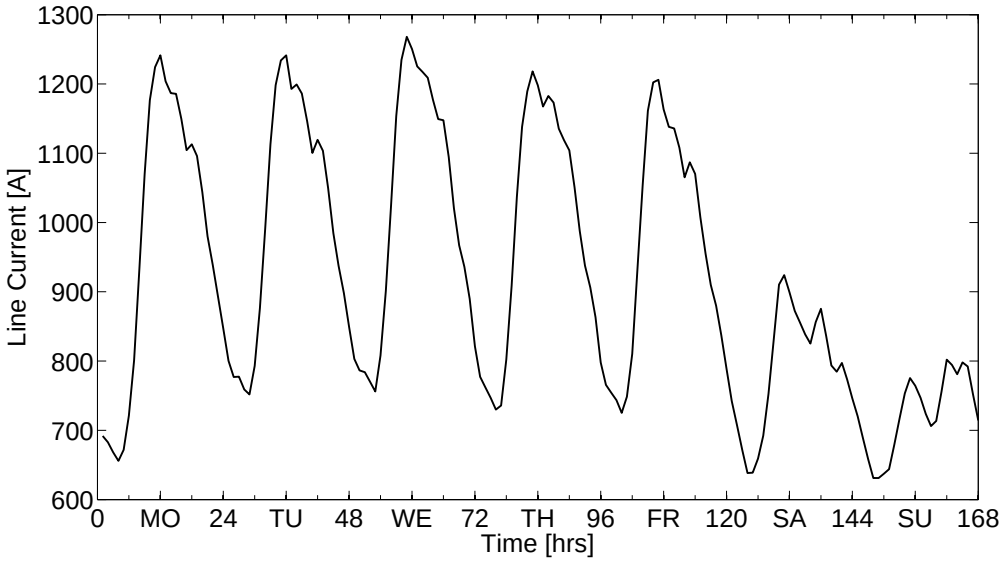

Figure 3.14: Assumed weekly load profile of line 5L011 with mean equals to 75% of nominal current

The frequency histogram of the location of the maximum wind speed and ambient temperature over the five year period is depicted in Figure 3.13. Statistical analyses of the weather parameters along the transmission line were performed and the results are presented in Table 3.3.

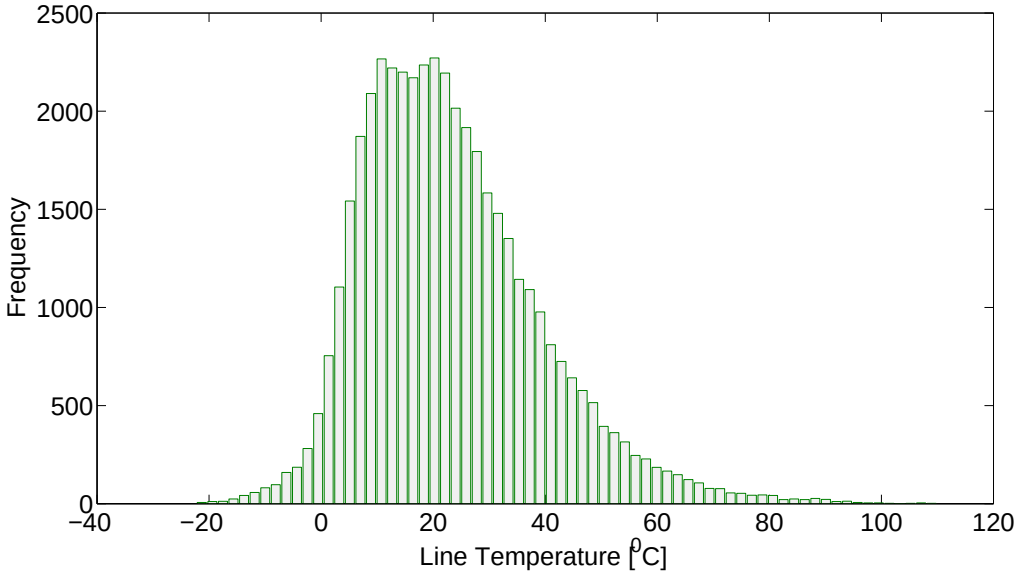

Figure 3.15: Temperature frequency histogram of tower 14 over five year period

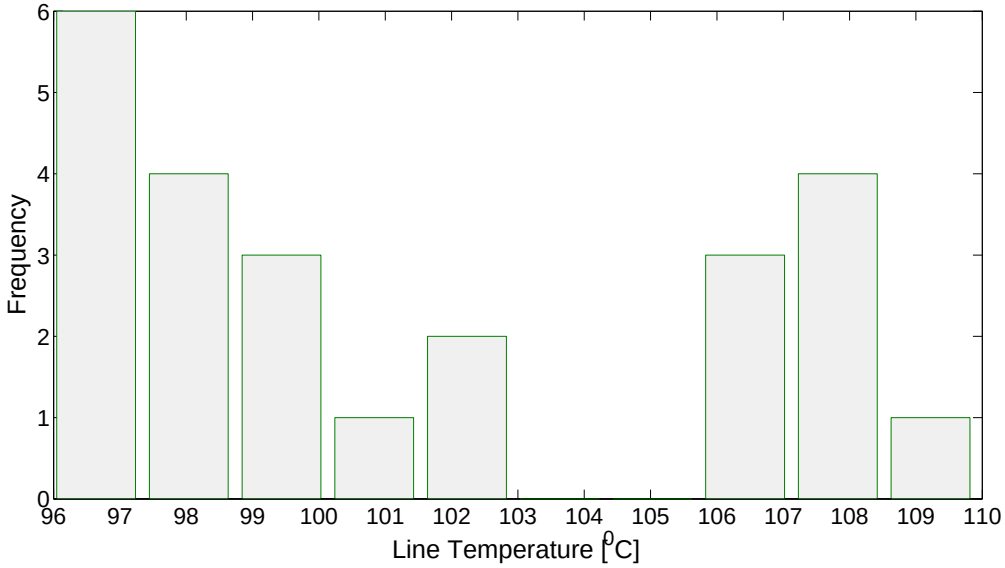

Figure 3.16: Frequency histogram of overload temperature of tower 14 over five year period

This case study takes into account a variable current load determined using a normalized weekly load profile [55] where the mean current equals 75% of the conductors nominal ampacity, i.e. 825A. The assumed load profile, used to simulate

Table 3.3: Basic statistical characteristics of weather parameters

	T_a [C]	V_m [m/s]
Mean	4.35	4.64
Standard deviation	9.4	2.33
90%-confidence interval	$\langle -11.05\ ;\ 19.00 \rangle$	$\langle 1.35\ ;\ 8.95 \rangle$
Range	$\langle -34.49\ ;\ 30.26 \rangle$	$\langle 0\ ;\ 19.79 \rangle$

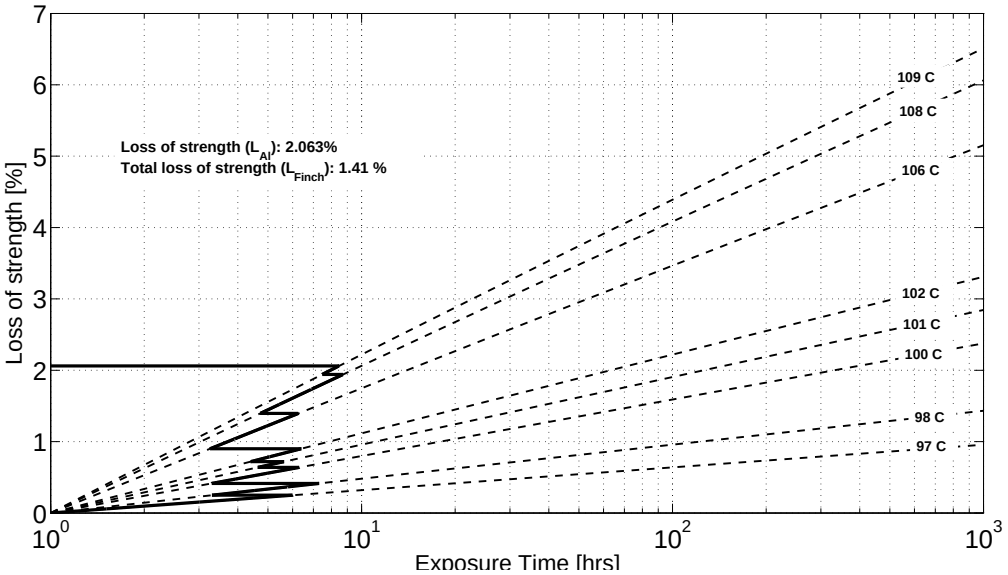

Figure 3.17: Graphical determination of loss of tensile strength for tower 14 over five year period (variable load)

the real operation of a transmission system, is shown in Figure 3.14. Using the point analysis methodology explained in section 3.2.1.1, conductor aging was estimated for each tower location. Results of this analysis for tower 14, located near the south end of the line (latitude 121.7750 °W, longitude 51.0396 °N), illustrate the applied methodology. Frequency histograms of overall conductor operating temperatures over the five year period and the temperatures above 95 °C are illustrated in Figures 3.15 and 3.16 respectively. A graphical method for the calculation of total loss of strength of an aluminum strand is depicted in Figure 3.17 using the exposed times for different annealing temperatures. Because they have a steel core, ACSRs exhibit very low loss of tensile strength. Over the five-year period, the loss of tensile strength of each aluminum strand is $L_{Al} = 2.063\%$, and the total loss of strength of

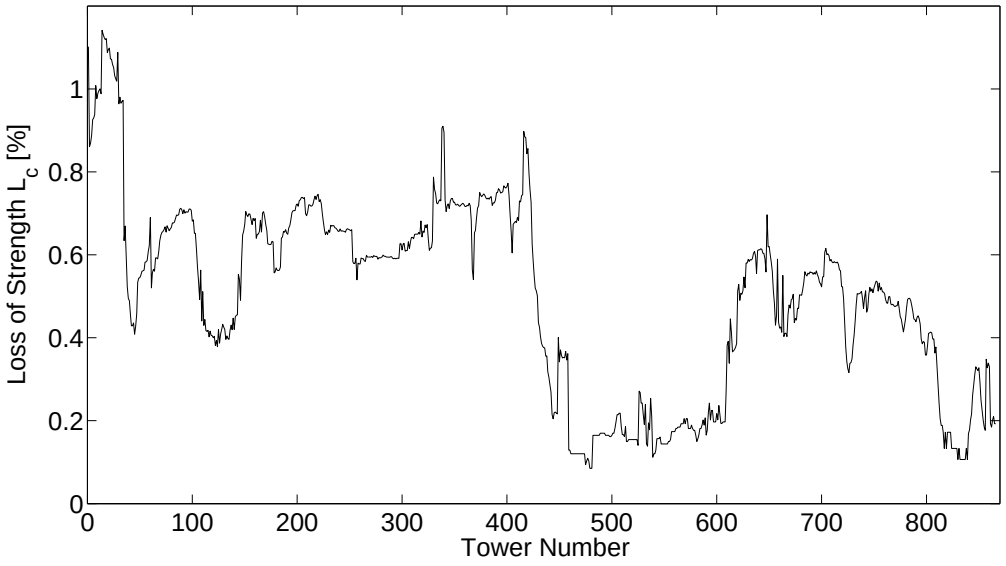

Figure 3.18: Spatial distribution of conductor aging over the five year period (variable load)

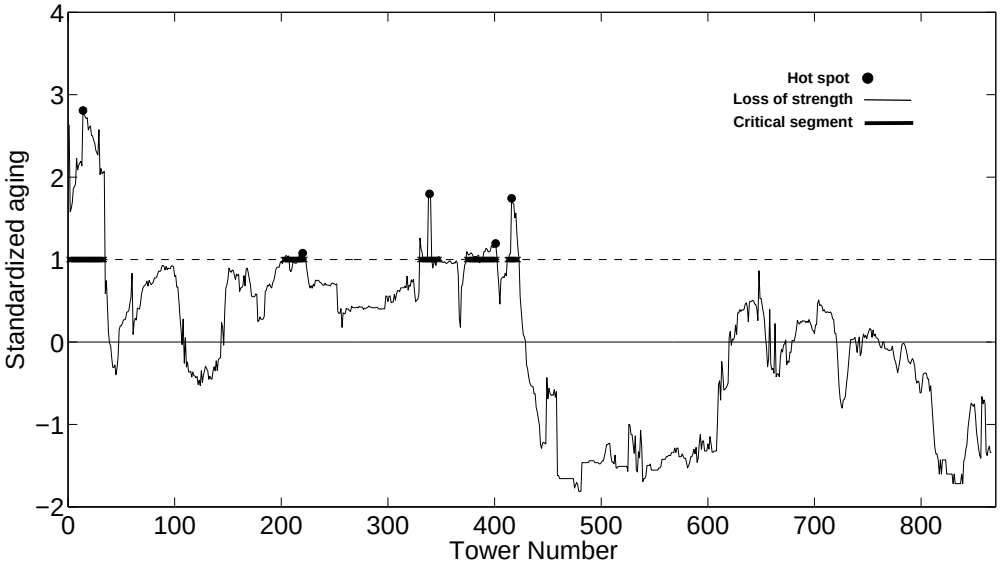

Figure 3.19: Standardized aging series $\{L_c\}$ with critical segments and hot spots (variable load)

the composite ACSR is $L_c = 1.141\%$.

Tower locations of critical aging segments and hot spots are identified using the spatial aging series along the transmission line according to methodology described

Table 3.4: Statistical parameters of spatial aging series $\{L_c\}$

Mean	$\mu = 0.49$
Variance	$\sigma^2 = 0.05$
Standard deviation	$\sigma = 0.23$

Table 3.5: Locations of critical aging segments, hotspots, and percentage loss of tensile strength for variable load current

Critical segment	Hot spot	L_c [%]
$\langle 1 \,;\, 34 \rangle$	14	1.141
$\langle 202 \,;\, 222 \rangle$	220	0.746
$\langle 330 \,;\, 348 \rangle$	339	0.910
$\langle 374 \,;\, 402 \rangle$	401	0.772
$\langle 412 \,;\, 422 \rangle$	416	0.898

in section 3.2.1.2. The second step begins with the concatenation of the spatial series of conductor thermal aging along the line $\{L_c\}$ shown in Figure 3.18. Then, a statistical analysis of aging series is performed and the sample mean and standard deviation are calculated and summarized in Table 3.4. The standardization of the spatial aging series is computed in the next step using equation (3.6). The contiguous sets of towers, whose standardized aging $\{L_c^{std}\}$ are greater than or equal to unity, are regarded as critical aging segments of the transmission line. Five different critical aging segments were identified in this case study while considering the variable current load from Figure 3.14; the first segment was between towers 1 and 34 near the south end of the line, the second, third, and fourth segments consisted of towers $202-222$, $330-348$, and $374-402$, respectively. The last segment was in the middle of the line between towers 412 and 422. Eventually, the locations of the global maxima of each critical aging segment were identified as hot spots in the transmission line, i.e. tower 14 (L_c=1.141%), 220 (0.746%), 339 (0.910%), 401 (0.772%), and tower 416 (0.989%). The standardized spatial aging series $\{L_c^{std}\}$ with critical aging segments and hot spots are depicted in Figure 3.19; the locations and corresponding values of the thermal aging of critical segments and hot spots are summarized in Table 3.5.

3.2.4.1 Sensitivity study

The load current, assumed for this sensitivity analysis varies from 75% to 125% of the conductor nominal ampacity, 1100 A, with an interval of 25 A. As a result, 23 different values of constant current loads were chosen from the interval $\langle 825A, 1375A \rangle$. The conductor is assumed to be 5 years old, therefore, the emissivity and solar absorption coefficients are equal to 0.76 and 0.95, respectively. The methodology for thermal aging evaluation explained in section 3.2 was used to evaluate critical aging segments (CAS) and hotspots for each constant load; the results are depicted in Figure 3.20. One can see that examined transmission line includes three main critical aging segments and their locations are consistent. The range and importance of thermal aging was determined by performing a statistical analysis of the total loss of tensile strength in the conductor. The result, illustrated in Figure 3.21, shows the exponential dependency of the degree of conductor aging on the current load. In the last stage of the sensitivity analysis the confidence intervals of CAS locations were determined. The most frequent critical aging segment is located between towers 208 and 215, with a probability of 0.95. Other significant critical segments are identified between towers 5 and 15, 142 and 154, and 164 and 252, with probabilities of 0.75. This outcome supports the independence of CAS locations on current throughput.

The sensitivity study results show that the total loss of strength of the conductor depends on the line current load and the locations of critical aging segments are insensitive to the line current.

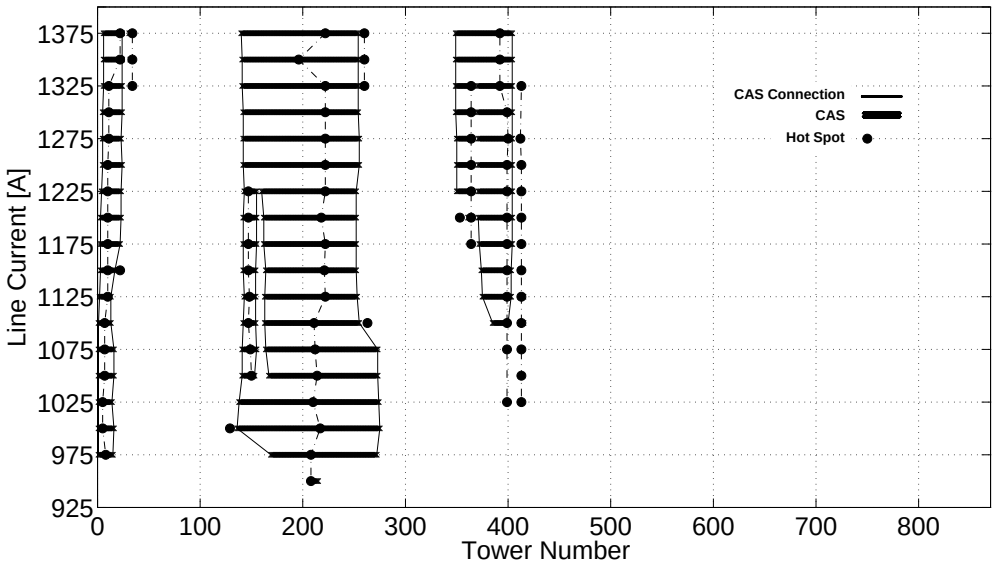

Figure 3.20: Spatial distribution of critical aging segments and hotspots for different load currents

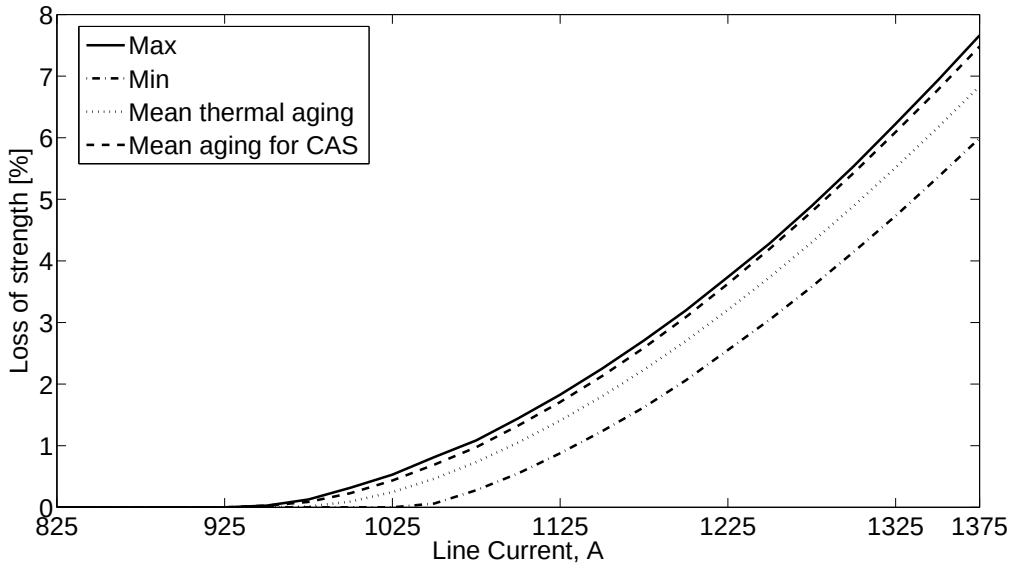

Figure 3.21: Ranges and means of thermal aging for different line current loads

3.3 Seasonal distribution of thermal aging [4]

This section analyses the seasonal distribution of conductor thermal aging using known characteristics of the transmission conductor, load information, and weather data. The dependency of conductor ampacity on different seasons is examined by analyzing the frequency histograms of line current-carrying capacities. Spatial distributions along the line of aging in different seasons are discussed and compared. This information is very important for transmission network operating procedures such as scheduling of line inspections and reconductoring, and for effective transmission asset management.

3.3.1 Seasonal dependency of conductor ampacity

The thermal overload of a transmission line depends mainly on the transmission capacity of the conductor. Ampacity is the maximum current a conductor may carry without exceeding a specified thermal limit; e.g., a typical maximum temperature for an ACSR conductor T_c = 95 °C. According to [19], weather phenomena in the transmission line region−particularly wind speed, wind direction, ambient temperature, and solar radiation−have significant impact on line ampacity. The seasonal variation in these meteorological parameters affects the line temperature as well as the thermal ampacity of the transmission line. The cold temperatures and common wind and precipitation events in winter increase the ampacity of the conductor, while the warmer temperatures in summer decrease the ampacity.

[4] *A version of this section has been published. Jana Heckenbergerova, Petr Musilek, M M I Bhuiyan and Don Koval, IEEE Conference on Innovative Technologies for an Efficient and Reliable Electricity Supply, Waltham, Massachusetts, USA, 2010, ISSN: 0278-0097, Vol:29, Issue:1, doi: 10.1109/MTS.2010.936470.*

3.3.2 Thermal aging behavior during different seasons

Variable weather conditions have a significant impact on conductor thermal aging. Thermal aging is expected to be higher during summer when higher temperatures warm the line and lower in the winter when frequent cool winds and precipitation cool the line. The locations of critical segments and hot spots in the line are unpredictable, as weather phenomena strike at variable points in different seasons. The seasonal effects on thermal aging are explained through the following case study.

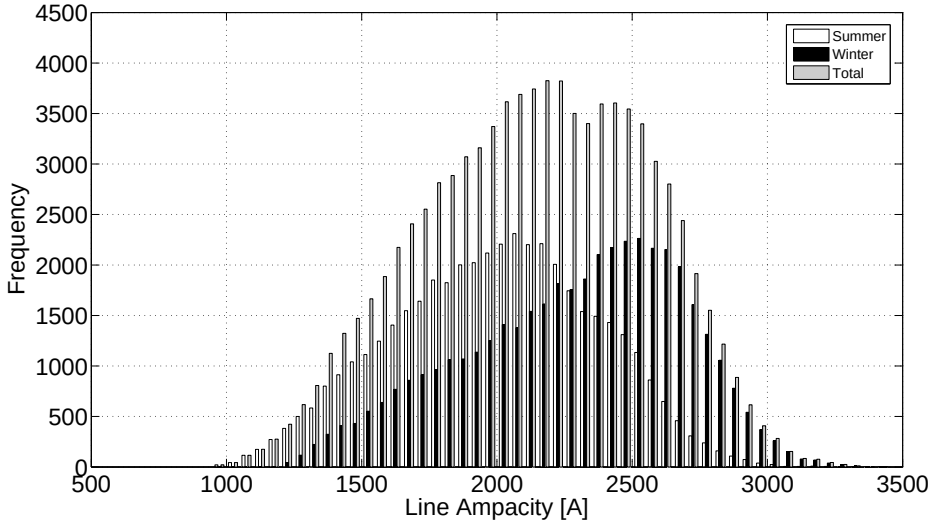

Figure 3.22: Frequency histogram of ampacities in hot spot over the ten year period

3.3.3 Case study

In order to show the seasonal effects on thermal aging and ampacity, weather information along the power transmission line (5L011) for a period of 10 years, from January 2000 to December 2009, was extracted. The conductor ACSR Finch has a nominal current load of 1100 A, an emissivity ε of 0.82, and a solar absorption coefficient α of 0.99. By implementing the line analysis method, the hot spot with the highest thermal aging was determined at tower 36, while tower 862 was defined as the spot with lowest thermal aging or cold spot. Ampacity distributions at these

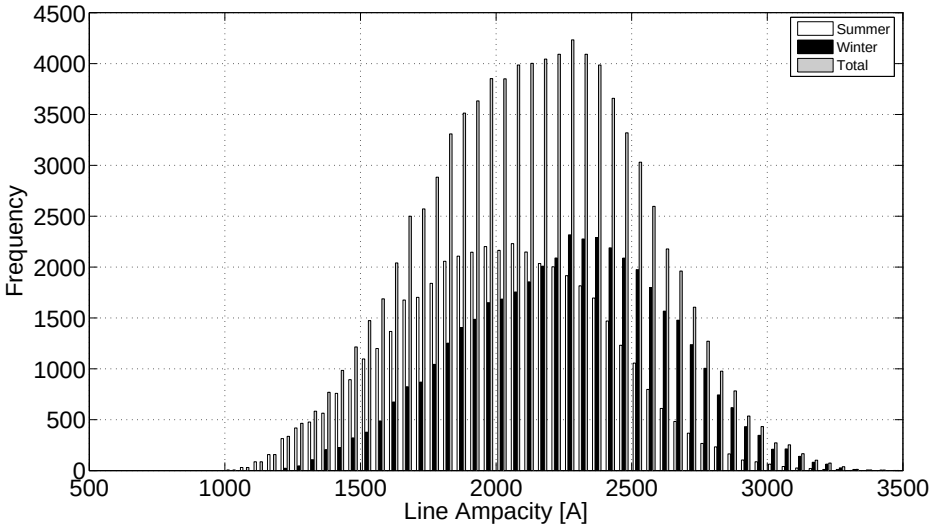

Figure 3.23: Frequency histogram of ampacities in cold spot over the ten year period

two locations were compared during winter (Nov−Apr) and summer (May−Oct) to evaluate the ampacity difference between the hot spot and the cold spot. The comparisons are depicted in Figures 3.22 and 3.23 using frequency histograms. These figures show that the expected difference between winter and summer ampacities is obvious in the case of hot spot (the difference between modes is 500 A), whereas it is much more delicate at the cold spot. Figure 3.24 illustrates the difference of ampacities at these two locations. It depicts that in winter hotspot has higher ampacity than coldspot and during summer coldspot has more available ampacity than hotspot, which significantly affect thermal aging of conductor.

To explore the seasonal dependency of conductor ampacity more precisely, four seasonal groups (winter: Dec, Jan, Feb; spring: Mar, Apr, May; summer: Jun, Jul, Aug; and fall: Sep, Oct, Nov) were constituted by splitting meteorological data. Figure 3.25 shows the probability density functions (pdfs) of conductor ampacity distribution at a hot spot tower corresponding to four different seasons. The domain of line ampacity for summer is the smallest whereas the total ampacity pdf has the

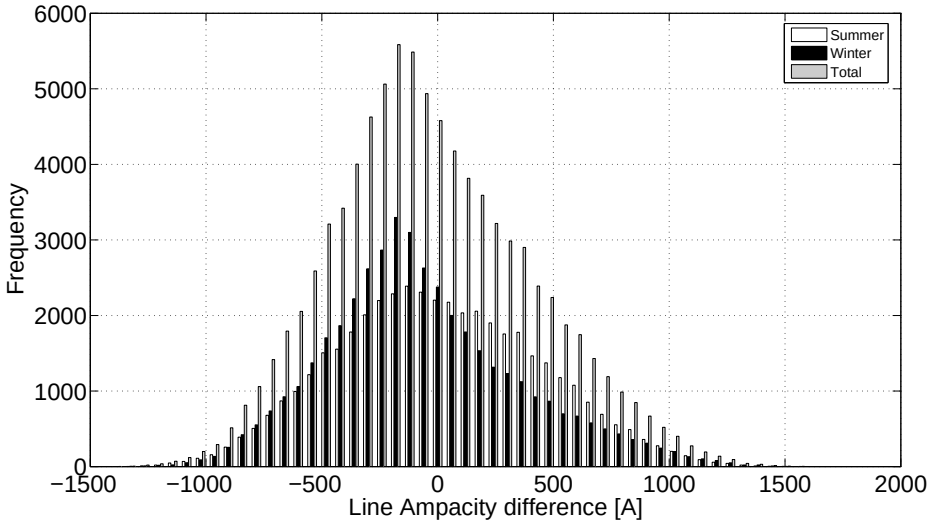

Figure 3.24: Frequency histogram of ampacity differences in cold spot and hot spot

largest domain of definition. Moreover, the summer pdf is shifted toward small values of ampacity, while the other pdfs are shifted to the right and therefore permit the line to transmit higher loads. According to summer pdfs, the temperature of the power transmission line should be higher during this season, producing a significant adverse effect on conductor thermal aging. During winter, lower temperatures permit more power to be transmitted through the conductor without imposing a risk of thermal aging.

To understand the dependency of thermal aging on the seasonal effect, an extension of conductor thermal aging was evaluated for each season according to methodology described in section 3.2. Figure 3.26 depicts the spatial thermal aging series for four different seasons and for the whole 10 years of simulation. Conductor temperatures are always below the thermal overload threshold (95 °C) during winter, hence, no aging occurs along the sample transmission line. The highest thermal aging is observed during the summer season, while spring and fall have a small aging effect on the conductor.

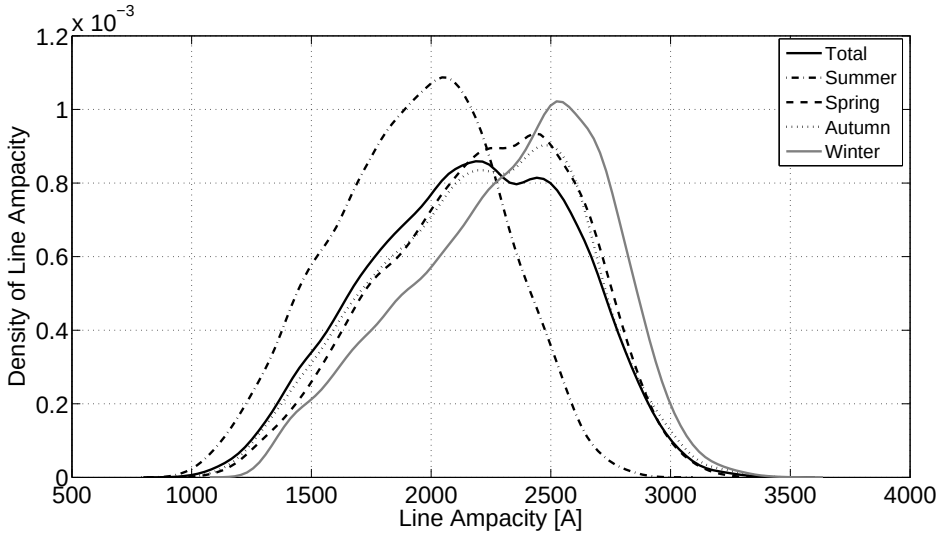

Figure 3.25: Seasonal probability density functions of conductor ampacity

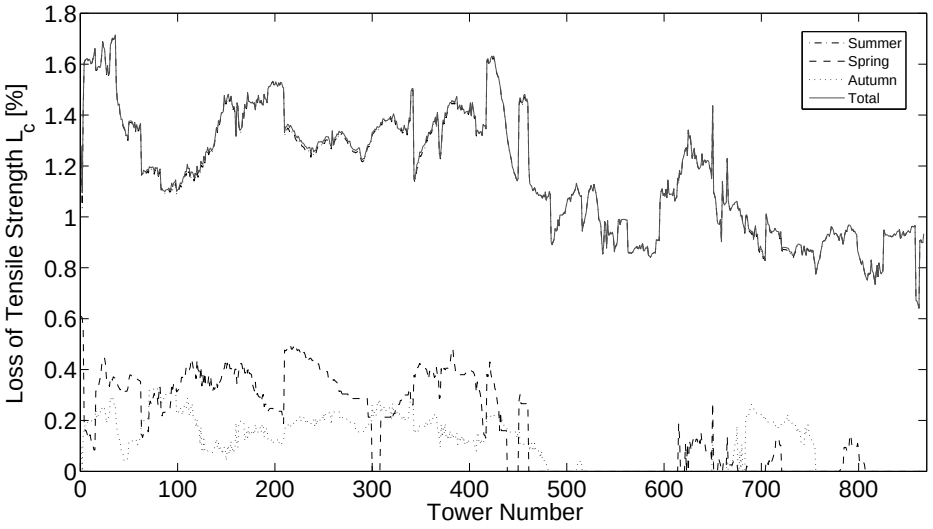

Figure 3.26: Spatial thermal aging for different seasons

The seasonal aging series was standardized using equation (3.6) and the results of statistical analyses are summarized in Table 3.6. Standardized thermal aging for different seasons and corresponding critical segments and hot spots are illustrated in Figures 3.27−3.29. Thermal aging during the summer and the total amount of aging are almost identical and their corresponding critical aging segments with hot spots are located at the same positions. Very low standard deviations are observed

Table 3.6: Statistical parameters (mean and standard deviation) of seasonal aging series

Aging	μ	σ
Total	1.178	0.232
Spring	0.177	0.172
Summer	1.173	0.230
Fall	1.114	0.098

for spatial aging during spring and autumn seasons; this signifies that the seasonal aging of all towers along the line is very close to the average. The south half of the power transmission line is thermally overstressed during spring and fall and its aging values impact the overall thermal aging values.

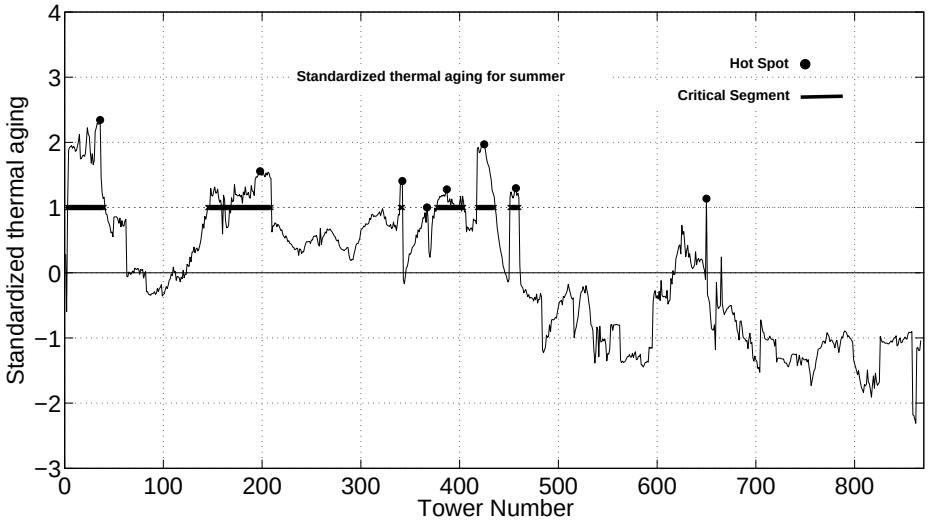

Figure 3.27: Standardized thermal aging series during summer season

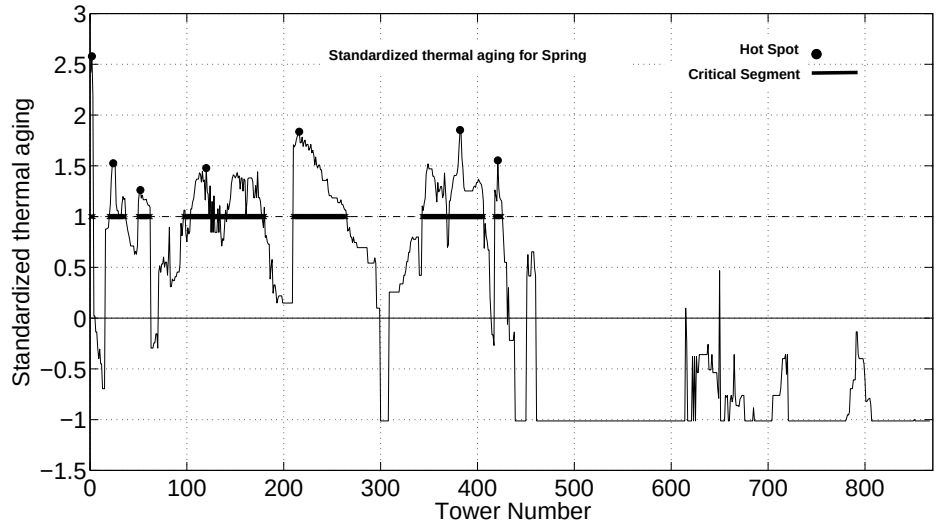

Figure 3.28: Standardized thermal aging series during spring season

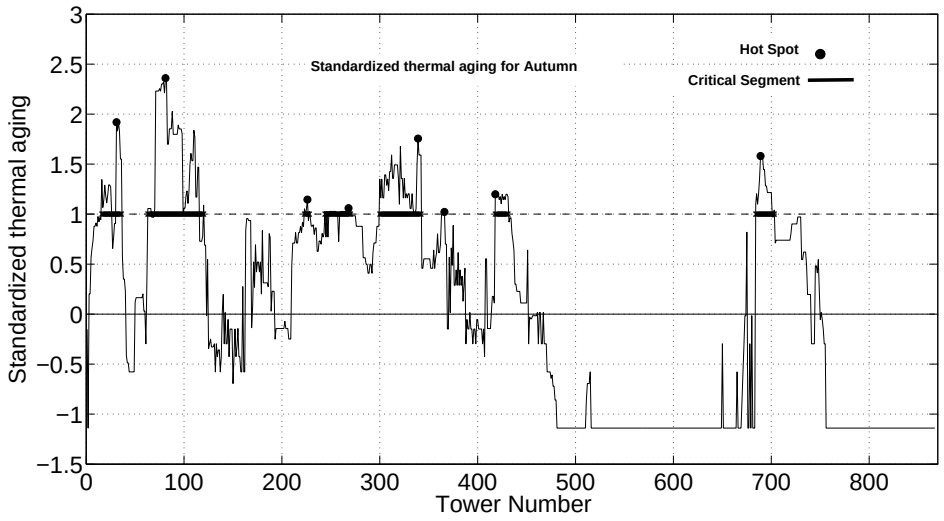

Figure 3.29: Standardized thermal aging series during autumn season

3.3.4 Evaluation of seasonal static thermal rating

Optimum utilization of overhead transmission lines can be obtained by devising a thermal rating strategy based on dynamic and probabilistic methods. Alternative rating strategies can be applied that consider weather conditions during different seasons and even during different times of day.

This section illustrates several seasonal rating paradigms, and compares their performance with actual ampacity. Several seasonal rating strategies are examined in a sample power transmission line in British Columbia, Canada. Simulation results show that, despite having a high degree of residual risk, seasonal ratings offer a modest increase in transmission line utilization compared to other probabilistic ratings.

Historical weather information along the transmission line plays a major role in determining probabilistic thermal rating [56]. Local weather stations, historical data sets, and numerical weather prediction (NWP) models are reliable sources of weather information. Weather information can be utilized to compute the ampacity of a transmission line by implementing an IEEE standard [19]. Subsequently, statistical analysis is applied to evaluate the cumulative distribution functions (CDFs) of line ampacities. The probabilistic thermal ratings are then determined as quantiles of the CDFs corresponding to a given risk tolerance. A 5% risk level is regarded as conservative enough for the use of most power companies. Nevertheless, there is no approved industrial standard or consensus for setting risk tolerance [57].

The procedure to determine seasonal static thermal ratings (SSTRs) is similar to the evaluation of basic probabilistic ratings STR_{prb}. However, in the former procedure, line ampacities are split into subsets according to a number of time periods before CDFs are calculated. Quantiles of line ampacities are then computed separately for each subset, and then used as static thermal ratings in corresponding time periods. The number of time periods is selected based on the seasonal and/or diurnal nonuniformity of weather information in the area of interest. A set of potential seasonal ratings can be demonstrated considering 1, 2, 4, and 12 rating periods per year. SSTRs with 4 (four seasons) and 12 (months) ratings can be further divided into different ratings for day and night. The categorization of SSTRs is shown in Table 3.7 which was adopted from [58].

Table 3.7: Classification of seasonal static thermal ratings (SSTR)

Label	Name	Description	Values
STR_a	Basic probabilistic STR	Fixed value of STR for a year	1
STR_b	SSTR for winter/summer	Two different SSTRs Winter : November - April Summer: May-October	2
STR_c	SSTRs for four seasons	Winter: December - February Spring: March-May Summer: June-August Fall: September - November	4
STR_d	STR for each month	Year is divided into each month	12
STR_e	Four seasons STR with day/night	Year is divided into four seasons Day-time is chosen as (6am - 6pm) and night-time is selected during (6pm-6am)	8
STR_f	Day/night Monthly STR	Year is divided into months and each day is divided into day-time and night-time	24

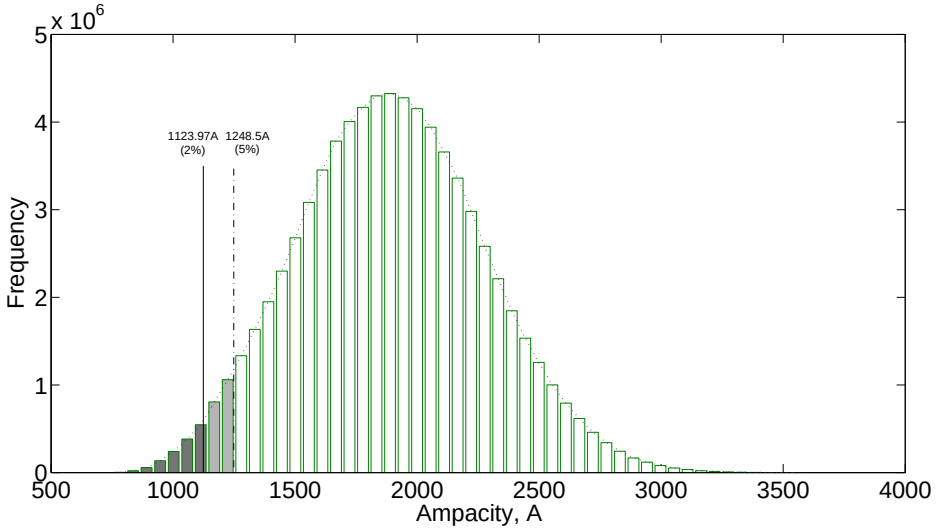

Figure 3.30: Frequency histogram of line ampacities

3.3.5 Case study

As in the previous sections, power transmission line 5L011 in British Columbia, Canada, was chosen for this case study. The 500 kV power transmission line consists of three phased ACSR Finch conductors where the emissivity and absorptivity coefficients of the conductor are assumed to be equal to 0.5. The maximum per-

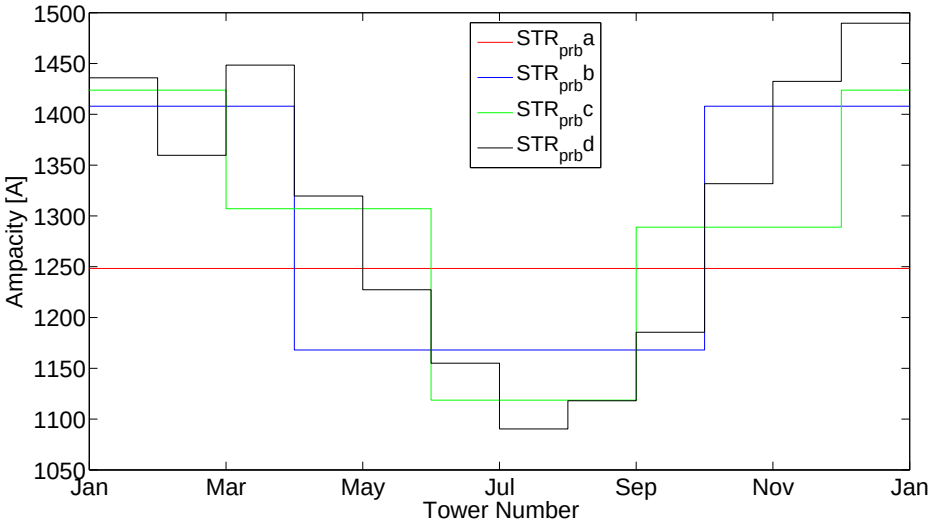

Figure 3.31: Seasonal thermal ratings STR$_{prb}a, b, c, d$

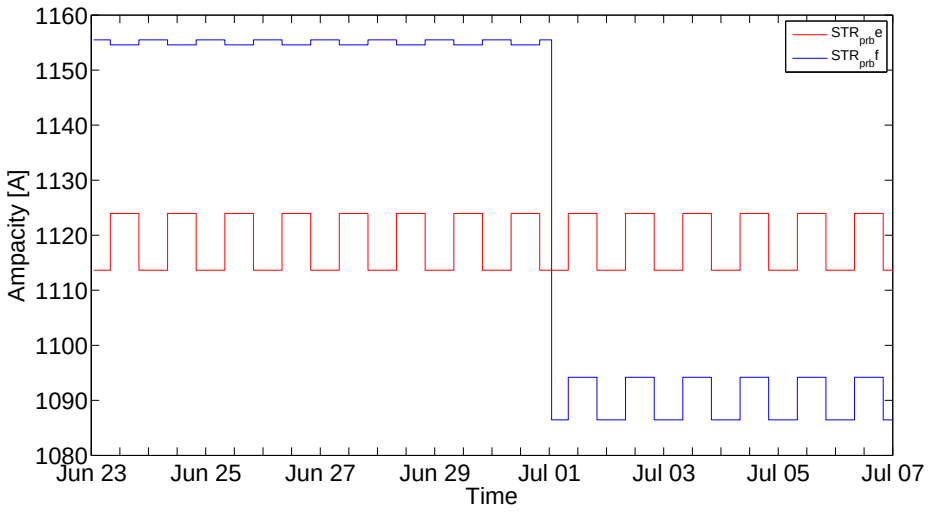

Figure 3.32: Seasonal thermal ratings STR$_{prb}e, f$

missible temperature of the overhead conductor is assumed to be 75 °C for normal operation. Over 860 towers of this line are considered in this study. Weather information over a period of 10 years, from January 2000 to December 2009, was extracted from historical datasets (NARR) for each tower of the transmission line.

Line ampacities were computed for each tower of the transmission line, implementing IEEE Standard 738 over a period of 10 years. Figure 3.30 shows the

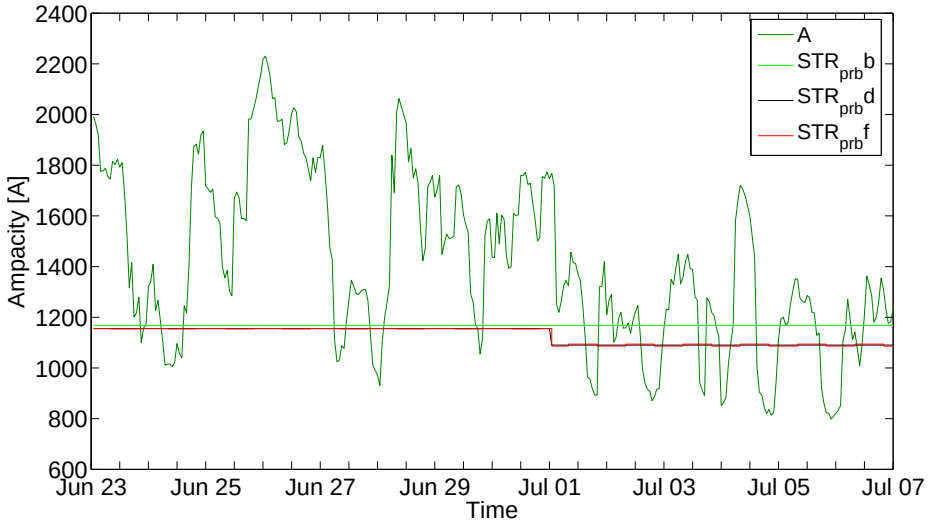

Figure 3.33: A time series of actual ampacity vs seasonal static thermal ratings (2 weeks duration)

frequency histogram of line ampacities of all towers at risk levels of 2% and 5%. Subsequently, line ampacity data were divided into subsets of seasons, months, and day/night-times, according to Table 3.7. A single static thermal rating value was determined for each subset of ampacity data by considering quantiles of CDFs corresponding to 5% risk tolerance. Results are shown in Table 3.8 and illustrated in Figures 3.31 and 3.32 for selected time periods. The actual current-carrying capacity of transmission line 5L011 over the entire year of 2009 was estimated by taking the minimum ampacity of all towers at each time step (1 hour). The estimated time series of actual ampacity (A) for June 2009 is depicted in Figure 3.33 together with other SSTRs. The most common way to compare thermal ratings, is to use cumulative frequency distribution functions (CFDFs), depicted in Figure 3.34. This plot reveals the risk associated with probabilistic ratings. One can see from Table 3.9 that application of such ratings can cause line overloading up to 8% of the simulation time. Table 3.9 also indicates that the percentage of exceeding the actual ampacity increases with increasing frequency of alternation among ratings.

Table 3.8: Evaluation of seasonal static thermal ratings ($STR_{prb}a-f$)

STR Label	STR [A]	STR Label	STR [A]	
			day	night
$STR_{prb}a$	1248.25			
$STR_{prb}b$				
summer	1168.00			
winter	1408.00			
$STR_{prb}c$		$STR_{prb}d$		
summer	1118.68	summer	1123.96	1113.64
autumn	1288.96	autumn	1305.60	1273.93
winter	1423.78	winter	1446.89	1403.88
spring	1307.09	spring	1318.28	1296.41
$STR_{prb}e$		$STR_{prb}f$		
January	1435.89	January	1457.63	1417.02
February	1359.63	February	1385.03	1336.87
March	1448.41	March	1455.43	1442.41
April	1319.63	April	1327.83	1310.38
May	1227.30	May	1244.69	1212.02
June	1155.06	June	1154.59	1155.50
July	1090.27	July	1094.19	1086.45
August	1118.03	August	1130.42	1106.59
September	1185.54	September	1195.44	1176.56
October	1331.74	October	1348.64	1316.17
November	1432.43	November	1458.77	1405.03
December	1489.62	December	1506.54	1474.84

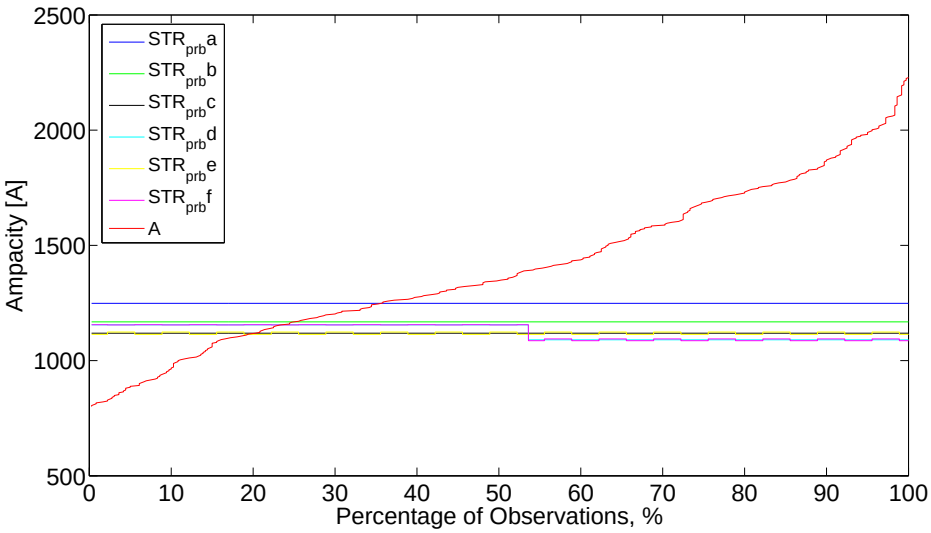

Figure 3.34: Cumulative frequency distribution functions for estimated ampacity and seasonal ratings for a period of 2 weeks

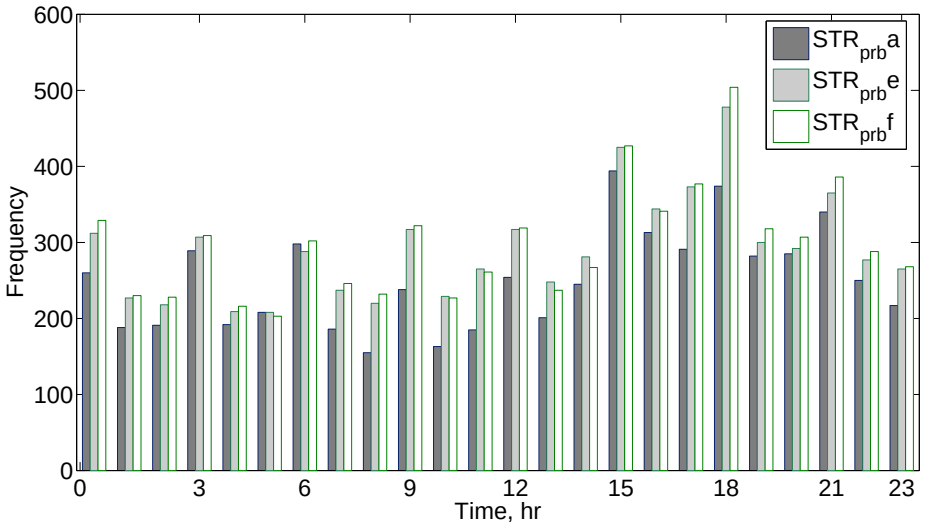

Figure 3.35: Frequency histograms of annealing temperatures for seasonal static line ratings $\text{STR}_{prb}a, e, f$ at each hour of a day

Numerical comparisons among different seasonal line ratings are presented in Table 3.9, showing the percentage of line utilization as well as the probability of exceeding the maximum permissible line temperature. Table 3.9 also summarizes the percentage of exceeding the actual ampacity for each static line rating. The

Table 3.9: Comparisons of different seasonal thermal ratings

Rating Label	Average Ampacity (AA) [A]	Line Utilization [% of AA]	STR $\geq$ A [% of time]	T_c >95 °C [% of time]
A	1514.56			
STR$_{prb}a$	1248.50	82.41	24.08	6.84
STR$_{prb}b$	1288.00	84.98	27.19	7.97
STR$_{prb}c$	1284.63	84.77	26.53	7.94
STR$_{prb}d$	1285.32	84.82	26.60	7.98
STR$_{prb}e$	1299.46	85.78	27.95	8.11
STR$_{prb}f$	1299.96	85.82	27.97	8.15

conductor temperature exceeds the thermal limit for normal operation during 24% of the simulation time for the STR$_{prb}a$ load and changes from 24% to 28% between different seasonal rating operations. Therefore, while the use of SSTRs increases the current throughput of the transmission line, it imposes further risk of thermal aging. A view of annealing temperature distribution is illustrated in Figure 3.35 for three different seasonal ratings. It can be observed that annealing temperatures mostly occurred at 6:00 p.m. for STR$_{prb}e, f$ ratings while the highest frequency of annealing temperature for STR$_{prb}a$ was 3:00 p.m. The figure shows that for almost each hour of the day, the frequency of annealing temperature is lowest for STR$_{prb}a$ and highest for STR$_{prb}f$; these results are supported in Table 3.9. Moreover, because of the severity of weather conditions, particularly, wind speed, temperature, and solar radiation as well as the elevated seasonal ratings, the highest frequency of annealing temperature is observed for STR$_{prb}e, f$ at 6:00 p.m. This information can be used by an asset management system created to determine the daily load profile that will incur the least risk of thermal aging; that is, the optimal utilization of the transmission line.

Chapter 4

An expert system for assessing conductor condition [1]

Over time, effects of thermal aging and exposure to environmental pollution gradually reduce the lifespan of energized ACSRs in overhead power transmission lines. This chapter demonstrates an expert system developed to diagnosis the current condition of overhead power conductors. Using a fuzzy inference paradigm, an expert system was designed to predict the current deterioration level of a conductor based on dominant phenomena such as thermal loss of strength LoS[%], environmental pollution, and conductor configuration. The parameters involved in the proposed expert system are highly nonlinear, uncertain, and categorical in nature. As a consequence, it is not possible to use a conventional analytical approach to implement the system. The use of neural networks is not possible either, due to the lack of numerical data describing the desired behaviour. Therefore, a fuzzy approach was selected for the implementation. It is able to use the categorical data provided by expert and deal with the vagueness of input and output parameters in an efficient way. Weather data for computing thermal aging can be extracted with high resolution at every tower location of the transmission line. Pollutant estimates for each tower location can be obtained from historical datasets of the National Pollutant

[1] *A version of this chapter has been accepted for publication. Md. Mafijul Islam Bhuiyan, Petr Musilek, and Jana Heckenbergerova 2011. IEEE Electrical Power and Energy Conference, EPEC 2011, Winnipeg, MB, October 3-5, 2011.*

Release Inventory (NPRI), Canada. The deterioration grades, the outcome of this model, will contribute to identify the predicted lifespan of the energized ASCR in the overhead power transmission line. Hence, a spatial view of this non-destructive diagnostic tool can be deployed for better economic scheduling of line inspections, refurbishment, and maintenance.

The expert system was developed under the expert guidance of Dr. Don Koval. His biography can be found in appendix A.3.

4.1 Observation of historical pollutant data

Data from the region of power transmission line 5L011 in the form of a historical pollutant dataset was obtained from the National Pollutant Release Inventory (NPRI) [59], Canada, 2008. The available one year data were rolled over five times based on the assumption that the amount of pollutants is almost similar each year. This dataset was further processed to estimate a pollution index for each tower of the transmission network. The processing of historical pollutant data collected from NPRI involves the following five steps:

I. Identification of facilities that emit pollutants having chemical agents responsible for corrosion (sulphur, ammonia, and chloride);

II. Calculation of the total amount of pollutants emitted from the identified facilities;

III. Determination of the geographic coordinates (longitude and latitude) of the identified facilities;

IV. Assessment of the total amount of pollutants released by identified facilities for each line span. This step consists of two sub-steps depicted in Figure 4.1:

- Calculation of distances among all tower spans and pollutant sources. If the computed distance is larger than a threshold value then the corresponding facility is ignored. Otherwise, a Sugeno fuzzy model [60] is used to estimate the amount of pollutant for each tower span.
- Both wind direction and speed influence the amount of pollutant that reaches a particular location. Therefore, the prevailing wind direction of each hour is taken into consideration to estimate the direction trend of floating pollutants. The schematic diagram in Figure 4.1 illustrates how these processes work.

V. Assignment of a numerical index to each tower span using predefined fuzzy membership functions, according to the estimated amount of pollutants.

The schematic diagram in Figure 4.1 illustrates how the pollutant amount is processed using wind direction and facility distance. According to information provided by a domain expert, the threshold distances were set to 5, 10, and 13 kilometres. However, these distances are highly geographic location oriented and can be modified by a power transmission company. As shown in Figure 4.1, the distances of facilities from transmission line, d1, d2, and d3, were evaluated based on wind direction. A projection line was drawn from the facility to the transmission line along with wind direction to calculate the distance. A facility will be ignored if it is situated outside of the largest threshold distance. Facility 1 will be ignored for wind directions wd2 and wd3 and facilities 2 and 3 will be ignored for wind direction wd1. Distances d1, d2, and d3 are used in the Sugeno fuzzy model to distinguish severity of effects in a tower span of a given facility.

The implemented Sugeno fuzzy model, described in Table 4.1, can be explained as follows:

- If x is *near* THEN $z = \mathrm{a} \cdot y$;
- If x is *medium* THEN $z = \left(\frac{x}{b} - 1\right) \cdot \mathrm{c} \cdot y$;
- If x is far THEN $z = (1 - \mu(x)) \cdot \mathrm{d} \cdot y$;

where, x is the distance between tower span and pollutant source, y is the amount of pollutant in that source, z is the estimated amount of pollutant at the facility, and the values of constants a, b, c, and d are chosen as 1.0, 10, 0.5, and 0.1, respectively; these values can be altered for different geographical locations and pollutant sources.

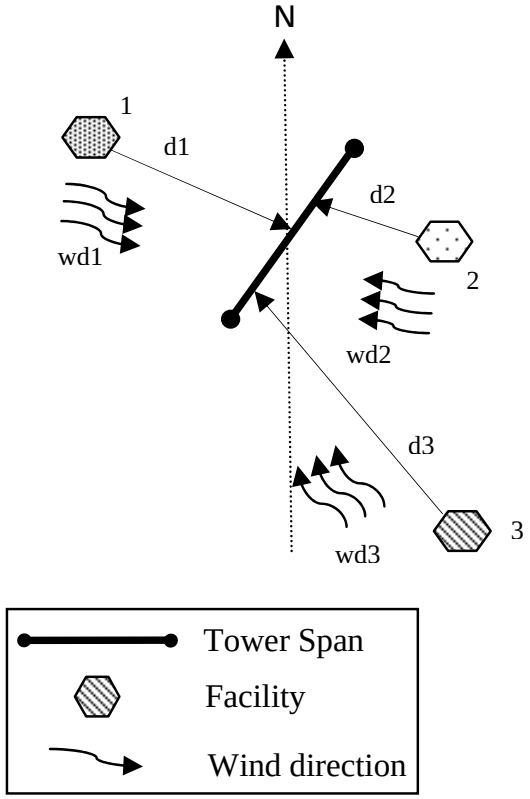

Figure 4.1: Schematic diagram of the analyzing of historical pollutant data

A weighted average defuzzification method [61] was applied to compute the final estimated amount of pollutant.

Table 4.1: Fuzzy membership functions of distance linguistic variable

Distance [Km]	
Variable	MF
Near	$\mu\langle 0,0,3,5\rangle$
Medium	$\mu\langle 3,7,10\rangle$
Far	$\mu\langle 8,11,13,13\rangle$

4.2 Structure of a fuzzy inference system

At elevated temperatures there is a risk of damage to a conductor due to an annealing effect. Annealing produces permanent damage that accumulates over time [15]. Therefore, thermal aging L_c was chosen as the prevailing input parameter in the proposed expert system. The deterioration level of a power conductor also depends on corrosion effects. ACSRs generally degrade due to atmospheric (pollutants) corrosion and galvanic (salt water spray) corrosion; the former is considered in this fuzzy system. The primary chemical agents of atmospheric corrosion are sulphate, chloride, sulphur dioxide, ammonia, and calcium [36].

Based on expert opinion, the nominal size of the conductor has a significant impact on the deterioration of power transmission line. Typically, conductors with a larger circular area have higher deterioration grades. Because contaminants, dust, and pollutants accumulate more readily on the surface of a larger conductor, a larger conductor corrodes faster and its lifetime is reduced relative to a smaller conductor.

The proposed fuzzy model quantifies the current condition of conductors using so called deterioration grade. The system classifies the grades as no deterioration, minor, partial and severe, as shown in Table 4.2. The fuzzy linguistic labels of each

Table 4.2: Classification of deterioration levels

Level	Interpretation
No Deterioration	Almost new conductor
Minor Deterioration	Normal condition
Partial Deterioration	Regular line inspection and maintenance
Severe Deterioration	Immediate reconductoring

level are summarized in Table 4.4. The numerical value of the deterioration grade can be used in asset management process to prioritize line inspection, maintenance, and reconductoring.

4.2.1 Fuzzy rule base systems

Fuzzy if-then rules, expressions of the form

If X is A then Y is B

interpret the relationship between fuzzy linguistic variables X and Y. A fuzzy rule based system generally encompasses five modules: input interface, fuzzy rules, database, fuzzy inference system (FIS), and defuzzified output [62]. The schematic diagram of the developed fuzzy model, adopted from [62], is depicted in Figure 4.2.

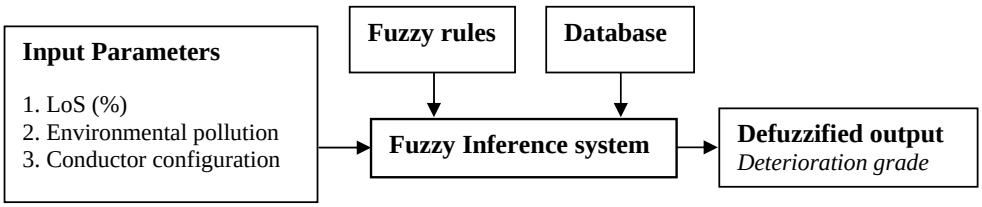

Figure 4.2: Schematic diagram of the proposed expert system

Tables 4.3 and 4.4 illustrate the qualitative values of input and output parameters classified into different linguistic variables of the proposed fuzzy model. The fuzzy database stores the types of membership functions and the universe of discourse of input and output parameters. These membership functions are highly problem dependent. Further, the fuzzy rules of the proposed model have been deduced based on the opinion of an expert in power transmission and conductor aging. By using these rules, the whole system can be quantified very easily rather than using a model based on a conventional mathematical tool, as the input and output parameters of the mathematical model are highly nonlinear, uncertain, and ill defined. In this case, input parameters LoS, pollution index, and conductor size are described by 5, 4, and 3 different linguistic variables, respectively. Therefore, the total number of fuzzy rules is 60 and they are listed in Appendix A.1.

4.2.2 Fuzzy inference system

The schematic diagram of the proposed fuzzy inference system is depicted in Figure 4.3. Here all the antecedents of a rule were combined with the *min* operation.

Table 4.3: Fuzzy membership functions of Input linguistic variables

Loss of strength L_c[%]		Pollution Index [-]		Conductor Size [mm^2]	
Variable	MF	Variable	MF	Variable	MF
Very Low	$\mu\langle 0,0,1,1.5\rangle$	Very Low	$\mu\langle 0,0,1.5,3\rangle$	Small	$\mu\langle 0,0,95,160\rangle$
Low	$\mu\langle 1,2.5,3.5\rangle$	Low	$\mu\langle 2,3,4\rangle$	Medium	$\mu\langle 160,350,480\rangle$
Medium	$\mu\langle 2.5,4.5,6.5\rangle$	Medium	$\mu\langle 3,5,7\rangle$	Large	$\mu\langle 410,560,590,590\rangle$
High	$\mu\langle 6,8,10\rangle$	High	$\mu\langle 6,8,10,10\rangle$		
Very High	$\mu\langle 8,10,12,12\rangle$				

Table 4.4: Fuzzy membership functions of output linguistic variables

Deterioration Grade [-]	
Variable	MF
No Deterioration	$\mu\langle 0,0,1.5,4\rangle$
Minor Deterioration	$\mu\langle 2,3,5.5\rangle$
Partial Deterioration	$\mu\langle 3,5.5,7\rangle$
Severe Deterioration	$\mu\langle 6,8,10,10\rangle$

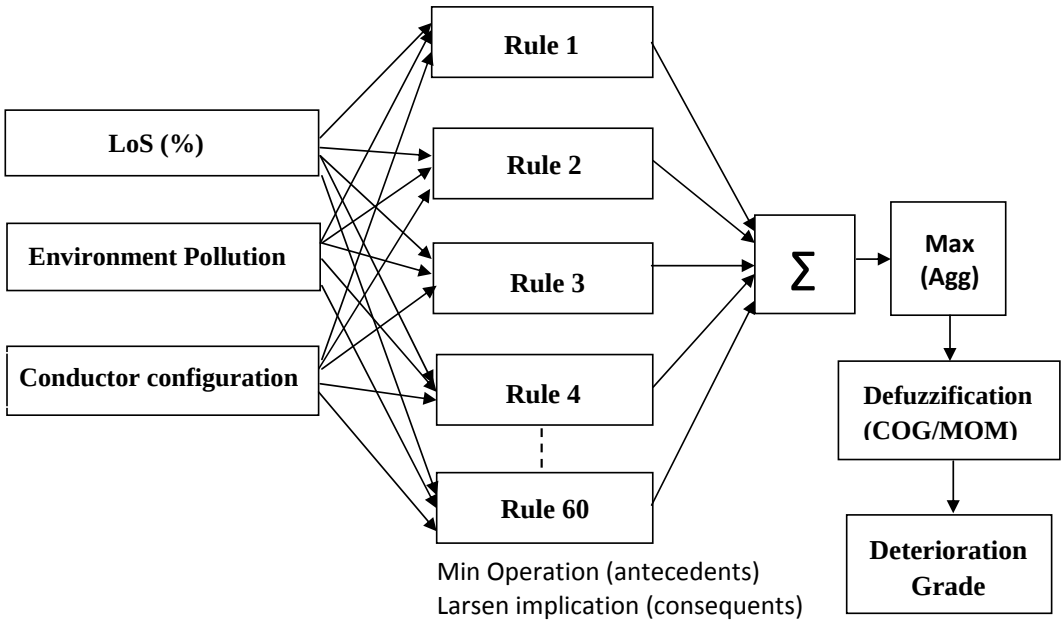

Figure 4.3: Structure of fuzzy inference system

The *Larsen* implication was applied to perform fuzzy inference between the consequence and the corresponding output of the *min* operation. All the fuzzy relations were then aggregated and the overall output was obtained using the *max* operation. Defuzzification (COG/MOM) methods were implemented to obtain the final deterioration grade as a crisp output. COG and MOM methods were compared with respect to defuzzification of this fuzzy inference model.

4.3 Case study

In order to validate the proposed expert system for assessing the condition of conductors, a sample overhead power transmission line (5L011) was selected from the Province of British Columbia, Canada. The structure and geographic location of the line is described in section 3.2.4. ACSR Finch is the conductor of the 5L011 transmission line. Its aluminum strand diameter and nominal current are 3.65 mm and 1110 A, respectively [48]. The emissivity and solar absorption coefficients were chosen as 0.23 and 0.4, respectively; these values are expected to increase with the use of the conductor.

Weather information over a five year period from 01/2005 to 12/2009 with a 3-hour time resolution was extracted from the North American Regional Reanalysis (NARR) historical dataset [49]. Weather data were interpolated to the locations of individual transmission towers using bilinear interpolation with 1-hour time resolution. Meteorological variables, including wind speed and direction, ambient temperature, and solar radiation, were applied to compute the line temperature as explained in [19]. This study considers variable load current derived using a normalized weekly load profile [55] with mean current equal to nominal ampacity, i.e., 1110 A. On weekdays, the daily peak of the specified load profile was about 26.95% above the mean value, whereas the load current was below the nominal ampacity during the weekend. The assumed load profile is shown in Figure 4.4.

Conductor thermal aging at each location of the power transmission line was estimated by applying the procedure described in chapter 3. The estimated amount of spatial loss of strength LoS is illustrated in Figure 4.5. The location of the nearest pollutant facilities are extracted from NPRI data (2008) and shown in Figure 4.6. The solid orange line on the map represents the real power transmission line and the bubbles along the transmission line symbolize the location of facilities. The density of pollution emission is distinguished through different colors of bubbles; yellow, purple, and green colors represent the highest, medium, and lowest pollutant emissions, respectively, in the air. The spatial pollution index of the whole transmission line, estimated using a procedure described in section 4.1, is depicted in Figure 4.7.

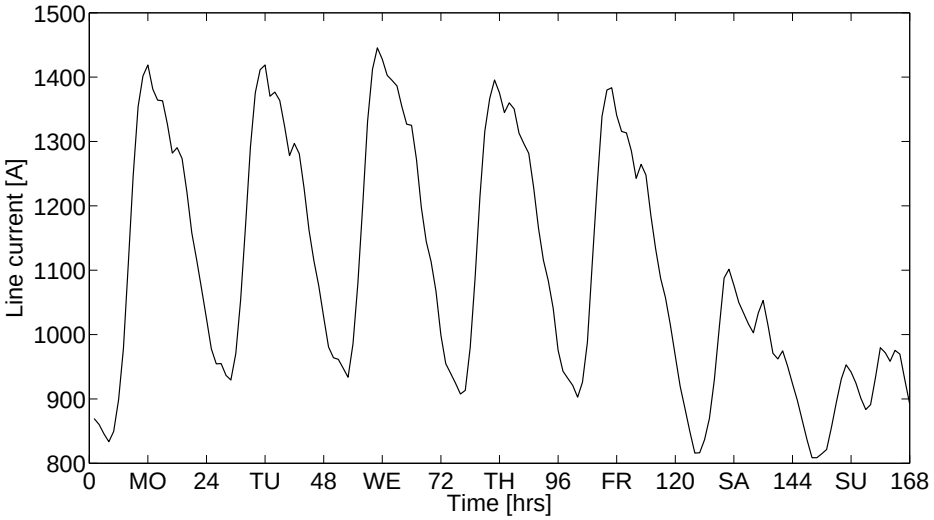

Figure 4.4: Assumed load profile with mean equals to nominal ampacity

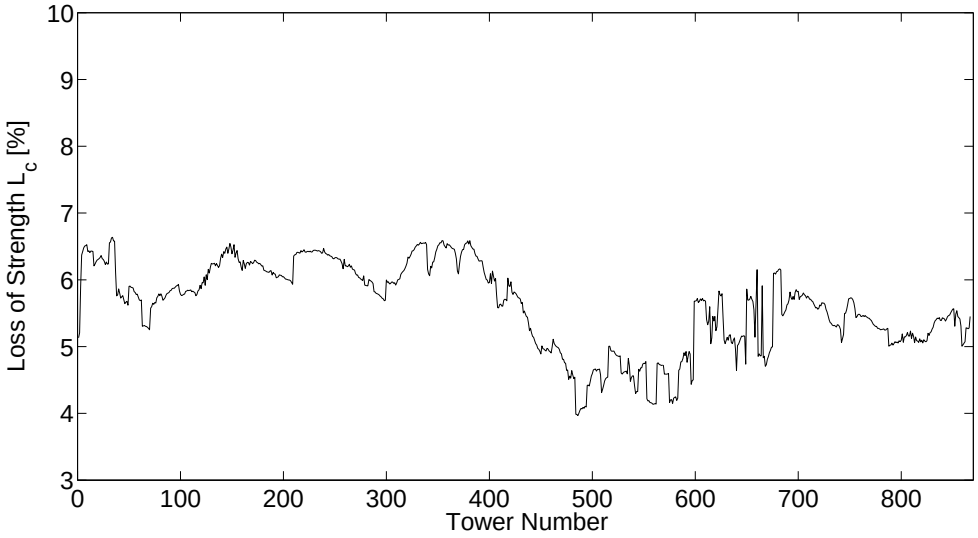

Figure 4.5: Spatial series of transmission line thermal aging over the five year period

4.3.1 Validation of fuzzy model

To validate the proposed fuzzy model, the complete input dataset has been randomly split into two mutually exclusive subsets. Sixty percent of the available data points (i.e., 520 towers) were used to determine the optimum values of universe of discourse for all linguistic variables and membership functions through applying

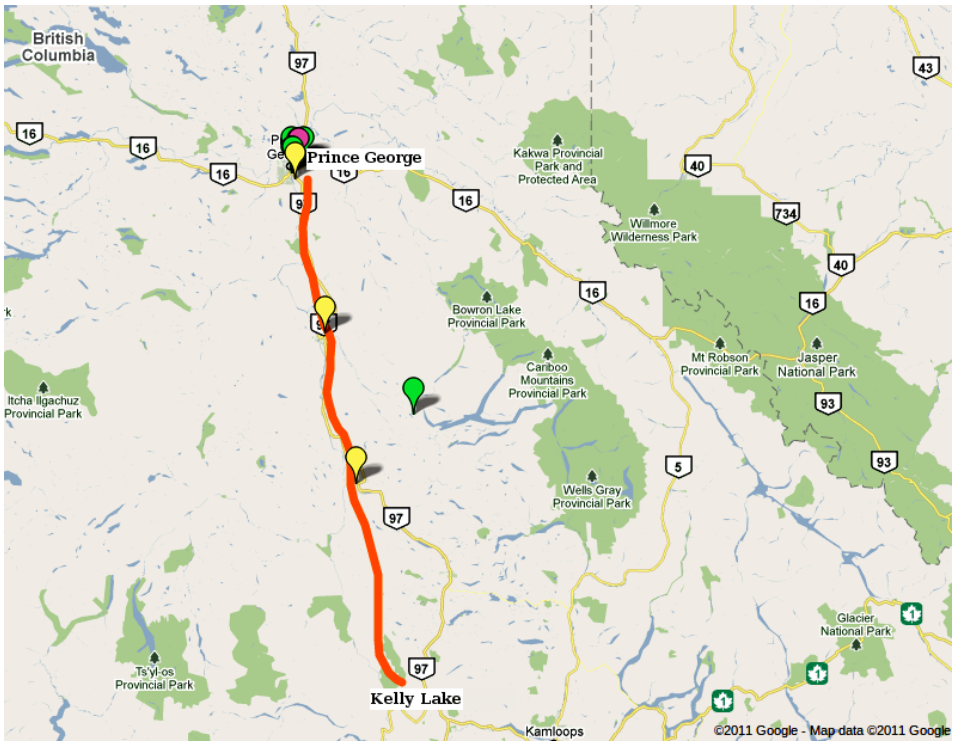

Figure 4.6: Locations of the nearest pollution facilities of power transmission line

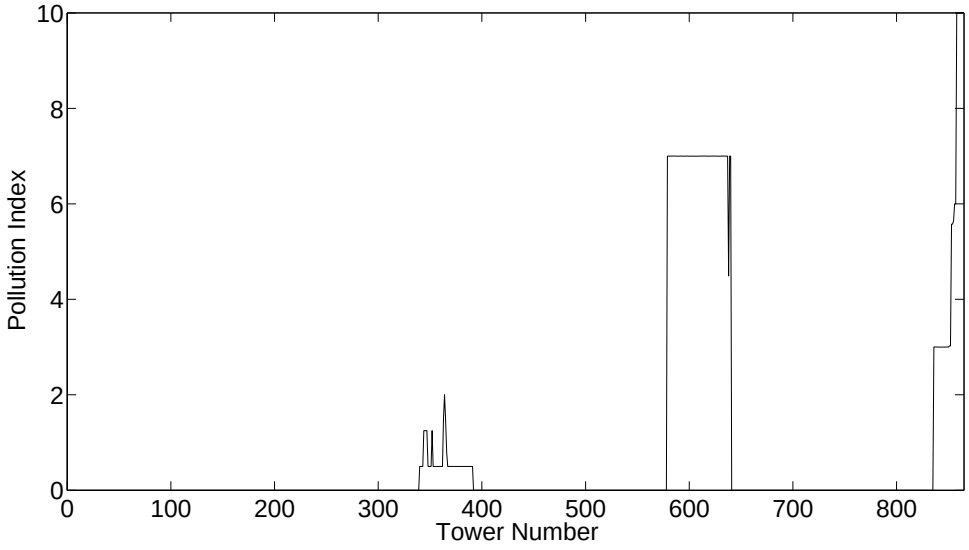

Figure 4.7: Spatial pollution index of transmission line

several iteration processes. Subsequently, the model was implemented to estimate the deterioration grades for the split dataset by using two defuzzification methods: COG and MOM. The resultant predicted deterioration grades, illustrated in Figures 4.8 and 4.9, should be compared with the desired deterioration grades. However,

such data are not available as they are highly expensive to acquire. Therefore, the spatial distribution of desired deterioration grades was estimated by the domain expert based on the thermal aging of ACSR Finch and pollution index. The procedure of estimating desired deterioration grades is explained in Appendix A.2. Figures 4.8 and 4.9 show the comparison of desired and predicted output for both COG and MOM defuzzification methods. It is observed that both methods can approximate the deterioration grades efficiently along the most severely deteriorated segments of the transmission line. However, the MOM defuzzification method was not able to provide accurate estimations along some sections with partial deterioration.

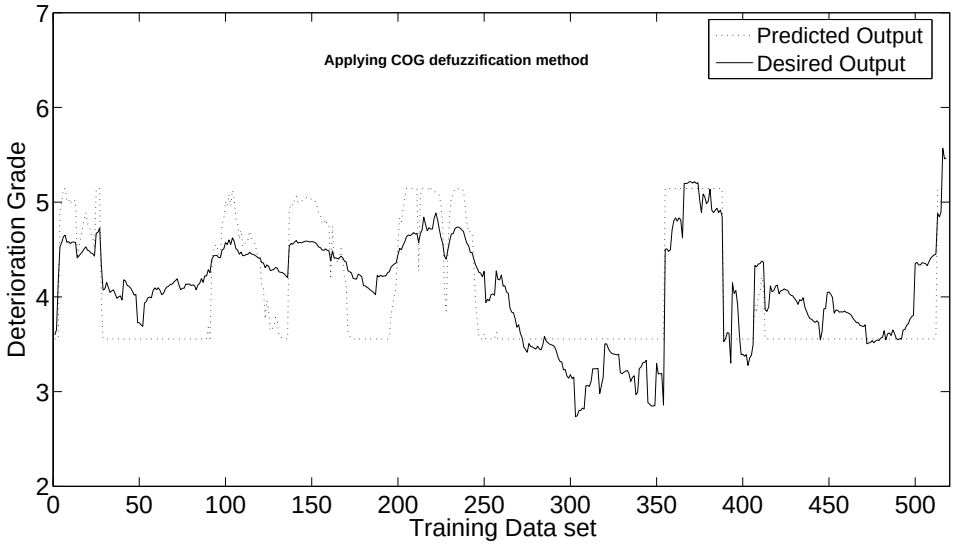

Figure 4.8: Estimated output of training dataset using COG method

Hence, the COG defuzzification method was chosen to estimate the deterioration grades of all the line spans in the transmission network; these values are illustrated in Figure 4.10. It is clearly shown in the figure that several segments of the power line are partially damaged after being energized for 5 years; these segments should be inspected regularly. Most critical segments are between towers $590-635$ and $850-865$ where higher environmental pollution was in evidence.

Although the proposed fuzzy expert system can be implemented for effective scheduling of line inspection and maintenance, the system must be further validated with actual deterioration grades acquired from field data of an energised transmission line. Historical data regarding forced power system outages could be

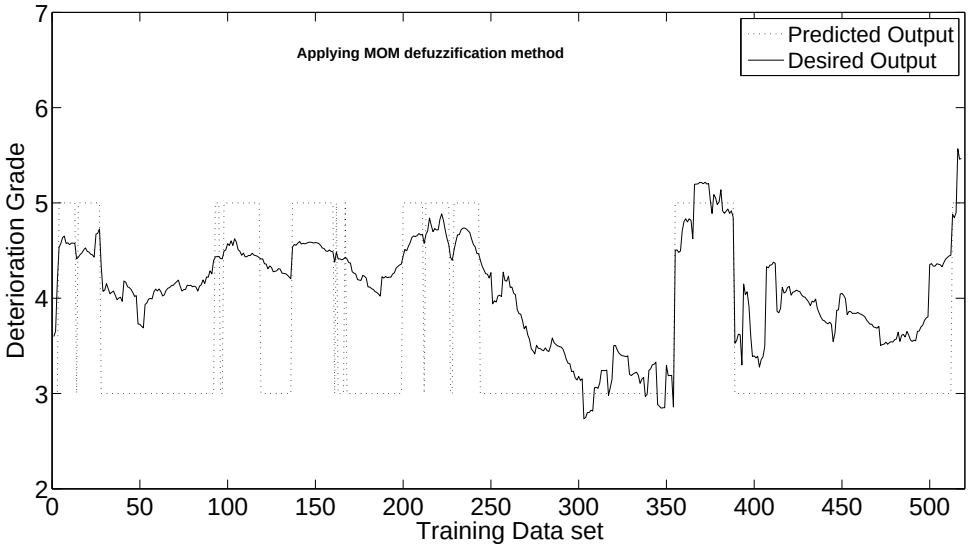

Figure 4.9: Estimated output of training dataset using MOM method

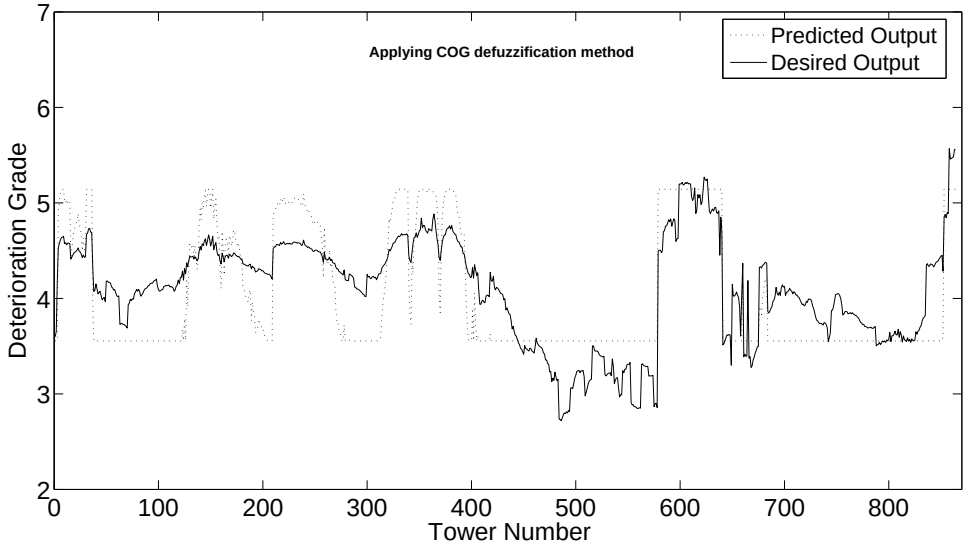

Figure 4.10: Predicted deterioration grade of all towers using COG method

an alternative source for further optimization and evaluation of system accuracy.

Chapter 5

Dynamic re-rating of overhead transmission lines

Energized ACSRs gradually elongate over time due to thermal expansion and mechanical loading [15]. Elongation causes the transmission line to sag, bringing it close to the ground where flashover can occur. A minimum ground clearance value is calculated and maintained to prevent damage to the power network and human injury. As line sag tends to increase as the conductor ages, it is very important to provide a basis for re-rating an existing line with respect to current sag, tension, and the ground clearance of the conductor. In this chapter, the southern part of BC Hydro transmission line 5L011 was selected to study how an energized transmission line can be optimally re-rated by considering factors such as thermal expansion, ice accretion, ice shedding, wind and ice load, metallurgical creeping, and geometrical settlement.

5.1 Thermal elongation of a transmission line

5.1.1 Thermal expansion evaluation

Composite ACSRs contract and expand with changes in conductor temperature. Homogeneous conductors comprised of a single metal−e.g., AAC (all aluminum)−undergo thermal elongation at a higher rate than nonhomogeneous conductors−e.g., ACSR (aluminum and steel). The elastic elongation due to thermal impact of a nonho-

mogenous conductor can be calculated using the following equation [63].

$$\alpha_{cond} = \alpha_{al} \cdot \left(\frac{E_{al}}{E_{cond}}\right) \cdot \left(\frac{A_{al}}{A_{cond}}\right) + \alpha_{core} \cdot \left(\frac{E_{core}}{E_{cond}}\right) \cdot \left(\frac{A_{core}}{A_{cond}}\right), \tag{5.1}$$

where α_{cond}, α_{al}, α_{core} are thermal elongation coefficients, E_{al}, E_{core}, E_{cond} are elastic moduli, and A_{al}, A_{cond}, A_{core} represent cross-sectional area of aluminum (Al), core, and conductor (cond), respectively.

The elastic deformation of an object, e.g., a metal conductor, can be expressed mathematically by a parameter known as the elastic modulus [15]. To compute the modulus of elasticity of a composite conductor, the following equation can be applied.

$$E_{cond} = E_{al} \cdot \left(\frac{A_{al}}{A_{cond}}\right) + E_{core} \cdot \left(\frac{A_{al}}{A_{cond}}\right). \tag{5.2}$$

Due to the complex behavior of the elasticity of a bimetalic conductor, thermal expansion is generally computed through stress-strain curves. However, in the computer aided numerical method, the thermal expansion of the core and thermal expansion of the whole conductor due to the increments of line temperature can be calculated as follows:

$$\Delta T = \alpha_{cond} \cdot (T_{applied} - T_{ref}) \cdot \left[L\left(1 - \frac{H}{(E_{cond} \cdot A_{cond})}\right)\right], \tag{5.3}$$

$$\Delta T_{core} = \alpha_{core} \cdot (T_{applied} - T_{ref}) \cdot \left[L\left(1 - \frac{H_{core}}{(E_{cond} \cdot A_{cond})}\right)\right], \tag{5.4}$$

where $T_{applied}$ [°C] and T_{ref} [°C] represent the current and previous line temperatures, respectively, H is the initial tension of the conductor, H_{core} is the initial tension of the conductor core, and L is the initial length of the conductor.

5.1.2 Permanent elongation of a transmission line

Creep is a nonelastic or permanent elongation of a conductor that generally occurs when the transmission line is operated at elevated temperatures with high mechanical loads. Creeping should be considered if the line temperature of an ACSR exceeds 95 °C [10]. Recursive procedures [22] for computing plastic elongation due to thermal metallurgical creeping include the following steps:

- Determination of metallurgical creep E_c by using line temperature (> 95°C),

$$E_c = 0.24 \cdot (\%RS) \cdot T_c \cdot t^{0.16}, \tag{5.5}$$

  where $\%RS$ is tension as a percentage of the rated strength, T[°C] is line temperature, t [hrs] is time duration, and E_c [$\mu\varepsilon$] represents metallurgical elongation;

- Determination of equivalent exposure time t_{i-1} for current line temperature T_c for the previous creep;

$$t_{i-1} = \left(\frac{E_c \cdot 4.617}{T_c \cdot \%RS} \right)^{6.25}. \tag{5.6}$$

- Summation of the current exposure time t_1 and the equivalent exposure time t_{i-1} and calculation of the creep elongation for the current line temperature using equation (5.3);

- Repetition of the previous steps until the last line temperature is encountered.

Geometrical settlement is another reason for irreversible elongation of a power conductor. It mainly depends on conductor maximum working tension MWT and happens rapidly during the first 24 hours when the conductor strands are settling [22]. It can be calculated as follows.

$$E_S = 750 \cdot (d-1) \cdot (1 - e^{\frac{-m}{10}}) \cdot \left(\frac{MWT}{RTS} \right)^{2.33}, \tag{5.7}$$

where E_s [m] is the geometrical settlement, m is the Al/St sectional area ratio, MWT is maximum working tension, and RTS [N$\cdot$ m^{-2}] is the rated tensile strength.

The permanent elongation of ACSR Finch for different line currents is shown in Figure 5.1, considering WRF weather data and a given simulation setup. Figure 5.1 shows constant permanent elongation caused by geometrical settlement for low line current and a sharp increase just above 900 A due to metallurgical creep.

5.2 The wind and ice load model

An estimate the impact of sag involves computation of all the forces acting on the transmission line, including wind and ice loads. First, an ice accretion model [44]

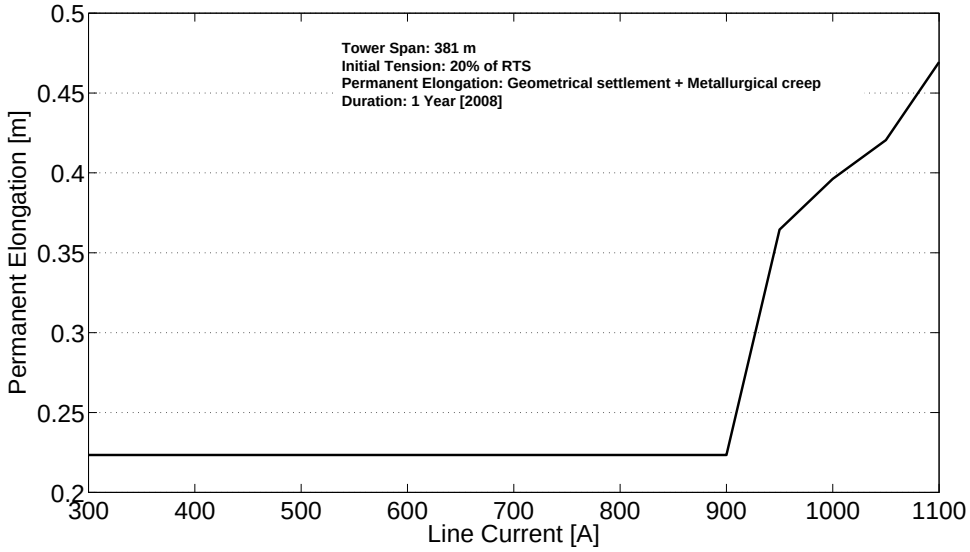

Figure 5.1: Estimated permanent elongation for different line currents

that takes into account weather parameters such as temperature and precipitation type, was used to estimate the amount of ice on the transmission line. Second, a mathematical ice shedding model that considers line current and heat propagation was implemented to estimate the resultant radial thickness of ice on the conductor. The resulting forces were estimated based on actual ice load and wind speed. This model was tested on several consecutive towers of the southern part of BC Hydro transmission line 5L011.

5.2.1 Ice mass load calculation

The ice accretion forecasting system (IAFS) is used to estimate the potential amount of ice on power conductors. This paradigm uses weather data in the region of interest and a precipitation type algorithm [44]. In this project, weather data along the southern part of power transmission line 5L011 operated by BC Hydro was estimated using the Weather Research and Forecasting (WRF) Numerical Weather Prediction (NWP) model [51]. Simulation time covers a one year period (from 01/2008 to 12/2008) with a time resolution of 10 minutes. It contains meteorological variables such as horizontal wind speed and direction, ambient temperature, atmospheric pressure, specific humidity, fraction of frozen precipitation, precipitation rate, etc. Finally, the amount of accreted ice on the transmission line at each

time stamp was calculated using an IAFS-GA (genetic algorithm) [44].

A mathematical model [64] of ice melting has been implemented to evaluate the resulting radial thickness of ice. It considers line current, heat propagation, and other parameters related to ice melting, and the boundaries between different materials.

$$Q_s = Q_h + Q_e + Q_l + Q_j. \tag{5.8}$$

The above heat balance equation contains the heat transfer due to convection Q_h, evaporation Q_e, radiation Q_l, and joule heat Q_j due to line current. The total propagated heat, Q_{tot} [J/m] through the surface area of a transmission conductor covered with ice can be computed by applying equation (5.7):

$$Q_{tot} = \left[(Q_h + Q_e + Q_l) \cdot \frac{\pi \cdot d}{3.85 \cdot 24} + Q_j \right] \cdot dt \cdot IFP, \tag{5.9}$$

where dt [s] is small time interval for simulation, d is the total diameter (conductor + Ice) [m], and IFP is initial freezing point. Finally, equation (5.8) is used to calculate the total diameter d_{new} of conductor with accreted ice.

$$d_{new} = \sqrt{d^2 - \frac{4 \cdot Q_{tot} \cdot d}{1000 \cdot \rho_i}}, \tag{5.10}$$

where ρ_i is the density of ice [kg·m^{-3}].

Figure 5.2 illustrates ice melting time versus line current for different radial ice thickness. Here, the air temperature and wind speed are kept constant at 3 °C and 4.5 m/s, respectively. According to the graph, there is an exponential reduction in ice melting time when the line current increases for different ice radial thickness. For an unenergized transmission conductor, the shortest melting time (about 47 min) is required for an ice radial thickness of 8 mm, whereas the longest melting time (about 97 min) is required for a 20 mm layer of ice.

After estimating the final radial ice thickness using the ice shedding model, the ice mass load can be evaluated. It corresponds to the volume of ice multiplied by its density.

$$m = \rho_i \cdot \pi (d \cdot R_{eq} + R_{eq}^2) \cdot \ell, \tag{5.11}$$

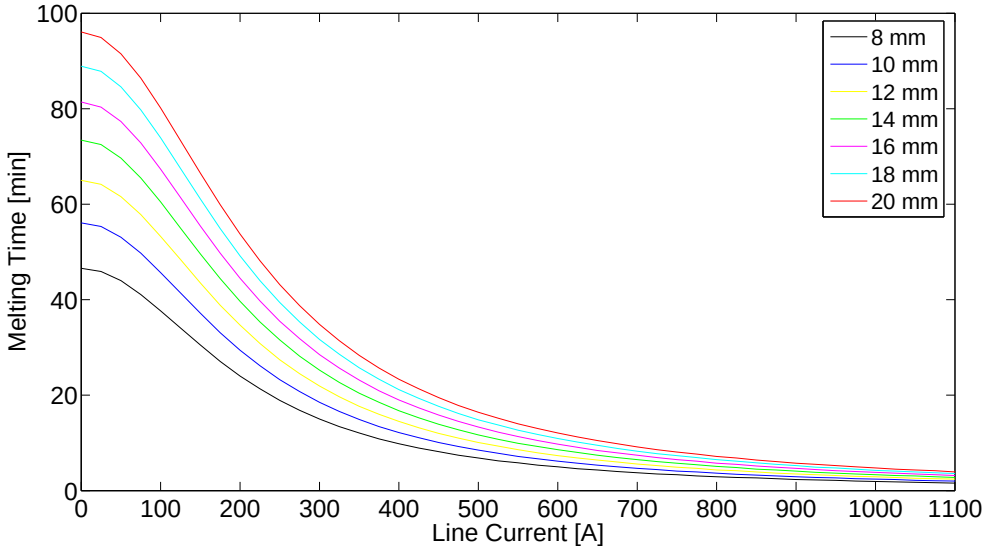

Figure 5.2: Ice melting time for different line currents and radial ice thickness

where m [g] is the ice mass, ρ_i is the ice density (0.0009 g·mm^{-3}), R_{eq} [mm] is the equivalent uniform radial ice thickness, d [mm] is the conductor diameter, and ℓ [mm] is the length of the conductor. The force f_{ice} exerted on the conductor due to the ice load can be obtained by multiplying the computed ice mass and the gravitational force, where the length ℓ of the conductor is standardized to one meter:

$$f_{ice} = 9.82 \cdot 10^{-3} \cdot \rho_i \cdot \pi(d \cdot R_{eq} + R_{eq}^2). \tag{5.12}$$

5.2.2 Wind force calculation

Wind load significantly affects the sag of overhead conductors. It can influence the design of a new power transmission line and is partially responsible for the permanent elongation of power conductors [15]. According to the National Electric Safety Code (NESC) [65], the wind force f_{wind} acting on an ice coated conductor can be expressed as:

$$f_{wind} = 0.5 \cdot \lambda \cdot \mu \cdot (K_R \cdot V_{RB})^2 \cdot K_Z \cdot G_{RF} \cdot I \cdot C_f \cdot \frac{(d + 2R_{eq})}{1000}, \tag{5.13}$$

where λ is a density correction factor normally equal to 1.0 [66], μ is the air mass density, K_R is an adjustment factor found in Table 4 of [67], V_{RB} is a reference wind speed, K_Z is a velocity-pressure exposure coefficient (line height dependent) found in Table 250-2 of [65], G_{RF} is the gust response factor (line length and line height

dependent) found in Table 250-3 of [67], I is importance factor set to 1.0 for utility structures and their supported facilities, and C_f is a force coefficient or the shape factor considered to be 1.0 for cylindrical structures and components.

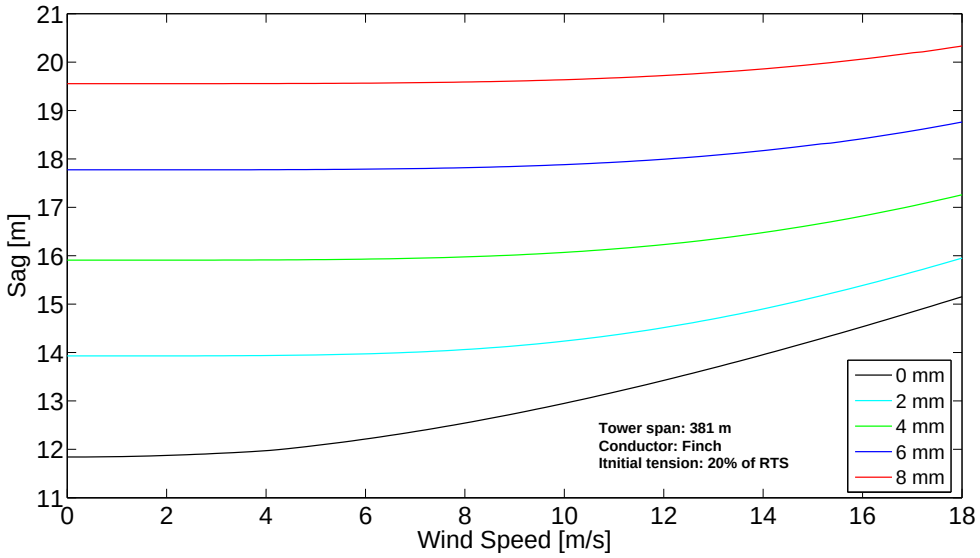

Figure 5.3: Sensitivity analysis of sag with different wind speeds

The dependence of sag on different wind speeds with constant ice radial thickness is shown in Figure 5.3 for a single tower span of power transmission line 5L011. The figure shows the impact of wind force on power transmission line sag; it also shows that wind speed has relatively higher impact on sag if small amount of ice is accreted on conductor.

5.2.3 Total mechanical load

The final step of the wind and ice load model entails a calculation of the total mechanical force exerted on the conductor. The vector sum of wind and ice forces represents the total mechanical load f_{tot}, expressed as:

$$f_{tot} = \sqrt{f_{ice}^2 + f_{wind}^2}. \tag{5.14}$$

The dependence of sag on the total mechanical load exerted on the conductor is shown in Figure 5.4. The sag of a particular tower span has been estimated by applying a hybrid numerical approach [8]. It can be observed that the sag is almost

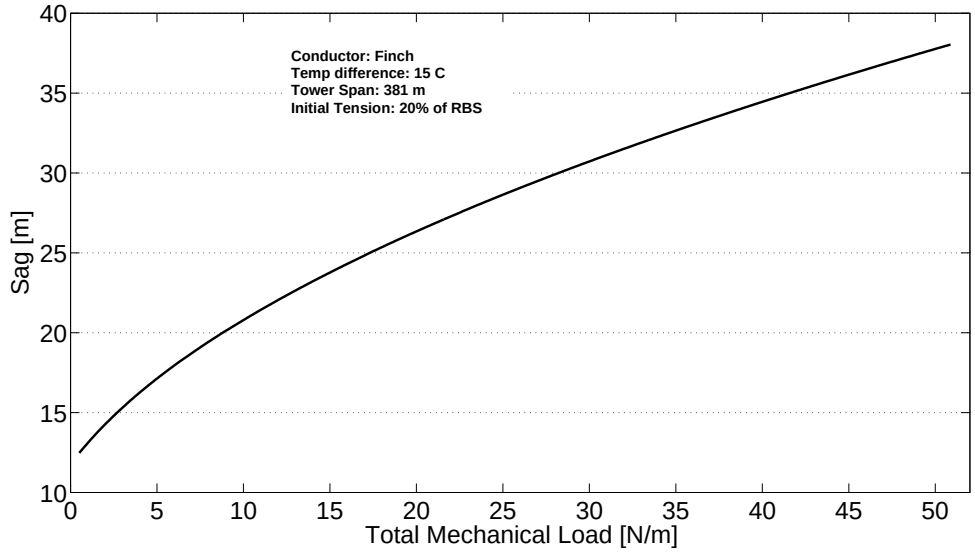

Figure 5.4: Sensitivity of sag on total mechanical load

linearly related to total exerted mechanical load for Finch conductor and constant temperature difference.

5.3 Estimation of final sag

Methods developed to calculate and predict sag for single metal and bimetallic conductors can be divided into graphical and numerical categories [8]. In most cases, the initial sag and tension of conductors are determined at the time of construction when the line is unenergized. The conductor is usually installed at ambient temperature between $10-25°C$ and tensioned to $15-25\%$ of the rated tensile strength (RTS). After installation, transmission lines are subject to elevated temperatures and high mechanical load (combined wind and ice) and elongation of the conductor takes place over time.

The hybrid sag method (HSM), a computer aided numerical sag computation procedure adopted from [8], is described in this section. A block diagram of HSM is shown in Figure 5.5 showing two parallel procedures to estimate sag. The process on the right of Figure 5.5 computes the sag of the total composite conductor and the process on the left of the figure calculates the sag using only the properties of the steel in the core of the conductor.

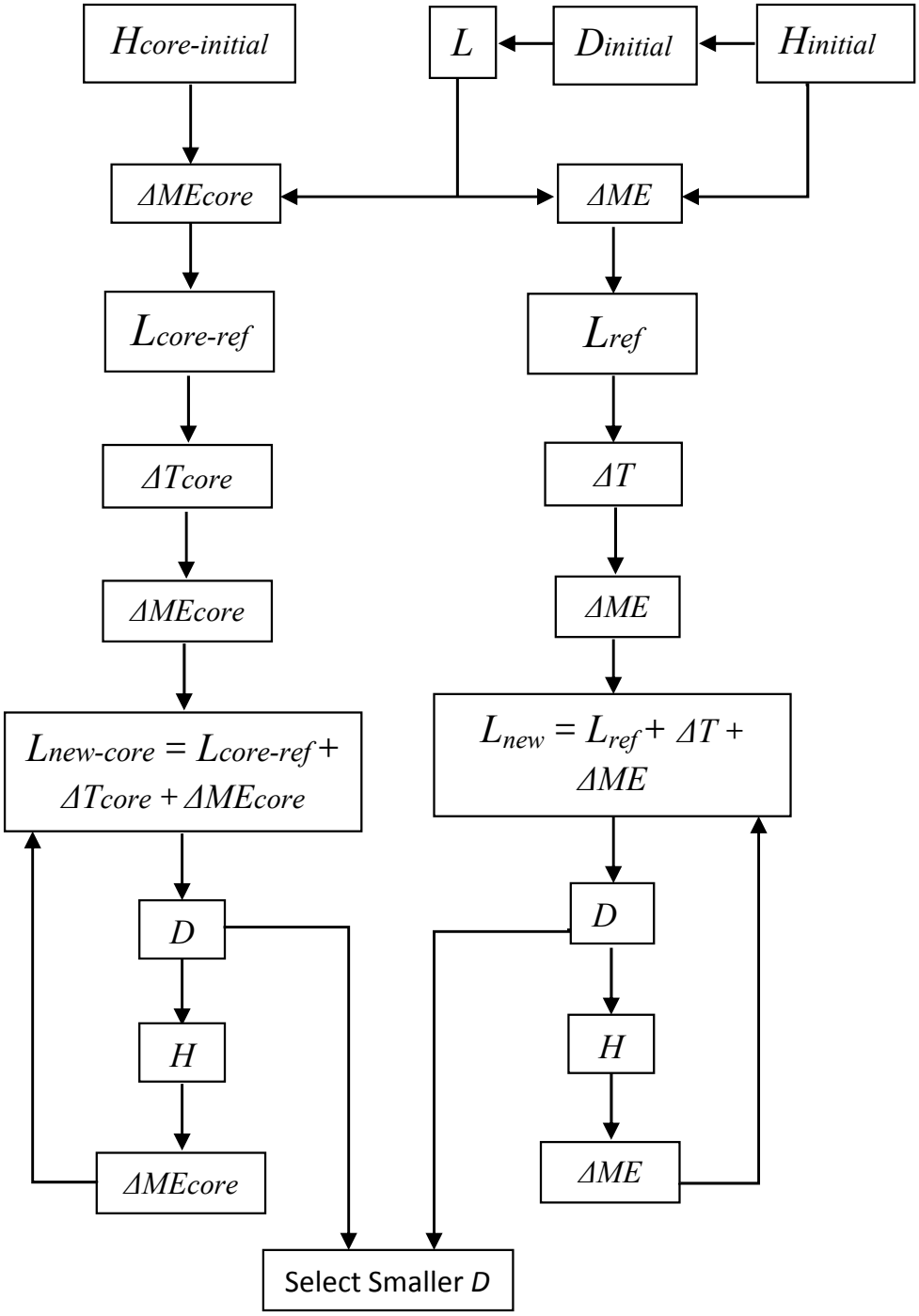

Figure 5.5: Schematic diagram of hybrid sag method (HSM)

In this numerical sag estimation approach, three different models are used to compute the mechanical load exerted on the power conductor: IAFS-GA [44], ice melting, and WILM [68]. The elongation of the core ΔME_{core} and elongation of the

whole conductor ΔME due to mechanical load can be computed as follows:

$$\Delta ME = \frac{L \cdot (H_{new} - H)}{E_{cond} A_{cond}}, \tag{5.15}$$

$$\Delta ME_{core} = \frac{L \cdot (H_{new} - H_{core})}{E_{core} A_{core}}, \tag{5.16}$$

where H_{new} represents the new tension of conductor, E_{core} and E_{cond} are elastic moduli, and A_{cond}, A_{core} represent cross-sectional area of core, and whole conductor, respectively.

Eventually, the final extracted or expanded length of the power conductor is computed considering thermal and mechanical effects, creep elongation, and geometrical settlement. The corresponding sag value can be determined using the following equation.

$$D = \sqrt{(3S(L-S)/8)}, \tag{5.17}$$

where S is tower span [m]. The temporal evolution of sag for different currents

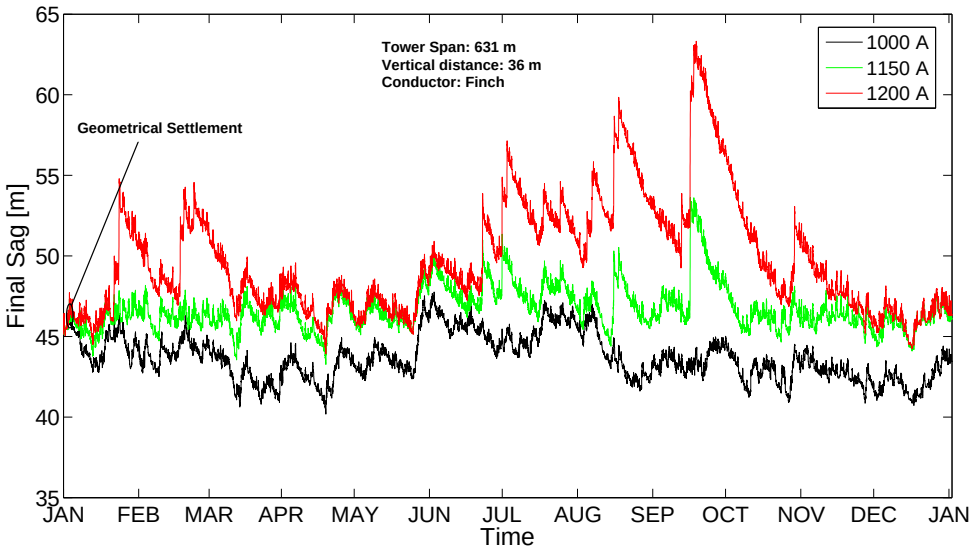

Figure 5.6: Temporal sag analysis

was studied on a segment of BC Hydro power transmission line 5L011. Results of this study are shown in Figure 5.6. Weather data along the transmission line was extracted from the WRF NWP model [51] to compute the mechanical load using the procedures described above. Transient line temperatures, necessary to estimate

the thermal elongation and loss of strength were calculated using IEEE Standard 738-2006. ACSR Finch, described in section 3.1.3, was assumed as the conductor of the transmission line. Figure 5.6 illustrates that sag gradually increases during summer (May−Oct) due to thermal effects and creep elongation. Sag is quite low during most of the winter (Nov−Apr), but increases sharply at the end of January and in February due to mechanical load and high fluctuations in line temperatures. Figure 5.6 also shows the behavior of sag for different line currents.

5.3.1 Comparison with SAG10

To verify the accuracy of the proposed sag computation method, the estimated output was compared with results computed from a widely used sag calculation program SAG10. A trial version of this software was used for this comparison.

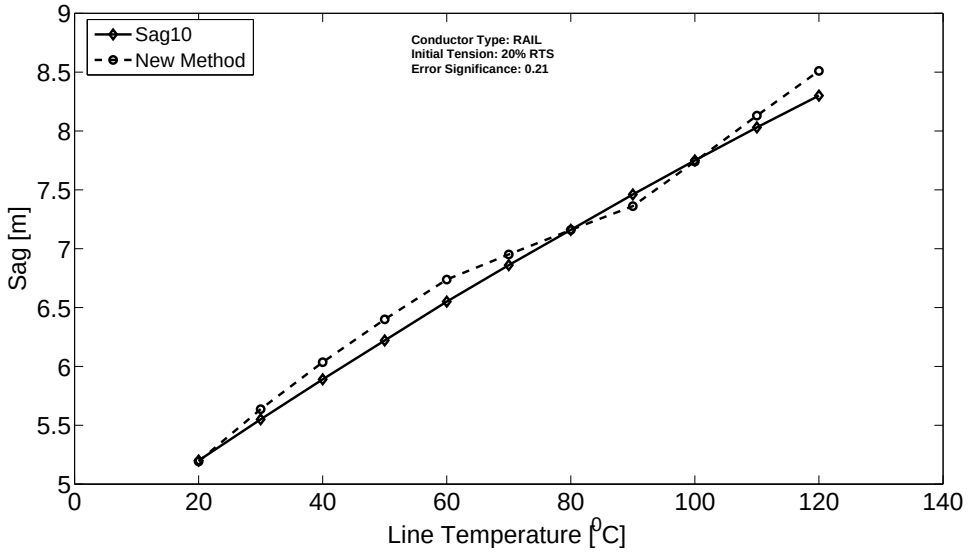

Figure 5.7: Comparison of proposed method and SAG10 considering creeping elongation

Figures 5.7 and 5.8 compare the results for creep elongation and wind and ice load, respectively. The conductor type, tower span, initial tension, and temperature were assumed as ACSR Rail, 247 m, 20% of RTS, and 20 °C, respectively. The figures confirm that the two methods provide very similar results. The mean absolute error (MAE) for creep elongation and wind-and-ice-load are 0.101 and 0.063, respectively.

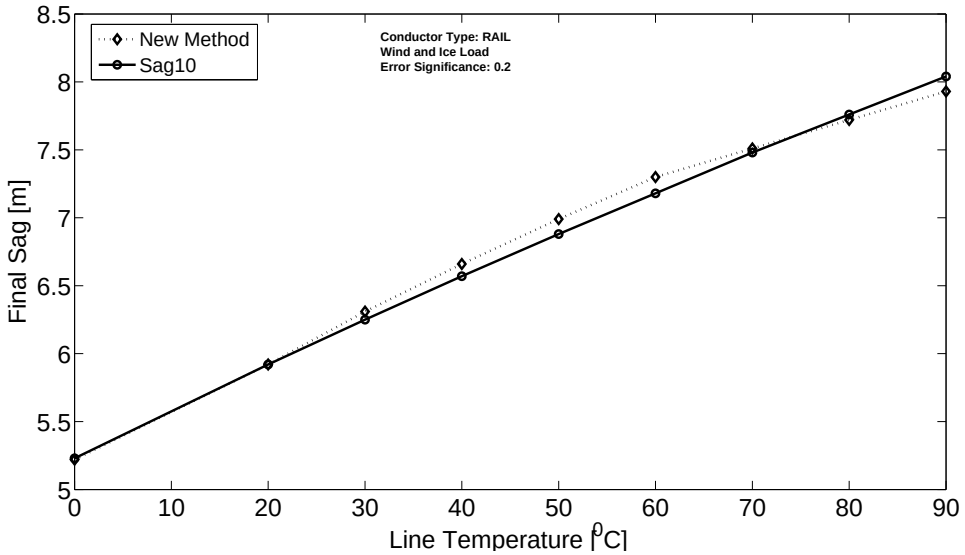

Figure 5.8: Comparison of proposed method and SAG10 considering wind and ice load

Compared to sag10 software, the proposed methodology has a number of advantages. Using the methodology, potential sag of transmission lines can be estimated for particular geographical locations based on weather parameters and assumed load profiles. This information can be used by design engineers for planning new transmission lines.

5.4 Computation of conductor ground clearance

The clearance to ground of inclined tower spans can be calculated using the following procedure outlined in [69]:

I. Determination of the maximum value of sag ($D_{S/2}$) at the midpoint of all tower spans by considering weather and thermal impact on the transmission line over a particular period of time;

II. Identification of the position (E_x) of the lowest sag point between two inclined towers:

$$x = \frac{S}{2} \cdot \left(1 + \frac{h}{4} \cdot D_{S/2}\right). \tag{5.18}$$

III. Computation of sag (D_x) at the lowest point of each tower span:

$$D_x = 4 \cdot D_{S/2} \cdot \frac{x}{S} \cdot \left(1 - \frac{x}{S}\right). \tag{5.19}$$

IV. Determination of the elevations of the positions computed in step II, using Google Maps API;

V. Calculation of the available ground clearances (a) of all towers:

$$a = H_0 - (H_0 - H_1) \cdot \frac{x}{S} - D_x - E_x, \tag{5.20}$$

where h is the vertical distance, $H_0 = h_0 + E_0$ is the total height of the higher elevation point, and $H_1 = h_1 + E_1$ is the total height of the lower elevation point.

The schematic diagram in Figure 5.9 shows how the minimum available ground clearances can be computed applying the above procedures for a single inclined tower span. However, this methodology does not work correctly for all cases, particularly, when the lowest sag point is not aligned with the lowest value of a. The segmentation method can be applied in this case to determine the lowest available ground clearance more accurately. In this process, the tower span is segmented into

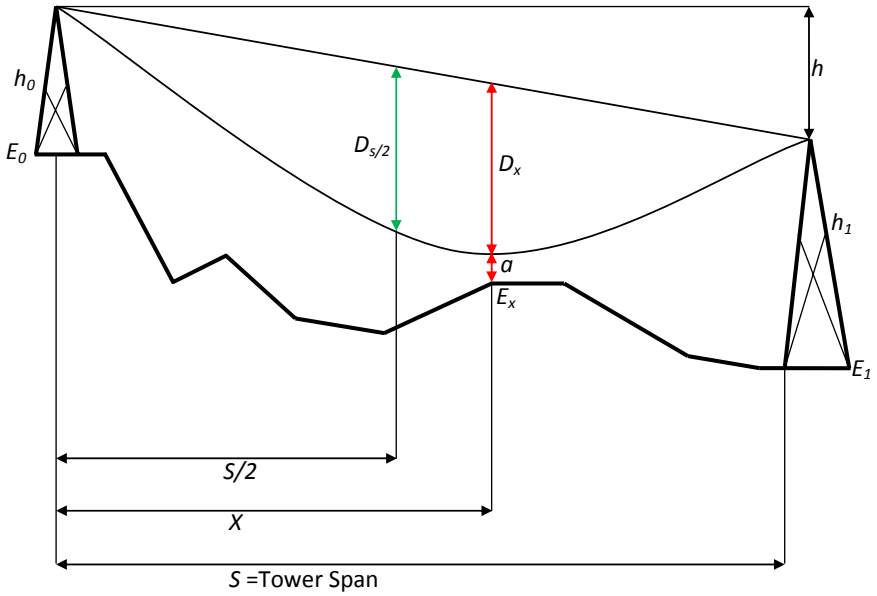

Figure 5.9: Schematic diagram for computing of available ground clearances

small and equal parts and the values of a are evaluated for the edges of each segment. Finally, the lowest value of a is selected as the minimum available ground clearance. The result will be more accurate if the segmentation interval is smaller.

Basic electrical clearance D_{el} is supposed to be approximately 3.5 m for a 525 kV overhead transmission line [70]. To mitigate the risk of flashover, a minimum ground clearance ($6+D_{el}$) [m] to the line surface must be maintained, especially during heavy wind and ice load and thermal elongation.

The described methodology was applied for 147 tower spans located at the southern part of BC Hydro transmission line 5L011 to evaluate the minimum available ground clearances after energizing the conductor over a 1 year period. Tower height, a significant parameter used in equation (5.20), was obtained from the asset management database of BC Hydro. Figure 5.10 shows the available ground clearances along the line for an 1100 A (nominal) line current. Ground clearance is also affected by changes in line current. The estimated spatial ground clearances show an inverse relationship with line current in Figure 5.11. The ground clearance is gradually reduced as line current increases.

Dynamic re-rating of overhead transmission lines based on weather conditions and thermal impact permits optimal utilization of power transmission lines and

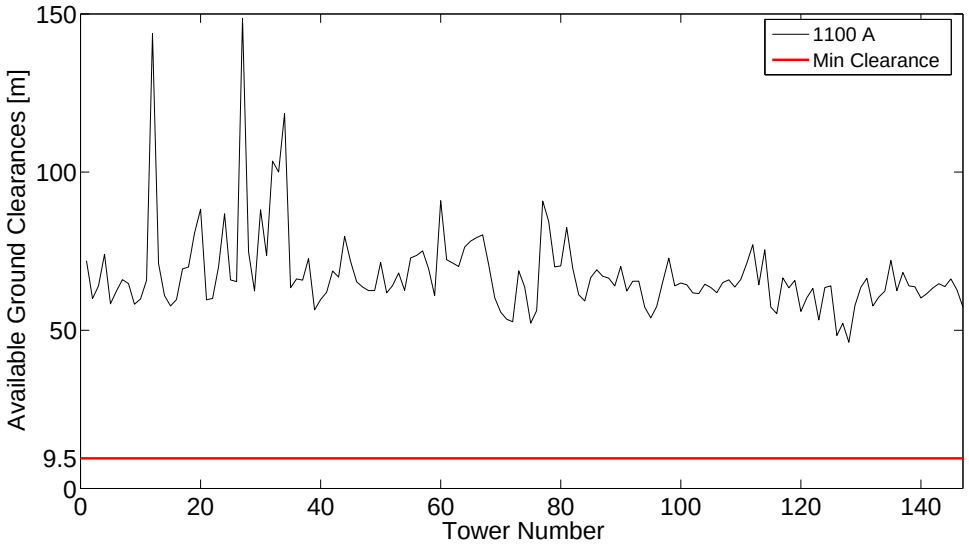

Figure 5.10: Available ground clearances after energizing over 1 year period

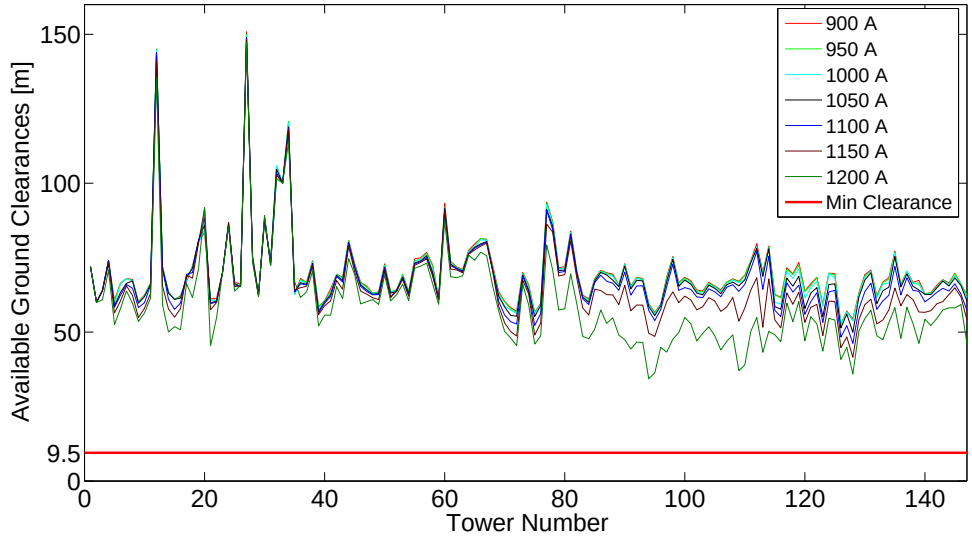

Figure 5.11: Available ground clearances for different line currents after energizing over 1 year period

avoids violation of safety requirements. To increase a line rating in an emergency, the current sag, available ground clearance, and aging must be monitored to avoid potential risks. Therefore, the spatial aging (chapter 3) and the ground clearance (this chapter) provide vital information for dynamic re-rating of an existing transmission line.

5.5 Risk analysis of outage and flashover

This section describes the estimation of spatial risks associated with the operation of the sample power transmission line, 5L011. The significance of thermal loss of strength and sag are considered in this study. The LoS and minimum ground clearances computed previously are used in this section to assess the risk of each tower span using a probabilistic method. This method evaluates not only the likelihood of outage of a particular segment of transmission line, but also the impact of that outage for given operating conditions. The total impact of thermal and mechanical overload is estimated as the sum of impacts on ground clearance and loss of strength for a given line current.

5.5.1 Risk quantification

Risk of an event can be expressed as the product of probability of occurrence and impact of the event [71],

$$\text{Risk(Event)} = \text{Probability(Event)} \cdot \text{Impact(Event)}.$$

The maximum permissible LoS of the conductor is 10% [72]. As mentioned earlier, the minimum ground clearance of an energized 500 kV transmission line is assumed to be 9.5 m [70]. The total risk assigned to a particular tower, due to thermal loss of strength and minimum ground clearance, can be quantified as follows:

$$R = \rho(LoS) \cdot Imp(LoS) + \rho(a) \cdot Imp(a), \tag{5.21}$$

$$\rho(LoS) = L_c/10, \tag{5.22}$$

$$\rho(a) = 9.5/a \; [a > 0], \tag{5.23}$$

where R is the total risk of a tower span for a given line current, $\rho(LoS)$ is the probability of outage, $\rho(a)$ is the probability of flashover due to sag, $Imp(a)$ is the impact of flashover, $Imp(LoS)$ is the impact of outage, L_c is the total thermal loss of strength, and a represents the minimum available ground clearance. The impact of an event depends on the length of the given tower span, as the cost of repair is higher for longer spans. The cost of reconductoring 1 kilometer of transmission

line is approximately $67,000 [73]. The impact due to line outage or flashover per meter can be estimated as follows:

$$Imp(LoS) = k \cdot L, \tag{5.24}$$

$$Imp(a) = 100 \cdot k \cdot L, \tag{5.25}$$

where L is the length of conductor and k is the reconductoring cost per meter, i.e., $67. In the event of flashover there is a high probability of damage to several consecutive towers at one time. Therefore, the repair cost for damage due to flashover is assumed to be 100 times higher than that of line outage due to loss of strength [71].

The dependence of risk on line current is shown in Figure 5.12 for transmission line 5L011 (Finch conductor with nominal current of 1100 A). The estimated risks are normalized according to line reconductoring costs. It can be seen that risk increases sharply when line current is higher than the nominal current (1100 A). The increased temperatures at higher line currents produce a higher frequency of annealing temperatures (occurring above 95 °C) which impacts both LoS and sag.

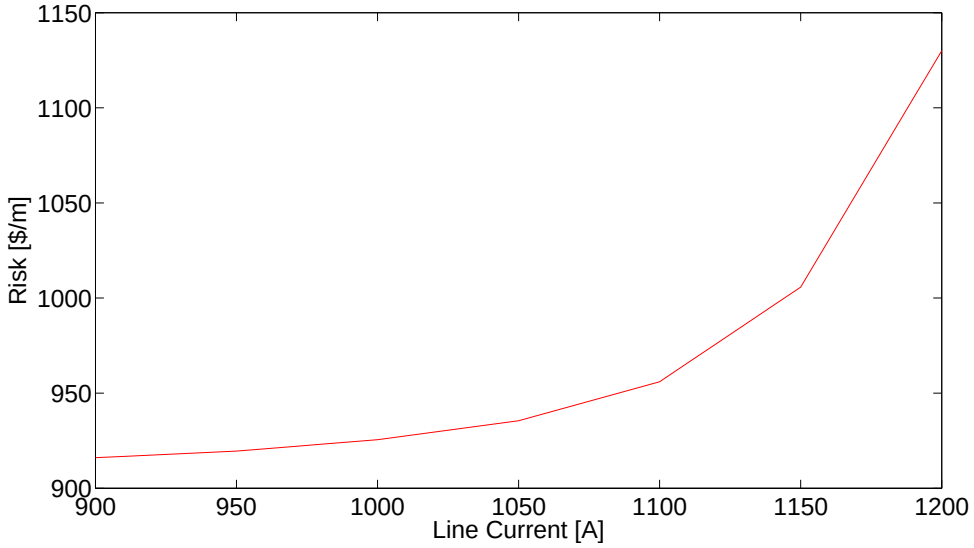

Figure 5.12: Dependence of total risk on line current

The spatial distribution of risk along the line is illustrated in Figure 5.13. The risk is estimated at each tower span of transmission line 5L011 for different line currents. As shown earlier, the percentage loss of strength increases (cf. Fig. 3.21)

and the available ground clearance decreases (cf. Fig. 5.11) with an increase of current. Hence, the total risk due to thermal outage and flashover increases for elevated transmitted loads, as shown in Figure 5.13.

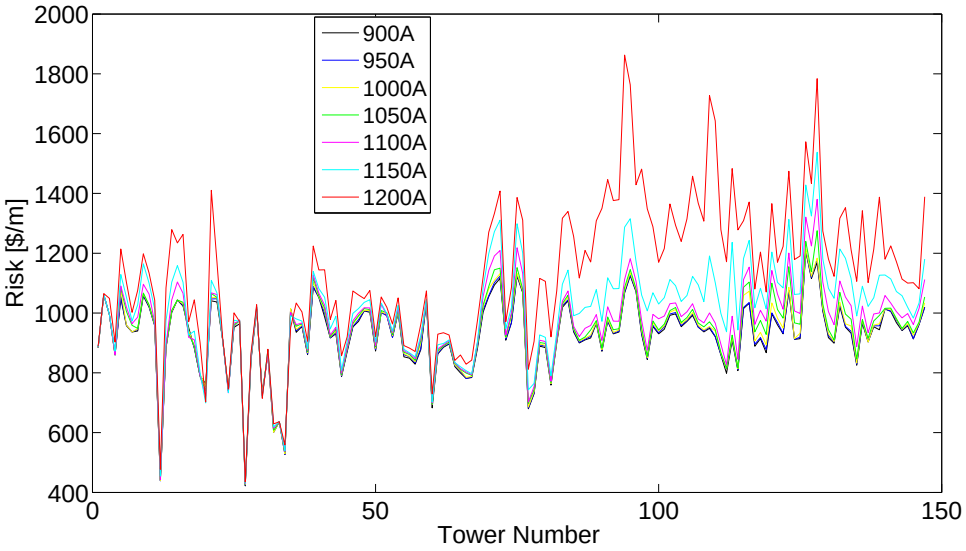

Figure 5.13: Spatial risk analysis for different line currents

Chapter 6

Conclusions, contributions, and future work

6.1 Conclusions

The main results of the thesis are summarized below.

- The dependency of thermal aging on load profile, local weather conditions, and conductor configuration were described in section 3.1 using the point aging analysis method. Using different load currents, it was shown that thermal aging of a single point of a transmission line is directly proportional to the load profile.

- The use of spatial aging analysis to identify critical aging segments and hot spots in a power transmission line was illustrated in section 3.2 using a historical variable load profile and weather data. Sensitivity analyses of this model, depicted in Figure 3.20, were examined on a real power transmission line located in the province of British Columbia and it was concluded that the aging segments and hot spots are independent of line currents. Seasonal dependency of thermal aging and static thermal rating were demonstrated in section 3.3. The highest loss of strength in a transmission line was evaluated during summer and no thermal aging was found during the winter season. Table 3.8 summarizes the numerical results for different seasonal thermal ratings and Table 3.9 presents the percent line utilization and percent of annealing temperatures for each rating.

- A fuzzy expert system for quantification of current condition of transmission conductors was described in chapter 4. It considers geographical location of pollution sources and wind direction to estimate chemical corrosion of the conductors. The final product of the system is the spatial distribution of conductor deterioration. This information can be used to effectively manage inspections and maintenance of power transmission systems.

- The sag and ground clearance of a real power transmission line were computed in section 5.3 and 5.4 based on wind, ice, and thermal stress to facilitate the dynamic re-rating of the transmission line. To estimate the seasonal dependency of sag at a single point of the power transmission line, temporal sag analysis was performed and shown in Figure 5.6. Sag gradually increased during summer due to thermal overload and decreased sharply during winter due to cooler temperatures that produced mechanical contraction.

6.2 Contributions

This thesis introduced a sequential approach to develop a spatio-temporal model of conductor thermal aging. The proposed model was used to analyze the thermal aging behavior of power transmission lines exposed to annealing effects at elevated line temperatures. Spatial aging was analyzed at two different levels: point and line. Point analysis was used to determine the thermal aging at a single point over a particular duration. Thermally critical segments and hot spots in a transmission line were identified using the line analysis approach. The components of the model are: an WRF NWP model, an algorithm for evaluating line temperature, and a graphical model for computing thermal loss of strength. A sample backbone overhead power transmission line, located in the province of British Columbia, was selected to illustrate the results of spatial aging analyses. Historical weather data along the transmission network was extracted using the NWP model and line temperatures were computed based on an IEEE thermal model. To examine the robustness as well as the confidence intervals of the proposed aging model output, sensitivity analyses were performed for various load currents. Temporal analyses were performed

by evaluating the seasonal dependency of thermal aging on a power transmission line for four seasons (winter, spring, summer, fall). In addition, to assess the current condition of an ACSR, a knowledge-based fuzzy expert system was developed that accounts for thermal aging and the impact of industrial air pollution. A fuzzy inference system was designed to estimate the deterioration grades of individual line spans considering three influencing parameters: loss of strength, industrial air pollution, and conductor configuration.

A mathematical model was proposed to compute sag and ground clearance for dynamic re-rating of an overhead power transmission line in order to reduce the risks of outage and flashover. The numerical hybrid sag method adopted from [8] is the core component of this model. It uses mechanical load and thermal stress to compute the elastic and plastic elongation of a transmission line span and the corresponding sag. Mechanical load due to a combination of wind and ice forces on the transmission line, was evaluated using an ice accretion forecasting system, an ice melting model, and a wind and ice load algorithm. Thermal stress along the transmission line was computed based on the fluctuation of line temperature and operation at elevated temperatures. Subsequently, sag at a single tower span was determined considering both mechanical and thermal loads using a numerical approach. The sag computed using this approach was compared with results of a commonly used software package, SAG10, considering two different cases: creep elongation and different wind and ice loads. Available ground clearance was estimated based on computed sag, tower heights, elevation, and vertical distance between towers. These methods were then applied to a sample transmission line. Sags and available ground clearances were calculated using historical meteorological data for various constant load currents. A simple spatial probabilistic risk analysis was performed considering both thermal aging and ground clearance to estimate the potential impact of any incident of outage or flashover.

6.3 Limitations and future work

6.3.1 Thermal aging model

The developed aging model can identify critical aging segments and the severity of single point aging of an energized transmission line. The methodology of area analysis [16] can be extended to design new transmission lines with lower potential thermal aging, similar to an approach proposed in [52]. Owing to the lack of weather data with higher time resolution, steady-state line temperatures were calculated using the proposed aging model. Transient calculations would likely provide more accurate results. To compute transient line temperatures, time resolution of weather data should be $5-15$ minutes [74]. Although the proposed aging model can play an important role in transmission asset management, a complete asset management system should also consider the aging behavior of other electric components.

6.3.2 Expert system

In order to validate the proposed expert system developed for assessment of a transmission line condition, the desired values need to be gathered from direct measurements of deterioration. In addition, conductors of different sizes could be used for further validation of this system. To estimate the pollutant amount in the air emitted from different facilities, wind direction and distance were taken into account as the primary parameters in the system. In addition, wind speed and stack height of a facility could also be considered in the model to estimate the pollution index more accurately.

6.3.3 Sag analysis

Structures within a backbone transmission network can be considered as a suspension structure that supports the power conductor vertically, but permits free movement of the conductor attachment points longitudinally or transversely. In contrast, the end spans are normally designed as strain structures that do not allow any longitudinal movement [15]. In the spatial sag analysis described in the thesis, all line sections within the entire transmission line were considered to be terminated

by strain structures, assuming that the sag at any tower span will not be influenced by the sag of an adjacent tower span. Hence, the computed sag values are slightly higher from real values. The ruling span method (see section 2.4.3) should be applied to get more accurate sag values that consider transversal and longitudinal movements of the conductor. The spatial sag analysis of the complete transmission line was not performed due to a lack of historical weather information with higher time resolution ($5-15$ min interval) in the area of interest. To identify the tower span with the most severe thermal aging and sag, historical weather information with higher time resolution should be acquired along the transmission line. In addition, the proposed sag model was not compared with SAG10 software for different types of ACSRs as such a package was unavailable. The model should be compared either with SAG10 software for different conductor types or real sag values collected from sensors installed at different towers. Vegetation characteristics near the power transmission line should be collected to estimate minimum ground clearances and risk of flashover more accurately. An extension of this thesis may develop a "health index" tool, where the most influencing factors−thermal aging, environment pollution, weather impact, sag, and tension of power conductor−are assigned weights and grades according to severity.

Bibliography

[1] G.M. Beers, S.R. Gilligan, H.W. Lis, and J.M. Schamberger, "Transmission conductor ratings," *IEEE Transactions on Power Apparatus and Systems*, vol. 82, no. 68, pp. 767–775, October 1963.

[2] D. Koval and R. Billington, "Determination of transmission line ampacities by probability and numerical methods," *IEEE Trans. on Power Apparatus and Systems*, vol. PAS-89, no. 7, pp. 1485, Sep. 1970.

[3] J.R. Harvey, "Effect of elevated temperature operation on the strength of aluminum conductors," *IEEE Trans. on Power Apparatus and Syst*, vol. PAS-91, pp. 1769–1772, Sep. 1972.

[4] Vincent T Morgan, "Effect of elevated temperature operation on the tensile strength of overhead conductors," *IEEE Trans. on Power Delivery*, vol. 11, no. 1, pp. 345–352, 01 1996.

[5] J. Lummis and H. D. Fischer, "Practical application of sag and tension calculations to transmission-line design," *Transactions of the American Institute of Electrical Engineers Power Apparatus and Systems, Part III.*, vol. 74, no. 3, pp. 402–416, Jan 1955.

[6] T.O. Seppa, "Factors influencing the accuracy of high temperature sag calculations," *IEEE Transactions on Power Delivery*, vol. 9, no. 2, pp. 1079–1089, April 1994.

[7] M. Keshavarzian and C.H. Priebe, "Sag and tension calculations for overhead transmission lines at high temperatures-modified ruling span method," *IEEE Transactions on Power Delivery*, vol. 15, no. 2, pp. 777–783, 2000.

[8] A. Alawar, E.J. Bosze, and S.R. Nutt, "A hybrid numerical method to calculate the sag of composite conductors," *Electric Power Systems Research*, vol. 76, no. 5, pp. 389–394, March 2005.

[9] M. Muhr, S. Pack, R. Schwarz, and S. Jaufer, "Calculation of overhead line sags," in *51st Internationales Wissenschaftliches Kolloquium*, 2006.

[10] F. Massaro and L. Dusonchet, "Risk evaluation and creep in conventional conductors caused by high temperature operation," in *43rd International Universities Power Engineering Conference*, 2008, p. 1.

[11] H. L. Willis, G. V. Welch, and R. R. Schrieber, *Aging Power Delivery Infrastructures*, Marcel Dekker. Inc., New York, 2001.

[12] Antonio Bracale, Amedeo Andreotti, Guido Carpinelli, and Umberto De Martinis, "Probabilistic index for increasing hourly transmission line ratings," *International Journal of Emerging Electric Power Systems*, vol. 119, 2007.

[13] V.T. Morgan, "The loss of tensile strength of hard drawn conductors by annealing in service," *IEEE Trans. Power apparatus and systems*, vol. PAS-98, no. 3, pp. 700–709, 1979.

[14] Md. Mafijul Islam Bhuiyan, P. Musilek, Jana Heckenbergerova, and D. Koval, "Assessment of the loss of strength in transmission line conductors over time due to thermal loading," *International Institue of Advanced Studies - Transactions on Systems Research and Cybernatics*, vol. X, no. 1, pp. 27–32, 2010.

[15] L.L. Grigsby, *The electrical power engineering handbook*, CRC Press, 2001.

[16] Musilek P., Heckenbergerova J, and Md. Mafijul Islam Bhuiyan, "Spatial analysis of thermal aging of overhead transmission conductors," *submitted to IEEE transaction on power delivery*.

[17] H.A. Smolleck and J.P. Sims, "Guidelines for the selection and operation of bare ACSR conductors with regard to current-carrying capacity," *Electric Power Systems Research*, vol. 5, no. 3, pp. 179–190, 1982.

[18] Arnold Dan, "An ice accretion and wind load forecasting system for power transmission networks using numerical weather prediction," M.S. thesis, University of Alberta, 2009.

[19] IEEE, "Standard for calculating the current-temperature of bare overhead conductors, Std 738," 2006.

[20] John Chan, "Tools for conductor evaluation: State of the art review and promising technologies," Tech. Rep., ELECTRIC POWER RESEARCH INSTITUTE (EPRI), December 2003.

[21] George A. Florea, Stelian Gal, Elena Mateescu, Nicolae Tulici, and Stefan Pastrama, "Romanian approach of ACSR overhead line conductor end of life using live line tehniques to get samples for testing," in *Electricity Distribution, 2005. CIRED 2005. 18th International Conference and Exhibition on*, june 2005, pp. 1–5.

[22] A. K. Deb, *Powerline Ampacity System-Theory, Modeling and Applications*, CRC, 2000.

[23] Henan Jiapu Cable Group, "http://jpcable99.en.made-in-china.com," .

[24] Alcan, "http://www.cable.alcan.com," .

[25] Ostendorp M., "Transmission line uprating guide," Tech. Rep., Electric Power Research Institute (EPRI), November 2000.

[26] Wang J., Lara-Curzio E., and King T., "Methodology for predicting the service life of high-temperature low-sag conductors," Tech. Rep., Oak Ridge National Laboratory, October 2006.

[27] R. Bergmann, H. Lobl, H. Bohme, and S. Grobmann, "Model to describe the chemical ageing behaviour of electrical busbar joints," *European Transactions on Electric Power*, vol. 7, no. 5, pp. 345–350, Sep 1997.

[28] R. Holm, *Electrical Contacts Handbook*, Springer, Berlin/Germany, 1958.

[29] M. Runde, H. Kongsjorden, J. Kulsetas, and B. Totdal, "Detection of a-spots in aluminum contacts," *IEEE Transactions on Components, Hybrids, and Manufacturing Technology,*, vol. 9, no. 1, pp. 77–85, March 1986.

[30] H. Weve, *Elektro- und Thennotransport in Metallen*, J. A. Barth, Leipzig/Gennany, 1973.

[31] R. Bergmann, H. Lobl, H. Bohme, and S. Grobmann, "Calculation of the lifetime of electrical busbar joints," *European Transactions on Electrical Power*, vol. 7, pp. 403–408, 1997.

[32] P. Pytlak, P. Musilek, and E. Lozowski, "Precipitation-based conductor cooling model for dynamic thermal rating systems," in *9th Electrical Power and Energy Conference (EPEC 2009)*. 2009, IEEE.

[33] T. L. Le, M. Negnevitsky, and M. Piekutowski, "Expert system application for the loading capability assessment of transmission lines," *IEEE Transactions on Power Systems*, vol. 10, no. 4, 1995.

[34] H.E. House and P.D. Tuttle, "Current-carrying capacity of ACSR," *Trans. AIEE Part III Power Appar Syst*, vol. 77, no. 3, pp. 1169–1173, Apr. 1958.

[35] M.M. Salama, "Thermal performance of an overhead transmission line under the influence of dust accumulation," *Energy Conversion and Management*, vol. 41, no. 12, pp. 1323–1334, August 2000.

[36] S.D. Kim and M.M. Morcos, "Diagnosis of useful life for ACSR conductors using a fuzzy inference system," *IEEE Power Engineering Review*, vol. 22, no. 5, pp. 61, May 2002.

[37] C.S. Taylor and H.E. House, "Emissivity and its effect on the current-carrying capacity of stranded aluminum conductors," *Power Apparatus and Systems, Part III. Transactions of the American Institute of Electrical Engineers*, vol. 75, no. 3, pp. 970–976, 1956.

[38] POWER Engineers, "Electrical transmission system long range plan (2004-2025)," Tech. Rep., Southern Maryland Electric Cooperative, Hughesville, Maryland, 2005.

[39] R. Thrash, G. Hudson, D. Cooper, and G. Sanders, *Overhead Conductor Manual*, Southwire Company, Carrollton, GA, 1st edition, 1994.

[40] J.R. Harvey, "Creep of transmission line conductor," *IEEE Trans. on Power Apparatus and Systems*, vol. PAS-88, no. 4, pp. 281–286, April 1969.

[41] J.R. Harvey and R.E. Larson, "Use of elevated-temperature creep data in sag-tension calculations," *IEEE Transactions on Power Apparatus and Systems,*, vol. PAS-89, no. 3, pp. 380 –386, March 1970.

[42] Z. Janjic, R. gall, and M.E. Pyle, "Scientific documnetation for the nmm solver," Tech. Rep., National Center for Atmospheric Research, February 2010.

[43] Ronald Stull, *Meteorology for Scientists and Engineers*, Brooks/Cole, Thomas Learning, 2nd edition, 2000.

[44] Pytlak P., Musilek P., Lozowski E., and Arnold D., "Evolutionary optimization of an ice accretion forecasting system," *American Meteorological Society*, vol. 138, no. 7, pp. 2913–2929, July 2010.

[45] L. Shan and D. Douglass, "Conductor and associated hardware impacts during high temperature operations: Issues and problems," Tech. Rep., Palo Alto, CA, 1997.

[46] D. Koval, "Determination of transmission line ampacities by probability and numerical methods," M.S. thesis, 1969.

[47] M.M.I. Bhuiyan, P. Musilek, J. Heckenbergerova, and D. Koval, "Evaluating thermal aging characteristics of electric power transmission lines," in *IEEE 23rd Canadian Conference on Electrical and Computer Engineering*. 2010, IEEE.

[48] J.D. Glover, M.S. Sarma, and T.J. Overbye, *Power system analysis and design*, Thomas Learning, 2007.

[49] F. Mesinger, G. DiMego, E. Kalnay, K. Mitchell, P.C. Shafran, W. Ebisuzaki, D. Jovic, J. Woollen, E. Rogers, E.H. Berbery, M.B. Ek, Y. Fan, R. Grumbine, W. Higgins, H. Li, Y. Lin, G. Manikin, D. Parrish, and W. Shi, "North american regional reanalysis," *Bull. Amer. Meteorol. Soc.*, vol. 87, no. 3, pp. 343–360, Mar. 2006.

[50] J. Heckenbergerova, P. Musilek, Mafijul Islam Bhuiyan, D. Koval, and E. Pelikan, "Identification of critical aging segments and hotspots of power transmission lines," in *EEEIC, Czech Republic*, May 16-19 2010.

[51] W.H. Press, S.A. Teukolsky, W.T. Vetterling, and B.P. Flannery, *Numerical Recipes in C: The Art of Scientific Computing*, Prentice Hall, 3rd edition, 1993.

[52] P. Pytlak and P. Musilek, "An intelligent weather-based system to support optimal routing of power transmission lines," in *Electric Power and Energy Conference (EPEC), 2010 IEEE*, Aug 2010, pp. 1–6.

[53] Robert W. Floyd, "Algorithm 97: Shortest path," *Communications of the ACM*, vol. 5, no. 6, 1962.

[54] A. Saltelli, Marco Ratto, Terry Andres, Francesca Campolongo, Jessica Cariboni, Debora Gatelli, Michaela Saisana, and Stefano Tarantola, *Global Sensitivity Analysis: The Primer*, John Wiley and Sons, 2008.

[55] M. Espinoza, J.A.K. Suykens, R. Belmans, and B. De Moor, "Electric load forecasting: Using kernel-based modeling for nonlinear system identification," *IEEE Control Systems Magazine*, vol. 27, pp. 43–47, Oct 2007.

[56] D.A. Douglass, "Weather-dependent versus static thermal line ratings (power overhead lines)," *IEEE Transactions on Power Delivery*, vol. 3, no. 2, pp. 742–753, Apr. 1988.

[57] Pei Zhang, Miaolei Shao, A.R. Leoni, D.H. Ramsay, and M. Graham, "Determination of static thermal conductor rating using statistical analysis method," in *Electric Utility Deregulation and Restructuring and Power Technologies*, 2008, p. 1237 1243.

[58] Heckenbergerova J., Musilek P., and Filimonenkov K., "Assesment of seasonal static thermal ratings of overhead transmission conductors," in *General meeting of the IEEE Power and Energy Society (PES)*, Detroit, July 2011, p. 8.

[59] Canada National Pollutant Release Inventory, "http://www.ec.gc.ca/inrp-npri/," .

[60] Fakhreddine O. Karray and Clarence de Silva, *Soft Computing and Intelligent Systems Design; Theory, Tools and Applications*, Pearson Education Limited, 2004.

[61] Guanrong Chen and Trung Tat Pham, *Introduction to Fuzzy Sets, Fuzzy Logic, and Fuzzy Control Systems*, CRC Press, 2001.

[62] Witold Pedrycz and Fernando Gomide, *Fuzzy System Engineering toward Human-Centric Computing*, John Wiley and Sons, 2007.

[63] D.G. Fink and H.W. Beaty, *Standard handbook for Electrical Engineers*, McGraw-Hill, 13th edition.

[64] K. Harstveit, "Using routine meteorological data from airfields to produce a map of ice risk zones in norway," in *Proc. of 10th International Workshop on Atmospheric Icing of Structures (IWAIS), Brno, Czech Republic*, June 17-20, 2002.

[65] David J. Marne, *National Electrical Safety Code (NESC) 2007 Handbook*, McGRAW-HILL, 2007.

[66] Canadian Standards Association, "Design criteria of overhead transmission lines," Tech. Rep., October 2006.

[67] Canadian Standards Association, "Overhead systems," Tech. Rep., October 2006.

[68] P. Pytlak, P. Musilek, E. P. Lozowski, D. Arnold, and J. Toth, "Wind and ice load model using numerical weather prediction," in *13th International Workshop on Atmospheric Icing of Structures IWAIS*, Andermatt, Switzerland, September 2009.

[69] F. Kiessling, P. Nefzger, J.F. Nolasco, and U. Kaintzyk, *Overhead power lines - Planning, Design, Construction*, Springer-Verlag, 2003.

[70] CENELEC, "En 50 341-1: Overhead electrical lines exceeding ac 45kv. part1: General requirements - common specifications," 2001.

[71] Hua Wan, James D. McCalley, and Vijay Vittal, "Increasing thermal rating by risk analysis," *IEEE Trans. on Power Systems*, vol. 14, pp. 815–828, 1999.

[72] K. Adomah, Y. Mizuno, and K. Naito, "Probabilistic assessment of the reduction in tensile strength of an overhead transmission line's conductor with reference to climatic data," *IEEE Transactions on Power Delivery*, vol. 15, no. 4, pp. 1221, Oct 2000.

[73] Y. Dai, J.D. McCalley, N. Abi-Samra, and V. Vittal, "Annual risk assessment for overload security," *IEEE Transactions on Power Systems*, vol. 16, no. 4, pp. 616–623, Nov 2001.

[74] Hosek J., Musilek P., Lozowski E., and P. Pytlak, "Eect of time resolution of meteorological inputs on dynamic thermal rating calculations," *IET Gener. Transm. Distrib.*, April 27, 2011.

Appendix A

Expert System

A.1 Fuzzy rules of the expert system [1]

1. IF (LoS is vl) AND (pollution is vl) AND (Conductor size is lar) then (conductor is not deteriorated) ELSE
2. IF (LoS is l) AND (pollution is vl) AND (Conductor size is lar) then (conductor is not deteriorated) ELSE
3. IF (LoS is med) AND (pollution is vl) AND (Conductor size is lar) then (conductor is minor deteriorated) ELSE
4. IF (LoS is h) AND (pollution is vl) AND (Conductor size is lar) then (conductor is partially deteriorated) ELSE
5. IF (LoS is vh) AND (pollution is vl) AND (Conductor size is lar) then (conductor is severely deteriorated) ELSE
6. IF (LoS is vl) AND (pollution is l) AND (Conductor size is lar) then (conductor is not deteriorated) ELSE
7. IF (LoS is l) AND (pollution is l) AND (Conductor size is lar) then (conductor is minor deteriorated) ELSE
8. IF (LoS is med) AND (pollution is l) AND (Conductor size is lar) then (conductor is minor deteriorated) ELSE
9. IF (LoS is h) AND (pollution is l) AND (Conductor size is lar) then (conductor is partially deteriorated) ELSE
10. IF (LoS is vh) AND (pollution is l) AND (Conductor size is lar) then (conductor is severely deteriorated) ELSE
11. IF (LoS is vl) AND (pollution is med) AND (Conductor size is lar) then (conductor is partially deteriorated) ELSE
12. IF (LoS is l) AND (pollution is med) AND (Conductor size is lar) then (conductor is partially deteriorated) ELSE
13. IF (LoS is med) AND (pollution is med) AND (Conductor size is lar) then (conductor is partially deteriorated) ELSE
14. IF (LoS is h) AND (pollution is med) AND (Conductor size is lar) then (conductor is partially deteriorated) ELSE

[1] vl = very low, l = low, med = medium, h = high, vh = very high, s = small, lar = large

15. IF (LoS is vh) AND (pollution is med) AND (Conductor size is lar) then (conductor is severely deteriorated) ELSE
16. IF (LoS is vl) AND (pollution is h) AND (Conductor size is lar) then (conductor is partially deteriorated) ELSE
17. IF (LoS is l) AND (pollution is h) AND (Conductor size is lar) then (conductor is partially deteriorated) ELSE
18. IF (LoS is med) AND (pollution is h) AND (Conductor size is lar) then (conductor is partially deteriorated) ELSE
19. IF (LoS is h) AND (pollution is h) AND (Conductor size is lar) then (conductor is severely deteriorated) ELSE
20. IF (LoS is vh) AND (pollution is h) AND (Conductor size is lar) then (conductor is severely deteriorated) ELSE
21. IF (LoS is vl) AND (pollution is vl) AND (Conductor size is med) then (conductor is not deteriorated) ELSE
22. IF (LoS is l) AND (pollution is vl) AND (Conductor size is med) then (conductor is not deteriorated) ELSE
23. IF (LoS is med) AND (pollution is vl) AND (Conductor size is med) then (conductor is minor deteriorated) ELSE
24. IF (LoS is h) AND (pollution is vl) AND (Conductor size is med) then (conductor is partially deteriorated) ELSE
25. IF (LoS is vh) AND (pollution is vl) AND (Conductor size is med) then (conductor is severely deteriorated) ELSE
26. IF (LoS is vl) AND (pollution is l) AND (Conductor size is med) then (conductor is not deteriorated) ELSE
27. IF (LoS is l) AND (pollution is l) AND (Conductor size is med) then (conductor is minor deteriorated) ELSE
28. IF (LoS is med) AND (pollution is l) AND (Conductor size is med) then (conductor is minor deteriorated) ELSE
29. IF (LoS is h) AND (pollution is l) AND (Conductor size is med) then (conductor is partially deteriorated) ELSE
30. IF (LoS is vh) AND (pollution is l) AND (Conductor size is med) then (conductor is severely deteriorated) ELSE
31. IF (LoS is vl) AND (pollution is med) AND (Conductor size is med) then (conductor is minor deteriorated) ELSE
32. IF (LoS is l) AND (pollution is med) AND (Conductor size is med) then (conductor is minor deteriorated) ELSE
33. IF (LoS is med) AND (pollution is med) AND (Conductor size is med) then (conductor is minor deteriorated) ELSE
34. IF (LoS is h) AND (pollution is med) AND (Conductor size is med) then (conductor is partially deteriorated) ELSE
35. IF (LoS is vh) AND (pollution is med) AND (Conductor size is med) then (conductor is severely deteriorated) ELSE
36. IF (LoS is vl) AND (pollution is h) AND (Conductor size is med) then (conductor is partially deteriorated) ELSE

37. IF (LoS is l) AND (pollution is h) AND (Conductor size is med) then (conductor is partially deteriorated) ELSE
38. IF (LoS is med) AND (pollution is h) AND (Conductor size is med) then (conductor is partially deteriorated) ELSE
39. IF (LoS is h) AND (pollution is h) AND (Conductor size is med) then (conductor is partially deteriorated) ELSE
40. IF (LoS is vh) AND (pollution is h) AND (Conductor size is med) then (conductor is severely deteriorated) ELSE
41. IF (LoS is vl) AND (pollution is vl) AND (Conductor size is s) then (conductor is not deteriorated) ELSE
42. IF (LoS is l) AND (pollution is vl) AND (Conductor size is s) then (conductor is not deteriorated) ELSE
43. IF (LoS is med) AND (pollution is vl) AND (Conductor size is s) then (conductor is minor deteriorated) ELSE
44. IF (LoS is h) AND (pollution is vl) AND (Conductor size is s) then (conductor is partially deteriorated) ELSE
45. IF (LoS is vh) AND (pollution is vl) AND (Conductor size is s) then (conductor is severely deteriorated) ELSE
46. IF (LoS is vl) AND (pollution is l) AND (Conductor size is s) then (conductor is not deteriorated) ELSE
47. IF (LoS is l) AND (pollution is l) AND (Conductor size is s) then (conductor is minor deteriorated) ELSE
48. IF (LoS is med) AND (pollution is l) AND (Conductor size is s) then (conductor is minor deteriorated) ELSE
49. IF (LoS is h) AND (pollution is l) AND (Conductor size is s) then (conductor is partially deteriorated) ELSE
50. IF (LoS is vh) AND (pollution is l) AND (Conductor size is s) then (conductor is severely deteriorated) ELSE
51. IF (LoS is vl) AND (pollution is med) AND (Conductor size is s) then (conductor is minor deteriorated) ELSE
52. IF (LoS is l) AND (pollution is med) AND (Conductor size is s) then (conductor is minor deteriorated) ELSE
53. IF (LoS is med) AND (pollution is med) AND (Conductor size is s) then (conductor is minor deteriorated) ELSE
54. IF (LoS is h) AND (pollution is med) AND (Conductor size is s) then (conductor is partially deteriorated) ELSE
55. IF (LoS is vh) AND (pollution is med) AND (Conductor size is s) then (conductor is severely deteriorated) ELSE
56. IF (LoS is vl) AND (pollution is h) AND (Conductor size is s) then (conductor is minor deteriorated) ELSE
57. IF (LoS is l) AND (pollution is h) AND (Conductor size is s) then (conductor is minor deteriorated) ELSE
58. IF (LoS is med) AND (pollution is h) AND (Conductor size is s) then (conductor is partially deteriorated) ELSE

59. IF (LoS is h) AND (pollution is h) AND (Conductor size is s) then (conductor is partially deteriorated) ELSE

60. IF (LoS is vh) AND (pollution is h) AND (Conductor size is s) then (conductor is severely deteriorated)

A.2 Estimation of desired deterioration grades

Table A.1 summarizes the desired values of deterioration grades for several tower spans chosen by an expert. The relative deterioration grades were estimated based on the magnitude of pollution index and thermal loss of strength. The impact of thermal loss of strength was given more significance than that of pollution index in estimating the grades.

Table A.1: Deterioration grades based on domain expert

Tower Number	Loss of strength [%]	Pollution index	Deterioration grade
346	6.27	1.25	4.6
372	6.35	0.50	4.7
597	4.49	7.0	4.8
624	5.78	7.0	5.3
638	5.13	4.5	4.9
833	5.39	0	3.7
852	5.30	3.0	3.75
856	5.43	6.0	5.1
860	5.03	10.0	5.1
863	5.28	10.0	5.6

Based on the data from Table A.1, the relationship between the deterioration, loss of strength, and pollution index was expressed in the following regression equation.

$$y = a + b \cdot x_1 + c \cdot x_2 + d \cdot x_1 \cdot x_2, \tag{A.1}$$

where y is the deterioration grade, and x_1 and x_2 represent loss of strength LoS and pollution index, respectively. Values of regression coefficients a, b, c, and d were found using nonlinear, multivariate regression analysis. Their values are a = -0.2747, b = 0.7548, c = 0.3906, and d = -0.039. In the final step, the desired deterioration grades of all tower spans were evaluated using equation (A.1).

A.3 Profile of Expert

Expert knowledge used to develop and evaluate the expert system described in this thesis was provided by Dr. Don Koval. He was a professor in the Department of Electrical and Computer Engineering at the University of Alberta. He taught classes in Power Systems, Reliability Engineering, and Industrial Power System Reliability. He also worked as a Distribution Special Studies Engineer in BC Hydro for 13 years and with Saskatchewan Power for 2 years. Don was a Registered Professional Engineer in the Provinces of Alberta and British Columbia, a Fellow of the American Biographical Institute, a Fellow of the IEEE, and a Life Fellow of the International Biographical Center, Cambridge, U. K. He was Chairman of

IEEE Std. 493 (IEEE Gold Book IEEE Recommended Practice for Design of Reliable Industrial and Commercial Power Systems). He was elected as one of the six Distinguished Lecturers of the IEEE Industry Application Society (IAS) for the period 2000-2001. Recently, he was also appointed to the rank of Distinguished Visiting Professor and elected Fellow by the International Institute for Advanced Studies in System Research and Cybernetics in Germany.